REACTION KINETICS OF METAL DEPOSITION BY SURFACE LIMITED REDOX REPLACEMENT OF UPD MONOLAYER

A Dissertation

Presented to

The Faculty of the Department of Electrical and Computer Engineering

University of Houston

In Partial Fulfillment

of the Requirements for the Degree

Doctor of Philosophy

In Electrical and Computer Engineering

by

Ela Bulut

August 2015

REACTION KINETICS OF METAL DEPOSITION BY SURFACE LIMITED REDOX REPLACEMENT OF UPD MONOLAYER

_____

Ela Bulut

Approved:

_____

Chair of the Committee,
Stanko R. Brankovic, Associate Professor,
Electrical and Computer Engineering

Committee Members:

_____

Paul Ruchhoeft, Associate Professor,
Electrical and Computer Engineering

_____

Jiming Bao, Associate Professor,
Electrical and Computer Engineering

_____

Lars C. Grabow, Assistant Professor,
Chemical Engineering

_____

James K. Meen, Associate Professor,
Department of Chemistry

_____

Suresh K. Khator, Associate Dean,
Cullen College of Engineering

_____

Badri Roysam, Professor, Chair,
Electrical and Computer Engineering

Acknowledgements

I could not have written this dissertation without the support and encouragement of my advisor, family, friends, and colleagues. To all of them, I would like to express my deepest gratitude. First, my deepest thanks go to my beloved husband, Alper Tolga Bulut, whose sacrifices made possible the completion of this research. Your love and support gave me the strength and motivation I needed to finish graduate school. I would also like to thank my precious daughter, my little angle, and my rock, Ipek Sare, whose arrival made me stronger than ever.

Second, I would like to thank my advisor Dr. Stanko R. Brankovic. I could not have completed this dissertation without your support and guidance. Your advice, comments, and timely interventions always eased my job. You were not only my academic advisor, but also my mentor. I will always remember and follow the valuable advices you gave whenever I needed on both my academic and personal life. I cannot express my gratitude for your understanding and support. I have learned so much during my PhD and still have a lot to learn from your incredible knowledge and expertise. I would also like to acknowledge my committee members, Dr. Jiming Bao, Dr. Paul Ruchhoeft, Dr. James K. Meen, and Dr. Lars C. Grabow. Their support and helpful comments helped to improve my work.

Third, I would also like to thank several of my graduate school friends. I would like to thank my former labmate, Dr. Dincer Gokcen, for his guidance and help when I was in the process of adapting to the PhD life. I also thank my labmates, Dr. Jinnie George, Dr. Qiuyi Yuan, Dr. Nikhil Dole, Milan Slavkovic, Ashish Tripathi, Shruti

Gopal, Rachit Sharma, and Dongun Wu for providing a joyful lab atmosphere. I also thank my friends, Sevda Agaoglu and Dr. Mehmet Naci Agaoglu for all of their help and support during my coding process. Your timely help came at a time when I was very desperate. “Allah ikinizden de razi olsun!” My labmate, Alexander Bello also deserves a big thank you for improving my LabVIEW code and making my experiments much easier. Many thanks to Carmen Pascente and Mahmut Unan for all of their help in the review and printing process. Wenlan Qiu, Rubabe and Hakan Haberdar, and all of my Turkish friends, thank you so much for your invaluable friendship. I am also thankful to the Turkish government and Ministry of Education for providing me the scholarship to pursue a graduate degree in the United States.

Finally, I would like to thank my parents, İmdat and Zennure Yılmaz, and my brothers, Selçuk and Erdal Yılmaz. Anneciğim, babacığım, abilerim: sizlere ne kadar teşekkür etsem azdır. Maddi ve manevi desteğiniz ve dualarınız vesilesiyle bugünlere gelmek nasip oldu. Allah sizlerden razı olsun. Bugünlere erişmemizi nasip eden Rabb’ime hamd-ü senalar olsun.

REACTION KINETICS OF METAL DEPOSITION BY SURFACE LIMITED REDOX REPLACEMENT OF UPD MONOLAYER

An Abstract

of a

Dissertation

Presented to

The Faculty of the Department of Electrical and Computer Engineering

University of Houston

In Partial Fulfillment

of the Requirements for the Degree

Doctor of Philosophy

In Electrical and Computer Engineering

by

Ela Bulut

August 2015

Abstract

Noble metal coatings have been used in many applications such as catalysts, corrosion protection, and microelectromechanical systems (MEMs). Using the monolayer coating concept lowers the ultimate cost by reducing noble metal content. Underpotential deposition (UPD) and Surface Limited Redox Replacement (SLRR) reactions are two significant monolayer deposition methods that have gained more attention lately in catalyst design community. To have a more precise deposition and control of monolayer catalysts morphology, it is important to know more about reaction kinetics, such as reaction rate constant and half time of the reaction. By varying the coverage of UPD layer using deposition via SLRR, it is possible to control the amount of monolayer deposit accurately down to a fraction of monolayer. Since in SLRR, galvanic displacement of UPD monolayer occurs at open circuit potential (OCP), conventional charge measurement method is not capable of monitoring deposited amount of noble metal. In addition, the OCP model equations derived from Bruckenstein-Swathirajan (BS) isotherm and rate equations have four or more fitting parameters which causes complexity of the fits and interpretation of the results. The objective of this research is to study reaction kinetics of Au deposition by surface-limited redox replacement (SLRR) of lead underpotential deposited (UPD) mono layer (ML) on Au (111) single crystal by surface reflectivity measurements. This approach involves fitting procedures that has only one adjustable parameter. Our system is proved to be successful in measuring reaction rate constants by fitting rate equation to the Pb UPD coverage transients during SLRR. Thus, this system is used to do reaction kinetics analysis in Au deposition via SLRR of Pb UPD ML.

Table of Contents

List of Figures

List of Tables

Chapter 1: Introduction

Last decades have witnessed the rise of electrochemical material synthesis and electrodeposition has become the enabling fabrication method in the high-tech enterprise (Edelstein and Cammarata, 1996; Cao, 2004). In many cases, electrochemical synthesis provides a convenient approach in terms of delivering the desired outcome. The use of electrochemical synthesis have proliferated in recent years through different applications such as growing multilayered metallic thin films and nano-structures (Nicewarner-Peňa et al., 2001; Schwarzacher, 1999; Pauling and Jüttner, 1992), nano-scale metallic architectures (Whitney et al., 1993; Sung et al., 2001; Bartlett, 2004; Whitaker et al., 2005; Kolb et al., 1997; Zach et al., 2000; Li et al., 1999), and a high quality single crystal overlayers (Yong et al., 1999; Sieradzki et al., 1999; Brankovic et al., 1999; Vasilic and Dimitrov, 2005). Electrochemical deposition techniques became quite popular in catalyst synthesis for fuel cells and metal-air batteries. These new applications offer new horizons for electrochemical material science research (Gokcen et al., 2011; Brankovic and Zangari, 2015).

This PhD dissertation consists of six chapters. In the first chapter, introduction, electrochemical deposition is briefly described. As an application of metal deposition via surface limited redox replacement reaction, core-shell nanoparticle catalyst synthesis is briefly discussed. This chapter reviews also literature on UPD and deposition via SLRR reaction and a brief definition of the reaction rate constant is described.

The second chapter describes the, experimental techniques, reviews literature on surface reflectivity measurements. Additionally, the theory behind the surface reflectivity

of gold electrodes is reviewed. Also, other experimental techniques such as cyclic voltammetry, chronoamperometry, and OCP measurements are described.

The third chapter covers experimental and describes our surface reflectivity measurement system by explaining its all significant components. This chapter also discusses the LabVIEW data acquisition algorithm and program that was developed as a part of this PhD thesis. In addition, the sample experimental preparation and our procedure for surface reflectivity measurements are described here.

The fourth chapter presents results and discussions. It gives the model equations we derived for reaction kinetics of Au deposition via SLRR of Pb UPD monolayer on Au (111). Effect of Au^{3+} concentration on reaction kinetics of Au deposition via SLRR of Pb UPD monolayer is discussed, and comparison between rate constants obtained from surface reflectivity measurements and rate constants from OCP transient measurements is presented. Same comparison is also done for effect of Pb^{2+} concentration and effect of supporting electrolyte (ClO_4^-) on reaction kinetics of Au deposition via SLRR of Pb UPD monolayer.

The sixth chapter gives a summary of the work with conclusions emphasizing the importance and accuracy of the system we built. In the final chapter, Chapter 7, brief suggestions on future work and on how to improve our surface reflectivity measurement system are discussed.

1.1. Electrochemical Deposition

Electrochemical deposition (electrodeposition) is one of the phenomena which can be used for thin film growth. This process can be described as deposition of ions

from a solution and incorporation of the metal ions into crystal lattices (Bockris and Reddy, 1970). The electrodeposition phenomenon includes three concepts, and these are charge transfer, surface diffusion, and lattice incorporation process. During the charge transfer reaction, metal ions pass through the electrified electrode-electrolyte interface and get discharged at the electrode surface by gaining electrons. This process is also described as the reduction of ions. After the charge transfer, adatoms tend to diffuse to the surface defects such as vacancies, kinks, and steps rather than staying on smooth terraces (Figure 1-1 from Gokcen, 2010). This is due to the fact that these are energetically more favorable than smooth terraces. This process follows a zigzag motion parallel to the surface until adatoms find the energetically most favorable locations where adatoms can easily bond with more atoms and is called as surface diffusion. Then, the adatoms finally incorporate into crystal lattices (Gokcen, 2010).

Electrochemical deposition (electrodeposition) can be expressed by a typical reduction expression of metal ions (M^{n+}) because metal ions reduce on a conductive surface by gaining electrons during deposition (Gokcen, 2010). The metal electrodeposition reaction can be written as

$$M^{n+} + ne^{-} \rightarrow M \,. \tag{1-1}$$

The equilibrium potential that needs to be exceeded to start a conventional electrodeposition is defined by Nernst equation,

$$E_{M^{n+}/M} = E^{0} + \frac{RT}{mF} \ln [a_{M^{n+}}] \,. \tag{1-2}$$

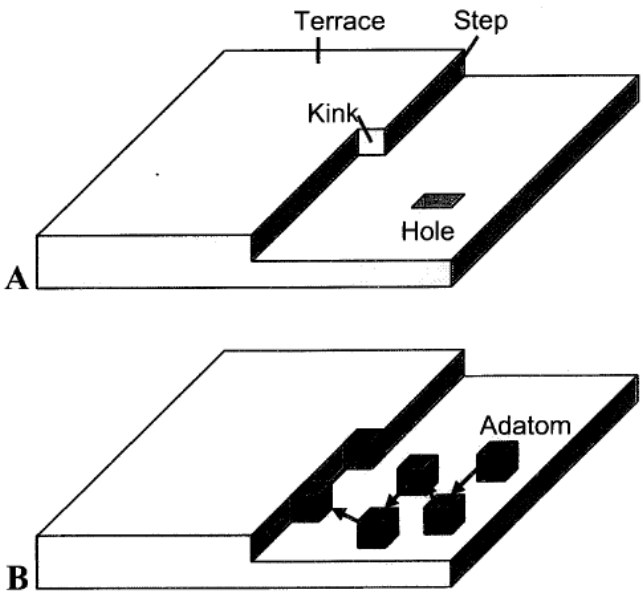

Figure 1-1. (A) Step, kink sites, holes and vacancies on crystal terraces, (B) Surface diffusion of adatoms through the kink site.

In Eq. (1-2), E^0 is the equilibrium (reversible) potential of the electrode surface at standard conditions (P^0=101 kPa, and T^0=298^{0}K, $a_{M^{n+}}$=1), R represents the universal gas constant, F is Faraday's constant**,** and T is the absolute temperature, $a_{M^{n+}}$ is the activity of the metal ions in the solution and n represents the number of electrons transferred in the redox reaction. The ion activity term, $a_{M^{n+}}$, can be approximated by the ion concentration in dilute solutions ($a_{M^{n+}} \approx C_{M^{n+}}$).

It can be stated from the Nernst equation that the actual value of the equilibrium potential can be adjusted by changing the concentration of the corresponding metal ions in the electrolyte. If the applied potential (E) is more negative than the equilibrium potential of the electrode (overpotential conditions: $\eta = E - E_{M^{n+}/M} < 0$), metal ions reduce on the surface through a cathodic reaction (negative current). In other words,

metal electrodeposition ($M^{n+} + ne^{-} \rightarrow M$) takes place at this overpotential condition (Overpotential deposition, OPD). In reverse, anodic reaction takes place (metal dissolution) on the surface when the applied potential is higher than the equilibrium potential (Brankovic, 2009).

1.2. Core-shell Nanoparticle Catalyst Synthesis by Using SLRR

Proton Exchange Membrane Fuel Cells (PEMFCs) seem to be an answer to the concern about energy resources. The cost of PEMFCs strongly depends on the amount of Pt catalyst needed since it requires a large amount of Pt in its cathode's catalytic layer due to the low catalytic activity of Pt for the oxygen reduction reaction (ORR) than for hydrogen oxidation (HOR). Some of the recent studies to improve electrocatalysts include alloying Pt to synthesize bi-metallic catalysts (Stamenkovic et al., 2007), core-shell nanoparticles catalysts (Zhang, 2005), the role of size, special structure, and shape of nanoparticles (Wang et al., 2009), and de-alloying of bimetallic alloys (Strasser, 2009). Electrodeposition method has several advantages on producing electrocatalysts when it is compared to other fabrication techniques, such as vacuum deposition and wet chemistry methods. Vukmirovic et al. (2011) studied the application of metal electrodeposition in the synthesis of a new type of electrocatalysts comprising a Pt monolayer (Pt_{ML}) on metal or alloy nanoparticles. To reduce the loading of Pt, or Pt-like noble metals, a Pt_{ML} shell on a nanoparticle substrate core can be achieved which will allow every atom to be available for catalytic activity (Fayette et al., 2011; Brankovic et al., 2002). The most efficient way to synthesize this type of 2D monolayer catalyst is deposition via surface limited red-ox replacement (SLRR) reaction which was first reported by Brankovic et al.

(2001; see also Gokcen et al., 2011). Galvanic displacement of a Cu UPD monolayer by Pt provides a simple and easy way to deposit a uniform metal monolayer on carbon-supported metal nanoparticles (Fayette et al., 2011). SLRR has a broad range of applications in design of core-shell nanoparticles, epitaxial ultra-thin film growth of highly active catalysts, and single crystal metal overlayers (Gokcen et al., 2011).

1.3. Activated-Complex Theory

The reaction rate can be defined as an increase in concentration of products or decrease in concentration of reactants in a constant-volume system per unit time (Laidler, 1969). It is very important to investigate reaction rates and the main factors which influence them, such as nature of the reactants and products, concentration of reacting species, temperature, and influence of catalysts.

There are two main theoretical aspects of reaction rates which arise as a result of Arrhenius' empirical study which was conducted in 1889 and was the fundamental realization on the temperature dependence of many chemical reactions (Arrhenius, 1889). Arrhenius (1889) expresses reaction rate constant as

$$k = Ze^{-E_a / RT} . \tag{1-3}$$

Here, Z is the frequency factor, and E_a is the activation energy, and these two terms are independent of temperature. When we take logarithm of both sides, equation will be expressed as

$$\ln k = -(E_a/R)(1/T) + \ln Z . \tag{1-4}$$

A plot of ln k vs. $1/T$ gives a line with slope $= -E_a / R$ and intercept = ln Z. This equation applies to all rate constants, regardless of the order of reaction. When the rate constant of a reaction at two different temperatures are measured, we can calculate the E_a of that reaction, or when E_a and the rate at one temperature is known, we can calculate the rate at a second temperature from

$$\ln k_1 - \ln k_2 = -E_a/RT_1 + E_a/RT_2 . \tag{1-5}$$

The main division of the theories of chemical reaction rates is based on whether they are related to potential energy surfaces or not. The theories based on passage over potential-energy surfaces are also classified in two divisions according to whether they make the assumption of equilibrium between reactants and activated complexes. A potential energy surface was first constructed in 1931 by Eyring and Polanyi (1931), and for a few years after that time a number of attempts were made to treat the dynamics of classical motion over potential-energy surfaces. However, at that time due to lack of high speed computers, there was a practical difficulty to carry out dynamical calculations since it requires a very large number of calculations to cover a variety of initial conditions and obtain meaningful results. Before the potential energy surface concept, researchers like Trautz and Anorg (1916) and McC (1918) studied the reaction rates by a collision theory in which molecules were considered as hard spheres. Due to the errors of this concept for many reactions, activated complex theory is developed by Rodebush (1923; 1933; 1935; 1936), later Rice and Gershinowitz (1934), Pelzer and Wigner (1932), and then by Eyring (1935), and Evans and Polanyi (1935; 1937) based on Marcelin's study (1915).

The reaction rate will increase if the concentration of the reacting molecules increases. Statistically, the number of collisions should increase when the concentration of colliding species is increased. The other method to increase the frequency of collisions is to raise the temperature of the system (Yerkes, 2011). Temperature is a measure of the average kinetic energy of the particles in the system, and in the gas phase, it is possible to calculate the increase in the collision rate as a function of temperature (Yerkes, 2011). It is discovered that even though the number of collisions increases dramatically with raising temperature, the rate of the reaction increases much less dramatically. This implies that only a small number of collisions actually prompt to a reaction.

We consider the reaction as A-B + C ↔ A + B-C and assume it proceeds to equilibrium. The activated complexes will also be in equilibrium with reactants and products even if the reactants and products are not at equilibrium with each other, and their concentration can be calculated in terms of A and B. Under these circumstances, activated complex theory is a reliable solution method for rate of the equation. In going from reactants (A-B and C) to products (A and B-C) there is one specific geometric configuration of all three atoms (A¨B¨C) called the *Activated Complex*, which must form before the reaction occurs. The point in the course of the reaction when this forms is called the transition state. At this point, the potential energy of the atoms is at a maximum. As it can be seen in Figure 1-2, the potential energy has reached a maximum at the transition state. The relative positions of the reacting species are that of the activated complex. The activated complex is completely unstable and cannot be isolated. It is simply a transition between the reactants and products, and resembles both the reactants and the products.

Reactions with large activation energies have slower rates. To increase the rate of these reactions, you can raise the temperature or add a catalyst. Catalysts speed up reaction rates by providing an alternate activated complex, with a lower activation energy (Yerkes, 2011).

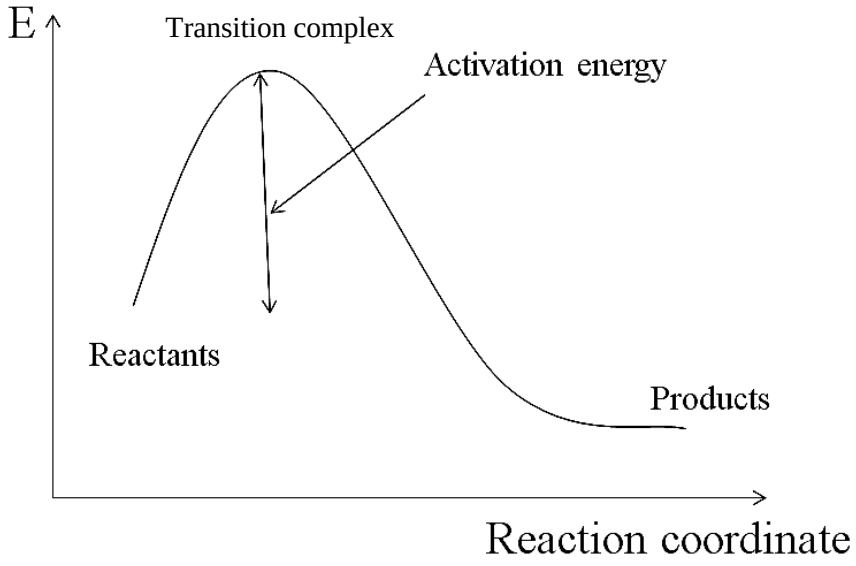

Figure 1-2. Schematic of activated complex.

1.4. Underpotential Deposition

Underpotential deposition (UPD) occurs in many electrochemical systems which include a metal electrode in solution with different metal ions. This phenomenon refers to potential dependent adsorption of metal atomic layers onto a foreign metal substrate at a potential which is more positive than the reversible Nernst potential (Herrero et al., 2001).

Figure 1-3 illustrates schematics of UPD phenomena. UPD deposition on bare substrate starts at a potential which is more positive than the reversible Nernst potential.

Ideally, adsorption and stripping peaks are symmetrical during UPD. After overpotential conditions are reached, bulk deposition takes place.

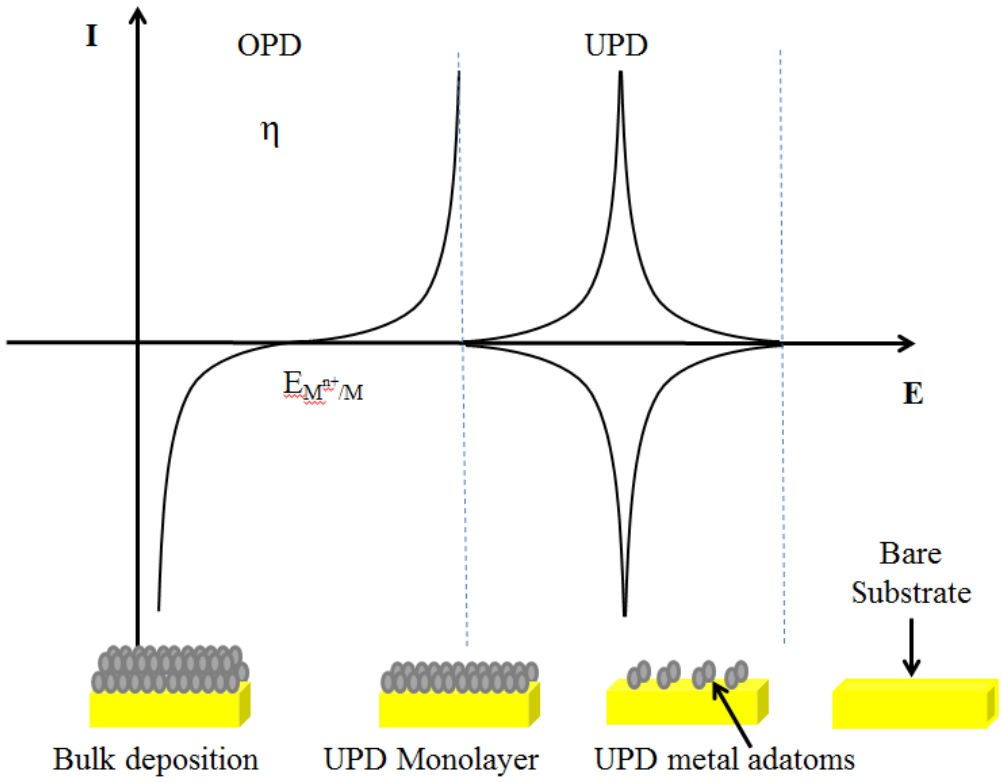

Figure 1-3. Schematic of underpotential deposition.

Different electroanalytical and surface characterization methods can be employed to examine UPD phenomenon. Since cyclic voltammetry (CV) provides control and measurements of the parameters, such as potential, current, and charge, it is one of the techniques used in our study. In a typical UPD process, several deposition or stripping peaks in a CV are observed. Purity of the solution and quality of the substrate define the cathodic and anodic peaks in the CV. The coverage and monolayer formation mostly

depend on the interactions among the adatoms in the UPD layer and the attractive forces between the substrate and UPD metal (Gokcen, 2010).

One of the first UPD studies is performed on deposition of radioactive Ag on polycrystalline Au and Pt by Rogers et al. (1949). A large number of comprehensive UPD studies were conducted on single crystal and polycrystalline electrodes in 1960's and 1970's (Trasatti, 1971; Kolb, 1978). UPD phenomenon has gained more attention with development of scanning probe microscopy and X-ray scattering techniques. During 1980's and 1990's, the detailed re-examination of many UPD systems led to more information about UPD process, its description, and diversity (Budevski et al., 1996; Herrero, 2001).

UPD represents a potential dependent adsorption process with great sensitivity and selectivity towards the nature of the metal surface and its termination (Trasatti, 1971; Budevski, 1996). Many applications such as, corrosion studies (Vukmirovic et al., 2012), measurements of surface area (Liu et al., 2009), and characterization of thin film quality and surface roughness (Fayette et al., 2011; Viyannalage et al., 2007) can be given as the examples of practical use of UPD phenomenon as a decoration technique for surface characterization. UPD has been often used in a broad range of electrochemical deposition protocols (Sieradzki et al., 1999; Brankovic et al., 1999; Vasilic et al., 2006; Kim et al., 2006; Viyannalage et al., 2007) since it precedes bulk deposition in many heteroepitaxial systems. UPD layers provide a route for enhanced catalyst activity and selectivity towards certain reactions, so that they are extensively used as a surface decoration protocol for catalytically active metals (Lipkowski and Ross, 1998). A new deposition technique in which UPD has an essential role was developed recently for fuel

cell catalyst synthesis (Brankovic et al., 2001; Fayette et al., 2011; Gokcen et al., 2011). In this protocol, the catalyst is deposited by a surface limited red-ox replacement (SLRR) reaction between the depositing metal and UPD metal layer. By depositing typically one monolayer (ML) or even submonolayer amount, this deposition technique provides the route to achieve a minimum catalyst loading on the substrate surface (Adzic et al., 2007; Sasaki et al., 2010).

As it was mentioned earlier, the main technique used to study UPD characteristics is cyclic voltammetry (CV). The UPD process is demonstrated by the presence of one or more deposition or stripping peaks in the underpotential region observed during the potential sweep in the cathodic (anodic) direction (Figure 1-4A). Generally, the preparation process and quality of the substrate surface define the identity of UPD peaks. On top of that, presence of one or more UPD layer superstructures (Will et al., 1995; Garcia et al., 2005) and/or the number of UPD MLs formed (Corcoran et al., 1994; Esplandiu et al., 1999) cause the complexity of the voltammetry characteristics.

Figure 1-4 shows the examples cyclic voltammograms (CVs) of Pb and Cu UPD on Au (111) from perchloric acid solution (10^{-3} M Pb^{2+} + 0.1 M $HClO_4$, sweep rate 10 $mV \cdot s^{-1}$) obtained by Gokcen et al. (2011). Here, insets show atomic resolution of full Pb UPD layer on Au (111). As it can be seen in the CV, the Pb UPD peak is very sharp and occurs at an underpotential of approximately +0.18 V and is preceded by several smaller and broader cathodic peaks, which occur at higher underpotentials (0.350 V and 0.240 V). As Brankovic and Zangari (2015) discussed that the Pb UPD process starts with the adsorption of Pb or Pb-OH species on defects at the Au surface like steps and dislocations (Budevski et al., 1996) and the broad cathodic peak at ≈0.375 V is associated

with the initial decoration of the Au (111) surface defects by Pb adatoms (Rath, 1983) while the broad shoulder and cathodic peak at ≈0.235 V is associated with nucleation and growth of Pb UPD layer on Au (111) terraces (Budevski et al., 1996). Majority of the current/charge related with the main Pb UPD peak is because of densification of the Pb UPD layer, which at first nucleates and grows as a low-density phase (Budevski et al., 1996). At 0.100 V underpotential, a fully dense Pb UPD layer (full monolayer) forms with an incommensurate hexagonal structure and ≈7% smaller interatomic distance than in bulk Pb (Hamelin and Lipkowski, 1984). Brankovic and Zangari also showed the STM image with atomic resolution of the Pb UPD layer on Au (111) at this potential in the inset of Figure 1-4A and the moiré pattern indicates compression in the Pb UPD layer having a packing density of 0.66 with respect to the underlying Au (111) (ρ_{Pb}^{UPD}=0.66) (Hamelin and Lipkowski, 1984; Brankovic and Zangari, 2015).

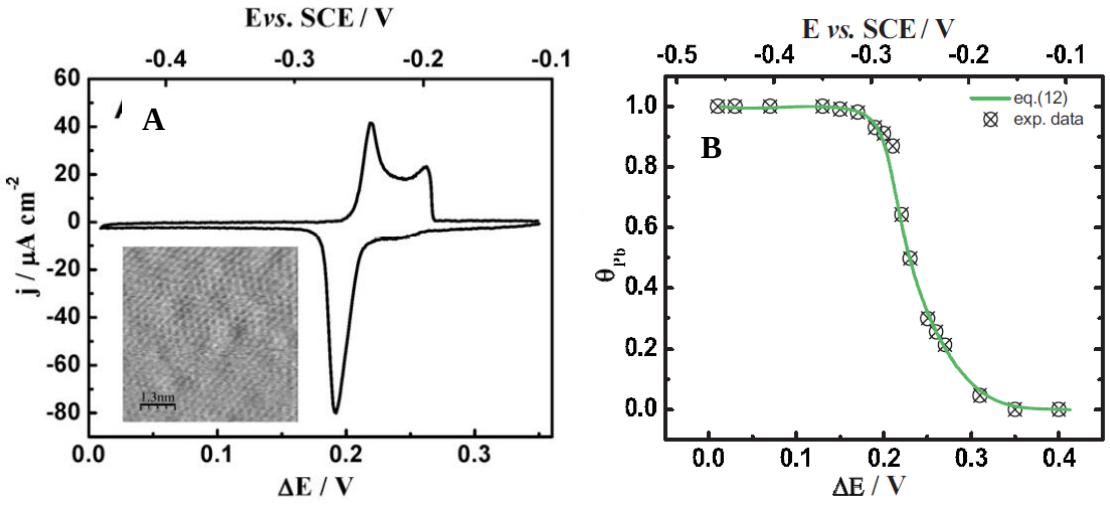

Figure 1-4. (A) Cyclic voltammograms for Pb UPD on Au (111), (B) θ vs. ΔE dependence for Pb UPD on Au (111) estimated from charge stripping experiments.

As Brankovic and Zangari (2015) mentioned, having stronger attractive interactions between the depositing metal and the substrate than the M-M, S-S bonds causes the UPD process. Kolb et al. (1974) conducted the first systematical study a with large set of M-S couples to define what M-S pairs would exhibit UPD and used these data to develop a model to correlate the underpotential shift ΔE_{UPD} to the work functions of M and S as

$$\Delta E_{UPD} = \alpha(\Phi_S - \Phi_M) \qquad \alpha = 0.5\,\text{V/eV}. \tag{1-6}$$

Sudha et al. (2005) generalized this model to take consideration of the effect of the electrolyte environment on UPD. A Born-Haber cycle was set up to decompose the UPD process in its fundemantal steps and along these lines create an expression relating ΔE_{UPD} to the thermodynamic quantities involved in such steps; the resulting expression is more rigorous, however, includes various parameters that cannot be promptly determined.

Various analytical models of adsorption isotherm (θ vs. E) were offered to interpret UPD process. Langmuir (Engelsmann et al., 1980; Schmidt et al., 1966), Temkin (Adzic et al., 1974), and Frumkin (Bewick and Thomas, 1977) isotherms have been used to explain the UPD monolayer/monolayers (ML/MLs) underpotential-coverage dependence (ΔE vs. θ, Figure 1-4B). Mostly, the attractive forces between the UPD metal and the substrate and repulsive interactions among the adatoms define this relationship. Moreover, the effect of strain because of the lattice mismatch between the substrate and the UPD layer, anion co-adsorption and the double layer effects are all found to be important for a complete understanding of this relation. When the UPD process

represents a single energy state, and its electrosoption valence is equal to the oxidation state of metal ions in the solution, Swathirajan and Bruckenstein (1983) described the underpotential-coverage dependence as

$$\Delta E = \Delta E^{0}_{\theta \to 0} - \frac{RT}{mF}\left[\ln\left(\frac{\theta}{1-\theta} \right) + f\theta + g\theta^{3/2} \right]. \quad (1\text{-}7)$$

The equation above will be called as *Bruckenstein-Swathirajan (BS) isotherm* in the future text. Here, θ refers to monolayer coverage, and $\Delta E^{0}_{\theta \to 0}$ represents the underpotential (equilibrium potential) of the most positive stripping peak of the UPD adlayer where UPD ML coverage approaches to zero.

The isotherm has a Langmuir basis and implies additivity of the various UPD adatom-substrate and adatom-adatom interactions. The term "*f*" refers to the Temkin parameter and takes consideration of the UPD layer-substrate interactions such as the electrode work function change with the UPD adlayer coverage. The term "*g*", on the other hand, refers to the Frumkin parameter which represents the lateral adatom interactions within the UPD adlayer (Swathirajan and Bruckenstein, 1983), and m is the oxidation state of the UPD metal. The BS isotherm fits to θ vs. ΔE data for Pb UPD on Au (111) discussed previously are shown as the full line in Figure 1-4B (Gokcen et al., 2011).

1.5. Surface-Limited Redox Replacement Reaction

Deposition of noble metal MLs as catalyst materials via surface-limited redox replacement (SLRR) reaction (metal deposition by galvanic displacement of UPD

monolayer) method is developed by Brankovic et al. (2001; see also Brankovic 2009; Gokcen et al., 2011). This approach/method has found extensive application in the synthesis of noble metal monolayers and catalyst materials (Brussel et al., 2003; Zhang et al., 2005). The SLRR method refers to a spontaneous irreversible surface controlled redox reaction and has been used in the synthesis of catalyst monolayers, functional surfaces, and nanostructures (Gokcen, 2010: 44). Figure 1-5 (Figure from Brankovic, 2009) illustrates basic steps of the SLRR deposition protocol. Here, redox replacement of UPD monolayer is initialized with the formation of UPD monolayer of the metal *M* on the *S(h,k,l)* substrate (Figure 1-5A and 1-5B). In general, the protocol is not limited only to formation of UPD metal layers but it could involve hydrogen UPD as well (Nutariya, 2013), or formation of other adlayers through adsorption processes involving charge transfer. The formed monolayer of metal M serves as a sacrificial material to allow deposition of a more noble metal *P*. After obtaining the required UPD monolayer coverage of the metal *M*, process is completed by immersion of the crystal in a more noble metal solution where the sacrificial less noble UPD metal layer is displaced by the more noble metal P^{p+} ions at the open circuit potential (OCP) (Brankovic, 2009). Another way could be to use a solution which contains both ions involved in the SLRR reaction in this step. In this way, "*one cell, one solution*" configuration will simplify the process (Fayette et al., 2011).

As Brankovic and Zangari (2015) mentioned in their study, a multilayer structure consisting of homoepitaxial or heteroepitaxial monoatomic layers can be achieved when the sequence in Figure 1-5 is repeated an arbitrary number of times (Vasilic et al., 2006). An experimental apparatus for *Electrochemical Atomic Layer Epitaxy* (ECALE) is

implemented by Stickney et al. (2002) to automate the film growth using this protocol (Huang et al., 1995). An additional variation of the SLRR protocol for thin film growth applications was reported recently (Fayette et al., 2011) which includes a SLRR step at open circuit potential, Figure 1-5C, and a short potential pulse resulting in the co-deposition of *P* and a UPD layer of *M* metal or hydrogen on the substrate surface. This leads to "*one cell, one solution*" concept which will provide a significant advantage for the applications where thicker films are needed with less stringent demand for purity (Fayette et al., 2011).

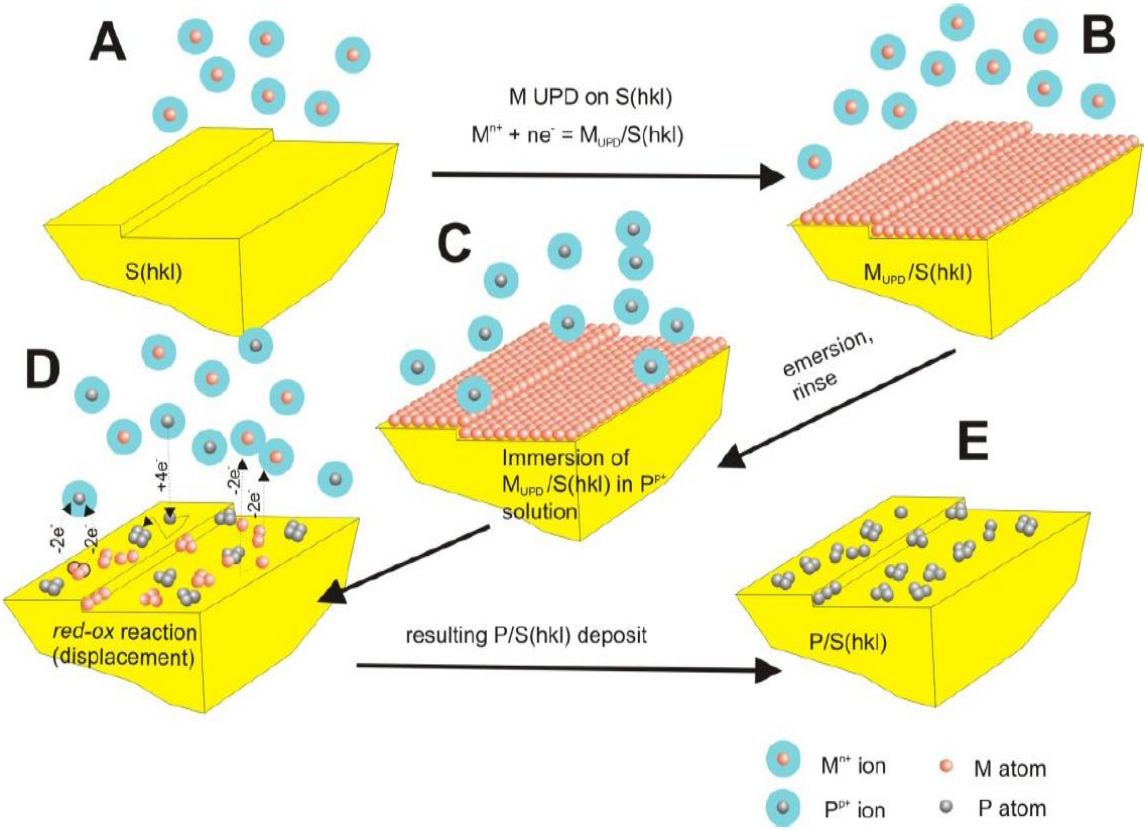

Figure 1-5. SLRR protocol of the *M* UPD monolayer by a more noble P metal on *S(h,k,l)*. (A-B): *M* UPD ML on *S(h,k,l)*, (B-C): Immersion of the crystal into P^{p+} solution, (C-D): SLRR reaction at OCP, (E): *P*/*S(h,k,l)* deposit.

1.5.1. Stoichiometry of SLRR Reactions and Deposition Process

With UPD process, it is possible to control layer coverage down to a fraction of a monolayer precisely. Therefore, deposition of metal *P* via SLRR of a UPD layer can be obtained with the same accuracy. This significant aspect introduces an array of new areas of application in catalyst monolayer design and synthesis. The amount of deposited metal *P* is controlled by reaction stoichiometry, structure and coverage of the UPD layer of metal *M* (Gokcen et al., 2011).

Coverage is controlled by the reaction stoichiometry of the redox replacement reaction whose general formulation is described by Brankovic (2009) as

$$\left(\theta_M \cdot \rho_M^{UPD}\right) \cdot M_{UPD}^{0} / S(h,k,l) + \left(\theta_M \cdot \rho_M^{UPD}\right) \cdot \left(\frac{m}{p}\right) P_{solv}^{p+} \Rightarrow \left(\theta_M \cdot \rho_M^{UPD}\right) \cdot M_{solv}^{m+} + \left(\theta_M \cdot \rho_M^{UPD}\right) \cdot \left(\frac{m}{p}\right) P_s^{0} / S(h,k,l) . \quad (1\text{-}8)$$

In this equation, m and p are the oxidation states of UPD metal M and the more noble metal P respectively. The factors , θ_M, and ρ_M^{UPD} are introduced in order to be able to express the amount of deposited metal P in ML units with respect to atomic areal density of the substrate *S(h,k,l)* (Brankovic, 2009). Here, θ_M, refers to the UPD ML coverage, and ρ_M^{UPD} is the packing density of M atoms in complete UPD ML with respect to the areal density of substrate *S(h,k,l)*. The subscript s indicates the deposition phase while the subscript solv refers to the solution phase. The coverage of the more noble metal *P* is controlled by the coverage of the UPD metal *M* (Brankovic, 2009).

Assuming that metal *P* forms a 2D, atomically thick deposit, from the above expression, the coverage of the deposited metal *P* with respect to the substrate can be

deduced. It can be expressed in terms of the M UPD layer coverage, its packing density and *m*/*p* ratio as (Gokcen et al., 2010)

$$\theta_P = \theta_0 + \theta_M \cdot \rho_M^{UPD}\left(\frac{m}{p}\right). \tag{1-9}$$

In this equation, the term θ_0 is takes the responsibility to accommodate the possibility that deposition of *P* may also occur via other processes, unrelated to the SLRR reaction (Gokcen et al., 2010; Brankovic and Zangari, 2015). This term could also describe the situation in which a pre-existing *P* layer was present on the substrate S before deposition via a SLRR reaction (Brankovic and Zangari, 2015).

Surface area characterization techniques, such as temperature programmed desorption or electrochemical adsorption (Fayette et al., 2011) can be used to determine the coverage and morphology of the deposited metal *P*. STM or AFM are also other alternative methods to be used (Gokcen et al., 2010; 2011; 2012). The overall stoichiometry of the SLRR reaction and deposition process also depends on specific experimental conditions favoring a certain oxidation state of the metal constituting the UPD layer. An example of this is shown in Figure 1-6 from Gokcen et al.'s (2010) study which shows Pt deposit coverage as a function of the Cu UPD layer coverage in SLRR reaction. Here, the reaction solution is 10^{-3} M $\{PtCl_6\}^{2-}$ + 0.1 M $HClO_4$. For $\rho_{Cu2x2}^{UPD} = 0.75$ the measured slope in θ_{Pt} vs. θ_{Cu} data is ≈0.19 indicating that *m*=1 instead of 2 as one would typically assume (Cu^+ vs. Cu^{2+}). SLRR reaction stoichiometry is $4Cu_{UPD}^0 + \{PtCl_6\}_{solv.}^{2-} + 2Cl^- \Rightarrow 4\{CuCl_2\}_{solv.}^- + Pt_s^0$ with *m*/*p*=0.25. The *m*=1 stoichiometric coefficient is the consequence of specific experimental conditions where the oxidation of

Cu UPD adatoms to Cu^{+} ions is thermodynamically more favorable than their oxidation to Cu^{2+}. The direct ligand transfer from depositing $\{PtCl_6\}^{2-}$ ions to dissolving Cu ions stabilizes the anionic species $\{CuCl_2\}^{-}$ where Cu has the 1+ oxidation state (Gokcen et al., 2010). This situation can be applied to most of the experimental studies where the supporting electrolyte contains anions having no complexing affinity towards UPD metal (Cu for example), such as a perchlorate based solution (Gokcen et al., 2010). This example stresses the general importance of the complexing anions in reaction solution for the overall stoichiometry of metal deposition *via* SLRR of UPD layers.

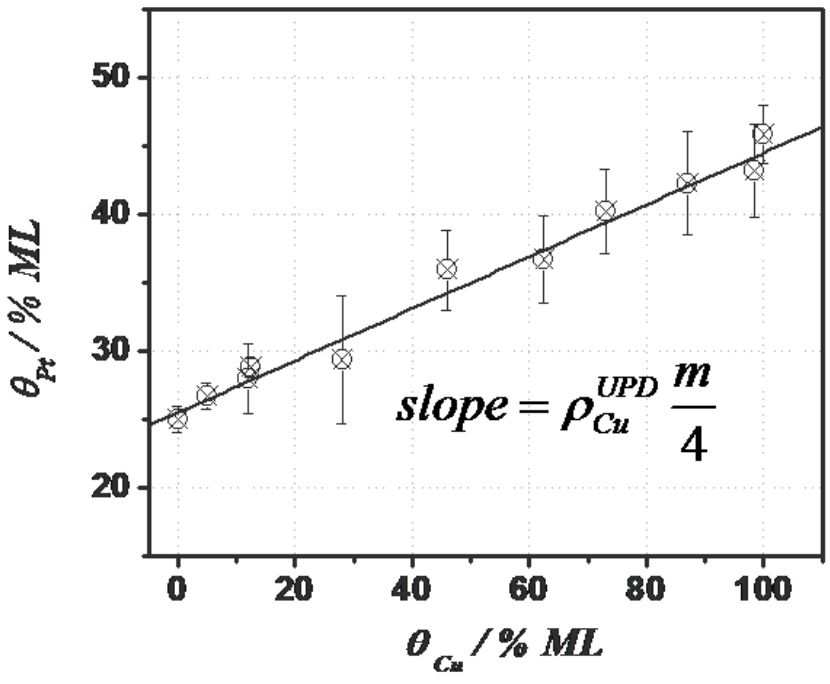

Figure 1-6. Data showing the dependence of Pt submonolayer coverage vs. coverage of Cu UPD monolayer on Au (111). The solid line in the graph represents the fit of the data using Eq. (1-9).

1.5.2. Driving Force for SLRR Reaction and Nucleation Rate of Depositing Metal

The electrochemical driving force for the SLRR reaction between the metal P and the M UPD layer is given by the difference between the equilibrium potential of metal *P* and that of the M UPD metal layer when its coverage approaches zero, $\theta_{UPD} \rightarrow 0$, (Brankovic et al., 2001; Brankovic and Zangari, 2015) (Figure 1-4A). This condition is defined as

$$\Delta E_{red-ox} = \Delta E^0_{EMF} - \Delta E^0_{\theta \rightarrow 0} - \frac{RT}{F}[\ln \frac{[a_{M^{n+}}]^n}{[a_{P^{p+}}]^p} > 0. \qquad (1\text{-}10)$$

In the equation above, ΔE^0_{EMF} represents the electromotive force defined as potential difference between the equilibrium potentials of *M* and *P* metals at standard conditions. The term, $\Delta E^0_{\theta \rightarrow 0}$, refers to the equilibrium potential of $M_{UPD}/S(h,k,l)$ where there is no UPD coverage ($\theta_{UPD} \rightarrow 0$) at standard conditions ($a_{M^{n+}} = 1, a_{P^{p+}} = 1$). Using different combination of the $M_{UPD}/S(h,k,l)$ and P^{p+} ions in the red-ox reaction will result different morphology and amount of *P* deposition (Brankovic, 2009). The departure from standard conditions is being described by the logarithmic term in the equation. Figure 1-7 (Figure from Brankovic and Zangari, 2015) shows the relation between the thermodynamic quantities discussed in the above equations which are graphically depicted (Brankovic and Zangari, 2015). The terms from Eq. (1-10) are identified in the Figure 1-7, and current–potential dependence for bulk *M* metal electrode and UPD of *M* on substrate *S* is represented with the gray lines while the current–potential dependence for bulk *P* noble metal electrode is illustrated with the dark line.

A close look to the equation above shows that the driving force for red-ox reaction can be modified by changing the activities of M^{m+} and P^{p+} ions in the reaction solution. The logarithmic term contributes notably to the value of $\Delta E_{red\text{-}ox}$ when there are no M^{m+} ions in reaction electrolyte. This means that under these experimental conditions, an extremely high nucleation overpotential can be achieved. As a result of this, a high nucleation rate and small size of stable P metal nuclei on the substrate surface will be obtained. This is illustrated by examples of the thermodynamic driving force and nucleation rate dependence on the ratios between the activity P^{p+} and M^{m+} ions in solution in Figure 1-8 (Figure from Brankovic and Zangari, 2015). Estimates in the figure are made for Pt deposition via SLRR of Cu UPD layer. Black line represents $2Cu^0_{UPD} + \{PtCl_6\}^{2-} = Pt^0 + 2Cu^{2+} + 6Cl^-$, and red line represents $4Cu^0_{UPD} + \{PtCl_6\}^{2-} + 2Cl^- = 4\{CuCl_2\}^- + Pt^0$ (Figure 1-8A and 1-8B). This dependence is calculated using parameters valid for Pt deposition on Au (111) via SLRR of a Cu UPD layer, (Figure 1-8A). There are two possible scenarios, both having a Pt(IV) salt ($\{PtCl_6\}^{2-}$ ion) in solution. In the first scenario, the oxidation state of Cu is 2+ (H_2SO_4 based reaction solution, m/p=0.5, $\Delta E^0_{EMF} - \Delta E^0_{\theta\to 0} \approx 0.1$ V). In the second case, the Cu oxidation state of 1+ ($HClO_4$ based reaction solution, m/p=0.25, $\Delta E^0_{EMF} - \Delta E^0_{\theta\to 0} \approx 0.2$ V). As presented in Figure 1-8A, the driving force for SLRR reaction, $\Delta E_{red\text{-}ox}$ is larger in the case of m/p=0.5 for $a_{Cu^{m+}} / a_{Pt^{4+}} < 0.1$. Indeed, it is apparent that the stoichiometry coefficient ratio has a large effect on $\Delta E_{red\text{-}ox}$. For example, an almost 0.4 V larger $\Delta E_{red\text{-}ox}$ is available for the SLRR reaction when m/p=0.5 than in the case of m/p=0.25 ($a_{Cu^{m+}} / a_{Pt^{4+}} = 5x10^{-6}$ and $a_{Pt^{4+}} = 0.01$). The dilution of Cu ions in the reaction solution and consequent decreasing value of their activity has a strong effect on $\Delta E_{red\text{-}ox}$. This is evident in particular for SLRR reactions

with larger *m*/*p* ratio, Figure 1-8A. In this case, for ultimately small values of $a_{Cu^{m+}} / a_{Pt^{4+}}$ mimicking the situation when no UPD metal ions are present in reaction solution ($a_{Cu^{m+}} / a_{Pt^{4+}} < 10^{-7}$), one can achieve a rather large nucleation overpotential, ($\Delta E_{red\text{-}ox} > 0.5$ V), but the value of $\Delta E_{red\text{-}ox}$ decreases due to the dilution of Pt ions in reaction solution and a lower value of their activity. This trend is stronger for SLRR reaction with smaller *m*/*p* ratio (Brankovic and Zangari, 2015).

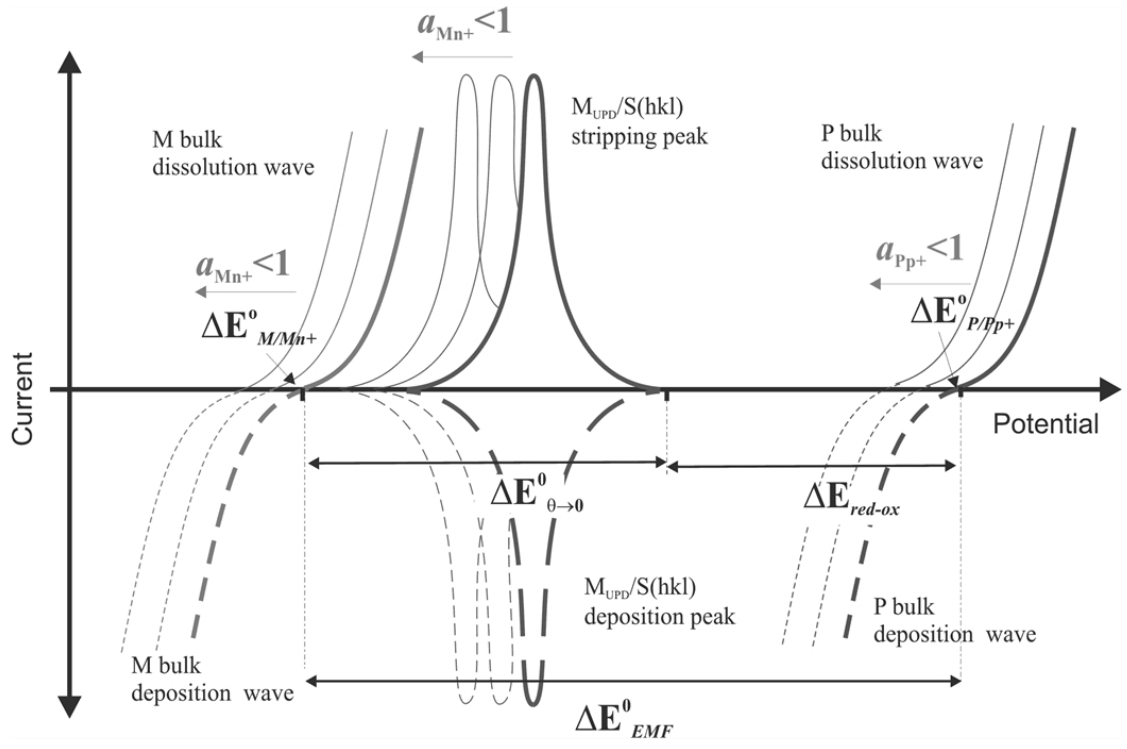

Figure 1-7. Schematics of the thermodynamic quantities determining $\Delta E_{red\text{-}ox}$ for a SLRR reaction and their mutual relation.

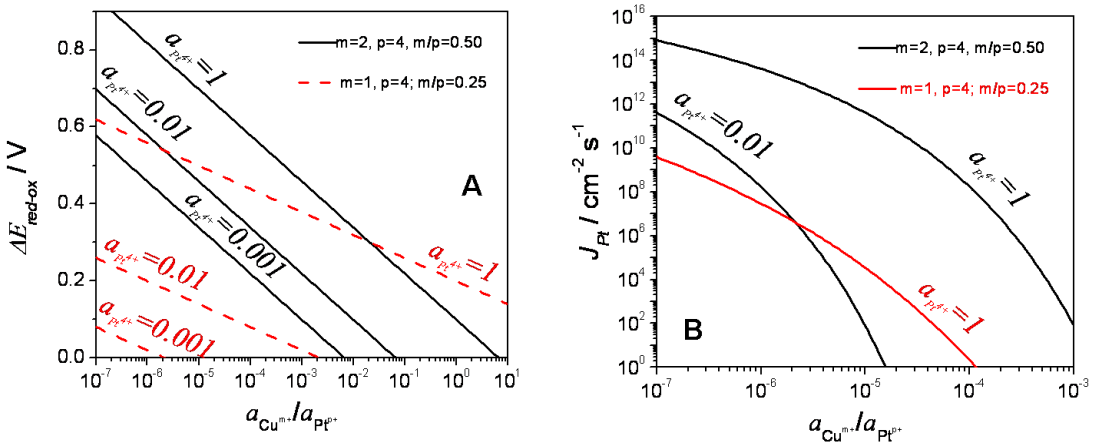

Figure 1-8. (A) Estimate of *ΔEred-ox vs.* $a_{Cu^{m+}} / a_{Pt^{4+}}$ ratio, (B) Nucleation rate vs. $a_{Cu^{m+}} / a_{Pt^{4+}}$ ratio.

To have a control on metal deposit morphology, the influence of the driving force for the SLRR reaction is very significant. The nucleation rate for Pt on Au (111) achieved during deposition via SLRR of a Cu UPD layer can be estimated roughly by classical nucleation theory (Markov, 1995). Brankovic and Zangari (2015) displayed the nucleation rate estimates as a function of $a_{Cu^{m+}} / a_{Pt^{4+}}$ ratio in Figure 1-8B for the two cases they investigated. It is discussed that the nucleation rate in both cases is very sensitive to the $a_{Cu^{m+}} / a_{Pt^{4+}}$ ratio and this is particularly important if $a_{Cu^{m+}} / a_{Pt^{4+}} > 10^{-5}$, corresponding to experimental conditions commonly reported in the literature, where this deposition protocol is used for catalyst monolayer synthesis (Adzic et al., 2007; Brankovic and Zangari, 2015). A tenfold variation in the $a_{Cu^{m+}} / a_{Pt^{4+}}$ ratio produces approximately 10^3-10^5 times change in nucleation rate.

Brankovic and Zangari (2015) also emphasized that the nucleation rate can quickly drop to values which are practically negligible if the $a_{Cu^{m+}} / a_{Pt^{4+}}$ ratio falls above about 10^{-4}. Brankovic and Zangari (2015) explained that the conditions during SLRR reaction favoring small nucleation rates will produce a Pt deposit which is not uniformly distributed over the Au (substrate) surface. Instead, the Pt deposit would preferentially nucleate at defect sites. This is an undesirable morphology if catalyst monolayer synthesis is sought for. The calculations in Figure 1-8B should be of general guidance for practitioners who are using this protocol for Pt monolayer catalyst design. One can see that a SLRR reaction with *m*/*p* ratio of 0.5 yields several order of magnitude higher nucleation rates at a given Cu and Pt activity ratio. This is a quite important fact which should be appreciated if one is after the control of Pt deposit morphology in terms of Pt cluster size and size distribution. In general, it can be concluded that SLRR reactions with larger *m*/*p* ratio will result in smaller average size of stable nuclei and thus a metal deposit consisting of smaller clusters.

The amount and coverage of metal deposit depend on the nature of M^{m+} and P^{p+} ions and on the UPD system adopted for the SLRR reaction. Brankovic and Zangari (2015) showed this in Figure 1-9 (Figure from Brankovic, 2009 and Brankovic, forthcoming) using the example of Pt deposition via SLRR of a Cu UPD layer on Au (111) (Figure 1-9A and 1-9C), and Pb UPD layer on a Cu UPD layer covered Au (111) (Figure 1-9B) in 0. 1 M H_2SO_4 based reaction solution. Here, $\theta_{Pt}\approx 0.5$ in Figure 1-9A, $\theta_{Pt}>0.6$ in Figure 1-9B, and $\theta_{Pt}\approx 0.42$ in Figure 1-9C.The deposit morphology varies from Pt monolayer continuous film to 2D mono-atomically high nanoclusters with very narrow size distribution and various coverage of the substrate (Brankovic and Zangari, 2015).

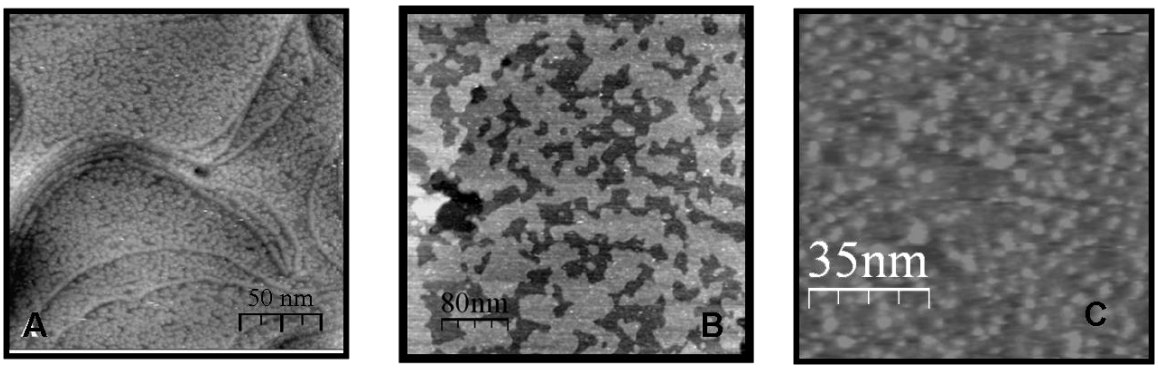

Figure 1-9. (A) Pt submonolayer on Au (111) by SLRR of Cu UPD layer, **(**B**)** Pt continuous submonolayer on Au (111) by SLRR of Pb/Cu UPD bi-layer, (C) Pt submonolayer on Au (111) by SLRR of Cu UPD layer.

Brankovic and Zangari (2015) pointed out the spatially uniform coverage of Pt nanoclusters on Au (111) in Figure 1-9A (Brankovic et al., 2009), and 1-9C. This shows that the nucleation process is independent of the availability of thermodynamically favorable nucleation sites such as surface defects. The Pt nanoclusters are uniformly distributed across the surface regardless of the presence of surface steps, where preferential nucleation and growth is typically observed during electrodeposition processes (Brankovic et al., 2009). This represents one of the major advantages of this deposition protocol over the traditionally used ones for catalyst synthesis application. The Pt nanoclusters are slightly smaller in Figure 1-9A than in Figure 1-9C, (3 nm vs. 4 nm) even though stoichiometry of SLRR produces Pt deposits with larger coverage in Figure 1-9A than in Figure 1-9C. This observation was in agreement with their previous discussion regarding the effect of SLRR stoichiometry coefficients on nucleation rate, i.e., SLRR reactions with higher m/p ratio yield higher nucleation rates and smaller stable nuclei. This is illustrated in Figure 1-9 (m/p=0.5 in Figure 1-9A, m_{Pb}/p = 0.5, m_{Cu}/p = 0.25 in Figure 1-9B, and m/p= 0.25 in Figure 1-9C) to demonstrate that manipulation of

the experimental conditions for SLRR reactions gives the opportunity to design and synthesize catalyst monolayers with different morphology, cluster size and coverage (Gokcen et al., 2012; Brussel et al., 2003; Kim et al., 2006; Brankovic, 2015; Brankovic, forthcoming).

1.6. Reaction Kinetics of Surface Limited Redox Replacement

Deposition protocol based on SLRR of UPD layers has gained lots of interest in the catalysis community due to the opportunities and challenges it provides (Brussel et al., 2003; Kowal et al., 2009). To achieve a success in the applications of this protocol, it is very important to understand the kinetics of metal deposition *via* SLRR reaction. A properly defined functional relation between experimental conditions and resulting reaction kinetics enables facile scale up of this deposition protocol to the level where the reaction volume and amount of synthesized catalyst material become adequate for industrial application (Brankovic and Zangari, 2015).

Gokcen et al. (2011) developed a phenomenological model describing the change in coverage of the UPD metal during the course of a deposition experiment to investigate the kinetics of metal deposition *via* SLRR reaction. The phenomenological description of the OCP transients during deposition *via* SLRR of UPD metal is an indirect way to achieve this. When a representative adsorption isotherm for the UPD metal-substrate system participating in the SLRR reaction is known (E *vs.* θ_{UPD}, Eq. (1-8)), the analytical model of the potential *vs*. time dependence during SLRR (E *vs.* t) is easily obtained by combining the appropriate expression for the rate equation (Smith, 1970) with representative UPD adsorption isotherm model. Thus, such E *vs.* t model can be used to

fit OCP transients from deposition experiments providing a direct way to study kinetics of metal deposition *via* SLRR of a UPD layer. In this way it is possible to quantify the effect of various experimental parameters on the resulting kinetic of the deposition process (Gokcen et al., 2011).

The analytical model developed by Gokcen et al. (2011) presents the appropriate theoretical framework to study and to measure the kinetics of metal deposition *via* SLRR reaction. Their results and analysis showed that kinetics of Pt deposition *via* SLRR reaction is the direct function of the nature of the UPD metal ML. Their comparative analysis between the deposition experiments with Pb_{UPD}/Au (111) and Cu_{UPD}/Au (111) in 0.1 M H_2SO_4 electrolyte indicates faster deposition kinetics with SLRR where the UPD metal has lower work function (Pb). On the other hand, Gokcen et al. (2011) also declared that the nature of the anions in the supporting electrolyte also has a significant effect and showed that the observed trend between the kinetics of Pt deposition *via* SLRR of these two UPD MLs can be reversed when the Cl^- is the only complexing anion in the supporting electrolyte for UPD metal adatoms. The choice of supporting electrolyte has a significant impact on the kinetics of the Pt deposition for Pb_{UPD}/Au (111) while the effect is modest for Cu_{UPD}/Au (111). Gokcen et al. (2011) explained that the choice of the supporting electrolyte and anions in the reaction solution together with the nature of the UPD metal determine the overall kinetics of Pt deposition *via* SLRR reaction and indicated that the concentration of depositing ions ($\{PtCl_6\}^{2-}$) in the reaction solution has the direct effect on the observed kinetics of the deposition reaction. The faster kinetics of deposition procedure *via* SLRR and transport limited redox replacement (TLRR) reaction are achieved with higher concentration of depositing ions contributing to a successful and

simple way to accomplish the optimum metal (Pt) deposition rate depending on the desired deposit morphology and its application. In their study, the quantification of the kinetics parameters for metal deposition *via* SLRR and TLRR of UPD ML using the developed theoretical framework provided the reaction half time and to further sophisticate the experimental design where the precise control of deposition flux, or manipulation of nucleation kinetics is required (Gokcen et al., 2011). Gokcen et al. (2011) emphasized that their work and conclusions apply only if the single replacement reaction is involved in deposition process and thus the considered UPD/substrate system is not changing overt the time. Gokcen et al. (2011) stated that in the case that the deposition *via* SLRR of UPD ML is considered for thin film growth which involves many consecutive steps of SLRR of UPD MLs the change of the parameters defining the deposition kinetics could be expected due to the gradual change of the UPD/substrate system. Gokcen et al.'s (2011) study improved understanding of the optimum experimental conditions for metal deposition *via* SLRR of UPD ML and helped the future applications of this method for monolayer catalyst design in situations where higher level of process control is required (Gokcen et al., 2011).

In the case of zero order reaction kinetics (N=0) in terms of θ_{UPD} (deposition via transport limited redox replacement, (TLRR) of UPD layer), the E vs. t model which can be used to fit OCP data from deposition experiments has the form (Gokcen et al., 2011)

$$E = E_{\theta\to 0} - \frac{RT}{mF}\cdot\left[\ln\left(\frac{1-k_0 t}{k_0 t}\right) + f\cdot(1-k_0 t) + g\cdot(1-k_0 t)^{3/2}\right]. \qquad (1\text{-}11)$$

In this equation, *t* refers to the reaction time, and k_0 is the TLRR reaction rate constant. The other terms are defined previously. The k_0 is defined as (Gokcen et al., 2011)

$$k_0 = \left(\frac{m}{p}\right) \cdot \frac{D_{P^{p+}} \cdot C^{\infty}_{P^{p+}}}{\Gamma_i^{UPD} \cdot \delta} . \tag{1-12}$$

Here $D_{P^{p+}}$ and δ represent the diffusion coefficient of P^{p+} ions, and the thickness of the diffusion layer, respectively. The term $C^{\infty}_{P^{p+}}$ represents the concentration of P^{p+} ions (noble metal-depositing metal) in the bulk solution and Γ_i^{UPD} is the surface concentration of a full and complete UPD layer.

In the case of first order reaction kinetics in terms of θ_{UPD}, *N*=1 (Deposition via SLRR of UPD layer), the *E* vs. *t* model is defined as (Gokcen et al., 2011)

$$E = E_{\theta \to 0} - \frac{RT}{mF}\left[f \cdot e^{(-k't)} + g \cdot e^{(-k't))^{3/2}} - (k't + \ln(1 - e^{(-k't)}))\right] . \tag{1-13}$$

The reaction rate constant, $k^{'}$, has the form (Gokcen et al., 2011)

$$k^{'} = k\left(C_P^{is}\right)^L , \tag{1-14}$$

where *k* represents a fundamental rate constant, C_P^{is} is the concentration of P^{p+} ions at the electrode/solution interface and *L* is the reaction order in terms of P^{p+} ion concentration.

For a N^{th} order reaction kinetics in terms of θ_{UPD}, (Deposition via SLRR of UPD layer, $N \neq 1$), the *E* vs. *t* model has the most general form (Gokcen et al., 2011) and is expressed as

$$E = E_{\theta\to 0} - \frac{RT}{mF}\cdot\left[\ln\left(\frac{(1+Kt)^{1/(1-N)}}{1-(1+Kt)^{1/(1-N)}}\right) + f\cdot(1+Kt)^{1/(1-N)} + g\cdot(1+Kt)^{3/(2-2N)}\right]. \quad (1\text{-}15)$$

In this case, the reaction rate constant, *K*, is defined as (Gokcen et al., 2011)

$$K = (N-1)\cdot k\cdot\left(C_P^{is}\right)^L\cdot(\Gamma_i^{UPD})^{N-1}. \quad (1\text{-}16)$$

An example of OCP transients of Pt deposition *via* SLRR of Pb UPD and Cu UPD layers on Au (111) in 0.1 M H_2SO_4 based solutions is shown in Figure 1-10A. Under these conditions, Pb and Cu oxidation state is 2+ which results in *m*=2 in both experiments. In this experiment, Pt is deposited from a hexachloroplatinate complex ($\{PtCl_6\}^{2-}$) i.e., *p*=4. Brankovic and Zangari (2015) stated that from the above stoichiometry coefficients it follows that two UPD adatoms (Pb or Cu) react with one Pt ion and explained the reactions and kinetics as it follows. These reactions are elementary ones, and the reaction order in terms of UPD metal adatom concentration/coverage can be obtained from the reaction stoichiometry as *N*=2, i.e., 2nd order (Smith 1970). The second order reaction kinetics for these UPD systems should be understood as a result of the cooperative involvement of more than one Cu UPD adatom during the red-ox process (Gokcen et al., 2011). In the most general case, regardless of the m/p ratio, whenever more than one UPD adatom is necessary for the reduction of the depositing metal ion, the reaction order in terms of the UPD metal coverage should be taken as 2 (*N*=2) (Brankovic and Zangari, 2015). In Figure 1-10, black lines represent the fits of the model, Eq. (1-15), to OCP data.

The values of the rate constants obtained from fitting for each reaction show that Pt deposition *via* SLRR of Pb UPD is approximately two times faster than Pt deposition

via SLRR of Cu UPD layer (Brankovic and Zangari, 2015). At constant temperature, the faster reaction kinetics suggests a lower activation energy for the activated complex (Smith, 1970). In their study, Brankovic and Zangari (2015) stated that this means lower activation energy for the activated complex of $\{PtCl_6\}^{2-}$ - Pb UPD adatom as compared to the activated complex of $\{PtCl_6\}^{2-}$ - Cu UPD adatom. The activated complex represents the entity with sufficient overall energy allowing direct electron transfer from the UPD adatom on one side to $\{PtCl_6\}^{2-}$ ion on the other. Brankovic and Zangari (2015) explained the relationship between kinetic, activation energy, and work function in their study as following. It is stated that the difference in kinetics and activation energies of these two deposition reactions must reflect the difference in bringing the Pb and Cu UPD adatoms to the activated state where the electron transfer to $\{PtCl_6\}^{2-}$ ion is possible. Since there is no significant difference in stability of Pb and Cu ions in 0.1 M H_2SO_4 electrolyte (Pauling, 1970), it is physically reasonable to expect that Pb as the UPD metal with lower work function would be more easily activated than the Cu UPD adatom. Whenever the two SLRR reactions of two UPD metals are compared in a supporting electrolyte that does not promote significantly the energetic of the UPD adatom dissolution of either one, the UPD metal with lower work functions should yield the faster reaction kinetics (Gokcen et al., 2011).

Gokcen et al. (2011) illustrated the OCP transients from the Pt deposition *via* SLRR of Pb UPD and Cu UPD on Au (111) in solution containing 10^{-3} M $\{PtCl_6\}^{2-}$ + 0.1 M $HClO_4$ in Figure 1-10B. Here, for SLRR reaction involving the Pb UPD, m=2, p=4 and the value of the rate constant K is significantly smaller than in a 0.1 M H_2SO_4 supporting electrolyte (K =0.87 [s^{-1}], for 0.1 M $HClO_4$ *vs.* K=9.7 [s^{-1}] for 0.1 H_2SO_4).

Brankovic and Zangari (2015) explained that the reason is that Pt deposition *via* SLRR of a Pb UPD layer depends strongly on the nature of the anion in the supporting electrolyte meaning the rate of Pt deposition *via* SLRR of a Pb UPD layer can be altered (increased/decreased) by appropriate choice of the supporting electrolyte. As it is stated, the basic difference between $\{SO_4\}^{2-}$ and $\{ClO_4\}^{-}$ anions in supporting electrolytes is that the $\{SO_4\}^{2-}$ is a relatively strong ligand, while $\{ClO_4\}^{-}$ has no complexing affinity towards metal ions (Pauling, 1970). For this reason, the metal (Pb) dissolution/oxidation process during the SLRR reaction in $\{SO_4\}^{2-}$ based electrolyte is significantly promoted due to a higher stability of the Pb ions in this electrolyte (Brankovic and Zangari, 2015). For Pt deposition *via* SLRR of Cu UPD in 0.1 M $HClO_4$ reaction solution, the $\{ClO_4\}^{-}$ does not complex Cu^{2+}. The ligands in the $\{PtCl_6\}^{2-}$ complex are Cl^{-} ions and they have a major effect on the final oxidation state of dissolved Cu. In this case, in parallel with the charge transfer process between the depositing metal complex and the Cu UPD adatoms, a simultaneous ligand transfer also occurs (Gokcen et al., 2010). The final oxidation state of Cu is determined by formation of the most stable Cu complex with ligands originating from the depositing metal complex ($\{PtCl_6\}^{2-}$). The presence of the residual chlorides in 0.1 M $HClO_4$ and Cl^{-} ions liberated after reduction of $\{PtCl_6\}^{2-}$ lead to the thermodynamically favorable path for Cu UPD adatoms dissolution into $\{CuCl_2\}^{-}$ ions with Cu oxidation state of 1+ rendering m=1. When they compared the extracted values of the rate constants, it is seen that the rate constants for SLRR of Cu UPD is slightly smaller than in the rate constant of 0.1 M H_2SO_4 electrolyte (≈10%). As a result, these findings show that that switching between sulfate and perchlorate based solutions does

not have a major effect on the Pt deposition rate or SLRR reaction kinetics (Brankovic and Zangari, 2015).

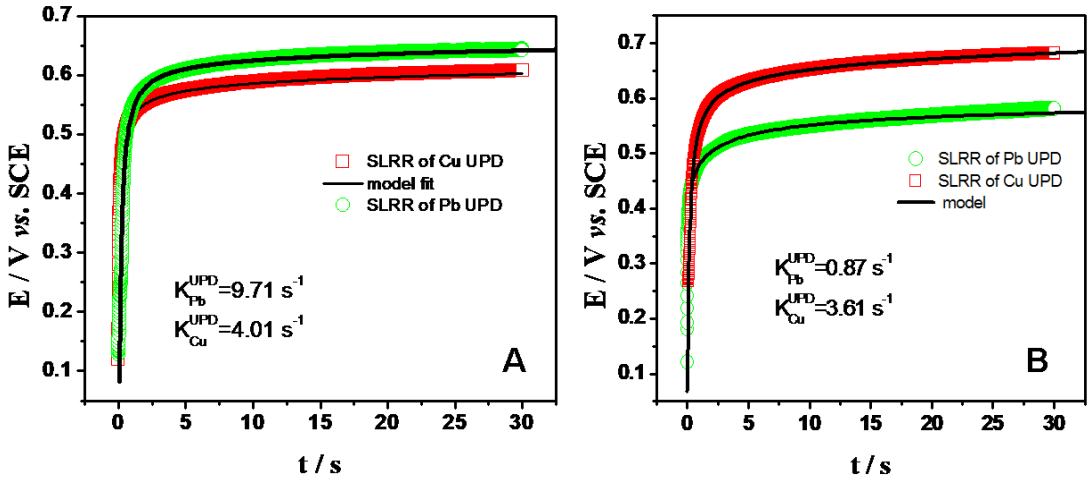

Figure 1-10. OCP transients for Pt deposition *via* SLRR of Pb UPD (green) and Cu UPD (red) on Au (111) with 1000 rpm rotation rate. (A) 10^{-3} M $\{PtCl_6\}^{2-}$ + 0.1 M H_2SO_4, (B) 10^{-3} M $\{PtCl_6\}^{2-}$ + 0.1 M $HClO_4$ solution.

When the rate constants of the SLRR reactions involving Cu UPD and Pb UPD in 0.1 M $HClO_4$ reaction solution are compared, it is expected to have a faster kinetics of SLRR with the Pb UPD system based on the previous argument related to the work function difference between Pb and Cu. On the other hand, Gokcen et al. (2011) obtained the inverse trend from the OCP transient analysis and explained that this was due to the fact that the activation energy of the UPD metal – $\{PtCl_6\}^{2-}$ activated complex is affected significantly by the solution phase i.e., the nature of anions in the supporting electrolyte. The lack of complexing ability of the $\{ClO_4\}^-$ as the dominant anions in the supporting electrolyte towards either Cu or Pb ions leads to the situation where the $\{CuCl_2\}^-$ complex is much more stable than the corresponding Pb ion in perchlorate solution. It is

explained that these results in comparatively lower activation energy for charge transfer between $\{PtCl_6\}^{2-}$ and Cu UPD adatom than between $\{PtCl_6\}^{2-}$ and Pb UPD adatom. Therefore, the faster kinetics for Cu UPD layer is not surprising. As Brankovic and Zangari (2015) stated, the nature of UPD metal in SLRR reaction and the nature of the complexing anions at the electrode/solution interface both have a significant effect on the kinetics of the metal deposition *via* SLRR of UPD layer (Brankovic and Zangari, 2015).

The rate constant of SLRR reaction is directly proportional to the surface concentration of depositing metal ions as Gokcen et al. (2011) showed in Eq. (1-14) and (1-16). The surface concentration of depositing metal ions (Pt ions in their study), $C^{is}_{\{PtCl_6\}^{2-}}$, is proportional to concentration in the bulk solution, $C^{\infty}_{\{PtCl_6\}^{2-}}$ (Gokcen et al., 2011). Thus, for the same SLRR with different $C^{\infty}_{\{PtCl_6\}^{2-}}$, a higher concentration of depositing metal ions, ($\{PtCl_6\}^{2-}$), in the reaction solution will result faster kinetics. The OCP transient for Pt deposition *via* SLRR of Cu UPD in 10^{-5} M $\{PtCl_6\}^{2-}$ + 0.1 M $HClO_4$ solution is illustrated in Figure 1-11A (Gokcen et al., 2011). Here, the $C^{\infty}_{\{PtCl_6\}^{2-}}$ is hundred times smaller than in Figure 1-10B. The rate constant is extracted as K(1.11A)=0.089 [s^{-1}] the model fit (Eq. 1-15) . This K(1-11A) is ≈40 times smaller than in 1-10B, K(1-10B)=3.61 [s^{-1}]). These findings showed how the depositing metal ion concentration in the reaction solution affects the control of the reaction kinetics. Faster SLRR kinetics and a higher metal deposition rate (Pt) are achieved with higher concentration of depositing ions ($\{PtCl_6\}^{2-}$) (Gokcen et al., 2011).

SLRR is being controlled by ion transport, i.e., to metal deposition *via* TLRR, Eq. (1-11) when the concentration of $\{PtCl_6\}^{2-}$ is low in the bulk solution or diffusion layer

thickness is large. Figure 1-11 (Figure from Gokcen et al., 2011)compares Pt deposition with or without rotation in the same electrolyte. In Figure 1-11A, open circuit potential transients for Pt deposition *via* SLRR of Cu UPD layer on Au (111) in 10^{-5} M $\{PtCl_6\}^{2-}$ + 0.1 M $HClO_4$ reaction solution with 1000 rpm rotation rate is displayed while Figure 1-11B shows open circuit potential transients for Pt deposition *via* TLRR of Cu UPD layer on Au (111) in 10^{-5} M $\{PtCl_6\}^{2-}$ + 0.1 M $HClO_4$ without the electrode rotation. Gokcen et al. (2011) showed the model fit Eq. (1-15) and Eq. (1-11) to the experimental data with the black solid lines, and the reaction rate constants extracted from the fits can be seen in each graph. Gokcen et al. (2011) successfully fitted the data set to the model for TLRR reaction (zero order), Eq. (1-11) and achieved a very good fit of the data except for the initial time interval of ~20 seconds. Gokcen et al. (2011) explained that this was due to conditions for transport limited reaction kinetics are not established immediately upon the reaction onset, but after some time, that required for $\{PtCl_6\}^{2-}$ ions to be depleted at the electrode/solution interface, i.e., to reach $C^{is}_{\{PtCl_6\}^{2-}}$ =0 condition. The reaction constant k_0 is extracted from the fitting as 0.0020 [s^{-1}] and also calculated the value of k_0 from the literature data to compare. For m/p = 0.25, $D_{\{PtCl_6\}^{2-}}$ = 7.13×10^{-5} [$cm^2\,s^{-1}$] (Nauma et al., 2005), δ=.05 [cm] (Prentice, 1991), and $\Gamma^{UPD}_{i,Cu}$ of the full Cu UPD layer calculated as the product of areal surface concentration of Au (111) and packing density of Cu UPD layer, $\rho^{UPD}_{Cu\ 2\times2}\times(1.5\times10^{15}/6.023\times10^{23})$, the value of k_0 is $0.0019s^{-1}$, Eq. (1-12). In this respect, it is proved that the extracted value of k_0 from experimental data and calculated value of k_0 agrees perfectly and the model describing the kinetics of TLRR reaction, Eq. (1-11), is sufficiently comprehensive to allow quantitative prediction of the reaction rate

constant when the transport limiting conditions are truly established (Gokcen et al., 2011; Brankovic and Zangari, 2015).

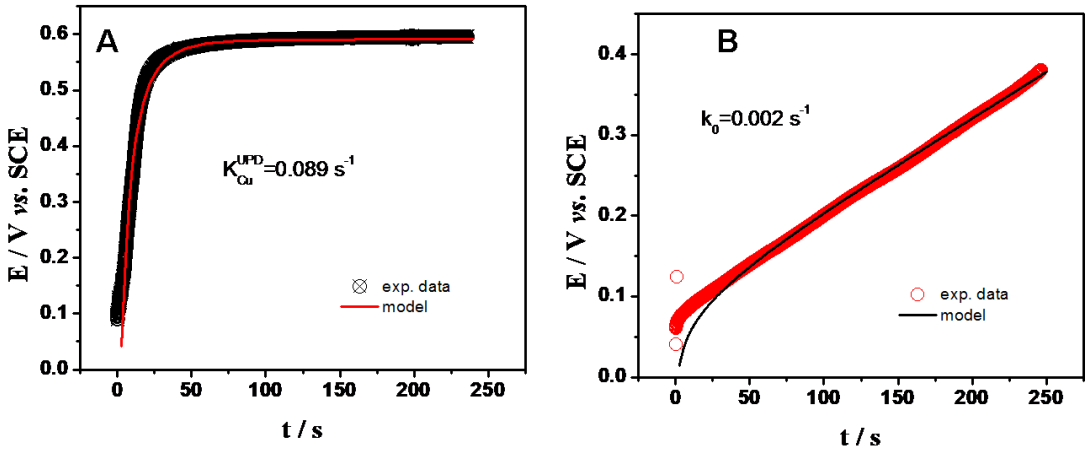

Figure 1-11. Open circuit potential transients for Pt deposition. (A) *via* SLRR of Cu UPD layer on Au (111) with 1000 rpm rotation rate, (B) *via* TLRR of Cu UPD layer on Au (111) without rotation.

Chapter 2: Experimental Techniques

Our approach is to use the surface reflectivity measurements to study reaction kinetics of SLRR. Previous chapter reviewed the literature on UPD and SLRR, and this chapter gives a short overview of some phrases and theoretical aspects of the experimental techniques used in this work such as cyclic voltammetry, chronoamperommetry, and surface reflectivity measurements. Cyclic voltammetry is collected for each UPD experiments and before each SLRR experiments to characterize Au (111) crystal surface. This chapter also reviews the relevant literature on reflectivity in detail paying specific attention to surface reflectivity measurements on electrode/electrolyte interface.

2.1. Surface Reflectivity Measurements

Depending on the physical characteristics of the light and also physical composition and characteristic of the matter, when light interacts with matter, three types of interactions may take place: light reflection, light absorption, and light transition.

The most important quantity in the discussion of surface scattering is the Bidirectional Reflectance Distribution Function (BRDF) which is the reflectance properties of a surface and describes how much light is reflected when light makes contact with a certain material. BRDF is an expression of the physical property of a material which describes the pattern of light reflected from a surface of the material to all directions above the surface, for all directions of incident light. When the light wavelength is ignored, BRDF can be defined as a four-dimensional function. For a

homogeneous surface, the BRDF determines the appearance of materials for different viewing directions (Ke, 1993).

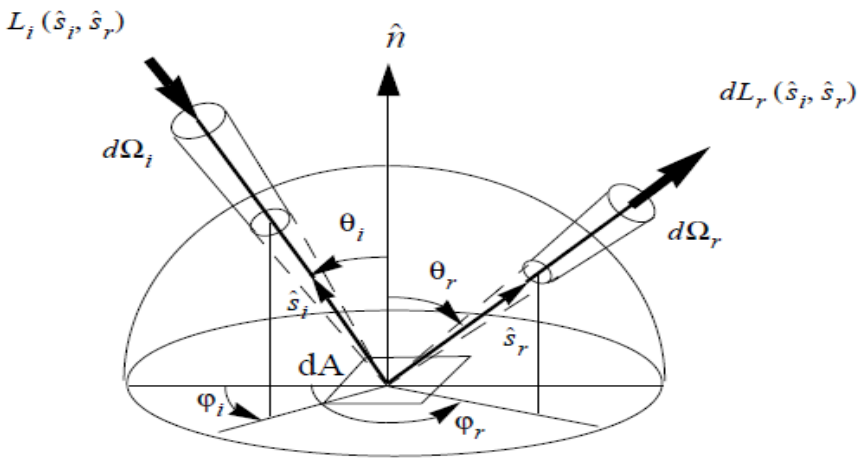

Figure 2-1. The geometry of bidirectional reflection process.

In the Figure 2-1 (Figure from Ke, 1993), a surface is shown illuminated from a direction (θ_i , ϕ_i) by a radiation centered within a solid angle $d\Omega_i$ with reflection in the direction (θ_r , ϕ_r), centered within a cone $d\Omega_r$. Units of the light measurement parameters are summarized in the Table 2-1.

Table 2-1. Units of light measurements.

Symbol	Name	Unit
L_i, L_r	Radiance	$Wm^{-2}sr^{-1}$
E_i, E_r	Irradiance	Wm^{-2}
$L_{\lambda i}$, $L_{\lambda r}$	Spectral radiance	$Wm^{-3}sr^{-1}$
f_r	BRDF	sr^{-1}

Radiance is a measure of the flux density per unit solid angle (or steradian) while spectral radiance is the radiance per unit wavelength and irradiance can be defined as a measure of radiometric flux per unit area, or flux density. BRDF can be expressed as the ratio between the directional reflected radiance and the directional incident irradiance,

$$BRDF = fr(\lambda, \hat{s}_i, \hat{s}_r) = \frac{dL_{\lambda,r}(\lambda, \hat{s}_i, \hat{s}_r)}{dE_{\lambda,r}(\lambda, \hat{s}_i)}. \quad (2\text{-}1)$$

In the equation above, $dE_{\lambda,i}$ refers to the incident spectral irradiance, and $dL_{\lambda,r}$ represent the reflected spectral radiance (Ke, 1993). In most BRDF measurements for global illumination, wavelength and polarization can be neglected, and in this case, BRDF equation can be simplified as

$$fr(\hat{s}_i, \hat{s}_r) = \frac{dL_{\lambda,r}(\hat{s}_i, \hat{s}_r)}{dE_{\lambda,r}(\hat{s}_i)}. \quad (2\text{-}2)$$

Gonioreflectometer is the device that used to measure BRDF. A gonioreflectometer needs at least four degrees of mechanical freedom to measure the complete function since the BRDF is a function of four angles. The typical design for gonioreflectometer contains a light source, a sample area that can be moved in relation to the light source, and a photometer that can be moved in relation to the sample area (Ke, 1993).

An early and basic gonioreflectometer designed by Murray-Coleman and Smith (1990). As another example of gonioreflectometer design, a basic device which uses imaging technology is created by Gregory J. Ward (1992) in Lawrence Berkeley Laboratory to estimate BRDFs. The main optical components were a half-silvered

hemisphere and a CCD camera with a fish-eye lens in his system. The combination of these elements takes care of the two degrees of freedom. Here, the hemispherical mirror collects the light reflected from the sample surface in holder A and reflects back into the fish-eye lens and onto the CCD array B (Ward, 1992).

In Figure 2-2 (Figure from Ward, 1992), the schematic on the right shows the advantage of using a half-silvered hemisphere. The lens is being focused at one half of the hemisphere radius allowing an image of luminance in all different reflected angles to be generated. The light source in this system is a 3 watt quartz-halogen lamp. To generate a parallel beam, Ward used an optical precise parabolic reflector. The half-silvered hemisphere permit the light beam to go through and illuminate the sample, and an exterior baffle shields the camera from stray radiation (Ward, 1992).

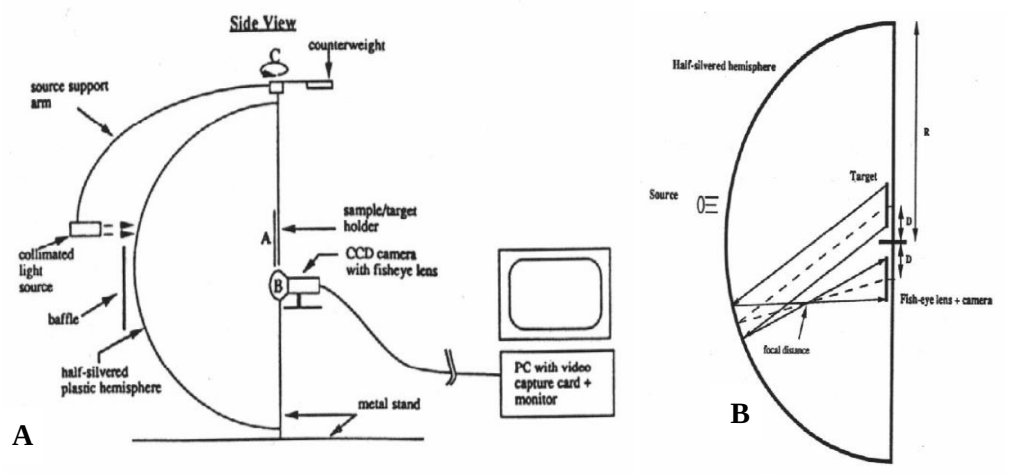

Figure 2-2. (A) Ward's silver hemisphere reflectometer, (B) Half-silvered hemisphere geometry of Ward's gonioreflectometer**.**

Turning the light source arm at point C and the sample holder at point A allows controlling the angle of incidence θ_i and ϕ_r mechanically in Ward's system. A computer controlled motor is used to move the light source during data collection, and the sample is

moved manually and also $m\phi_i$ is changed manually. Free variables in Ward's system are shown in Figure 2-3 (Figure from Ward, 1992).

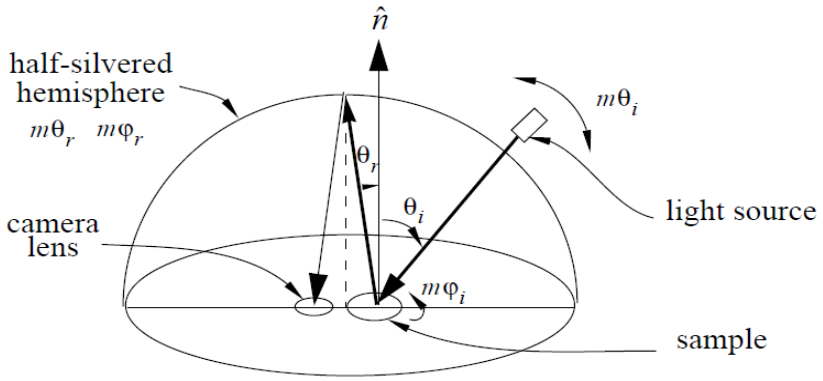

Figure 2-3. Free variables in Ward's gonioreflectometer.

The most significant contribution of Ward's device is that the hemisphere of reflection is captured in a single image, which enables fast data collection. Using his system a complete BRDF measurement can be recorded in a few minutes, including time for manual rotation of the sample (Ward, 1992).

Other than Ward's device, there are two other systems that were built to measure BRDF. One of them was built by the Columbia Automated Vision Environment research group. This system uses a robotic manipulator and a CCD camera to allow simultaneous measurement of BRDF and BTF (Bidirectional Texture Function) (Dana et al., 1996). The other device was built by the Light Measurement Laboratory at the Cornell University, and it is used to acquire reflection and emission data. A light sensor is used as the light measuring instrument in Murray's reflectometer and Cornell's gonioreflectometer used a light sensor while at Columbia University used a camera.

Automatization of the measuring process will be useful since BRDF requires huge amount of data. The previous systems are not totally automated and required human intervention at some point of the process, thus, Ke (1993) built a new system to measure the BRDF automatically after the initial setup. His system is called ACME (Active Measurement Facilities) with two degrees of freedom for the direction of incident light and another two degrees of freedom for the direction of reflected light. ACME is an integrated robotic system which is created to obtain optimum measurements in order to achieve accurate computational models. In this system, a 3 Channel CCD Camera is used as the light measuring device. In his research, Ke used several materials as sample such as paper and silk, and reached estimated overall error less than 8%. (Ke, 1993).

2.2. Reflectivity on Gold Electrodes

We developed our own surface reflectivity measurement system to the reaction kinetics of SLRR building on the systems that were created by Ward and Ke. In order to understand the phenomena behind the change in the reflectivity during UPD and SLRR, this part of my dissertation focuses on literature on reflection studies at the electrode/electrolyte interface.

One of the earlier studies of the reflection of light from an electrode surface was done by Plieth in 1970 on adsorption of methylene blue on a platinum electrode (Plieth, 1970). Arguing that the multiple specular method has disadvantages, the author used both, a multiple reflection and a single reflection cell and investigated the intensity of the reflected light from gold and platinum electrodes for both specular and diffuse

reflectivity. Plieth combined the single-reflection studies with a modulation of the reflectivity of the interface and modulated the potential drop across the electrolytic double layer. He investigated the adsorbed layer without interference by light absorption in electrolyte with the electro-reflection technique.

The properties of the electrode/electrolyte phase boundary are connected with its light reflectivity. Measuring the parameters of the reflected light will give some information about the state of the interface.

2.3. Reflection of Light from an Electrode

The reflection of light from a surface can be characterized by the reflectivity, *R*, it is a function of wavelength and also a function of the electrode potential for an electrode. Plieth defined the reflectivity as (Plieth, 1970)

$$R = I_r / I_0 . \tag{2-3}$$

Adsorption on the electrode surface is a critical factor in terms of affecting the state of an electrode surface. In his paper, Plieth classified the influence of adsorption on the reflectivity of an electrode into two parts: First, adsorbed molecules can change the electronic states of the electrode surface and the additional amount of the adsorbed substance in the adsorption layer can lead to an increased absorption of the light equal to decreased reflectivity of the surface. In this regard, he defined the overall reflectivity in terms of reflection of the light from the electrode metal atoms, $R_{M,}$ and the transmittance of the adsorption layer, T_{ad}, as

$$R = R_M / T_{ad} \,. \tag{2-4}$$

The terms, R, R_M, and T_{ad} are functions of the wavelength, λ, of the incident light, the electrode potential, and the coverage of adsorbed species, θ (Plieth, 1970).

Beside the interface effect, the measurable intensity of the secularly reflected light also depends on its absorption in the electrolyte phase. This effect also depends on several other factors such as, the thickness of the electrolyte, the concentration of the absorbing substance, and the wavelength of the incident light. Plieth also notes that eliminating the absorption in the electrolyte is possible by using an extrapolation procedure. In addition, when electrolyte layers are very thin and concentrations of an absorbing substance are small, the absorption of light in the electrolyte can be neglected compared with the decrease in the light intensity during reflection from the electrode surface. Lastly, the influence of the electrolyte can be neglected in a wavelength range where the electrolyte is non-absorbing (Plieth, 1970).

As mentioned earlier, Plieth argued that the multiple specular reflection method has disadvantages compared to the single reflection method, which is based on a modulation technique. With this method, several parameters were modulated to have more sensitive changes in the intensity of the specular reflected light. A modulation of the amplitude and of the wavelength is possible. The modulation of the reflectivity is known from semiconductor investigations (Cardona, 1968; 1969; Lax, 1968). This method is also ideal for especially metal electrodes (Plieth, 1970).

The intensity of the reflected light is defined as (Plieth, 1970)

$$I_r = I_0 R . \tag{2-5}$$

When we take the differentiation, it will give

$$dI_r = I_0 dR . \tag{2-6}$$

When the Eq. (2-6) is divided by Eq. (2-5), it will give

$$dI_r / I_r = dR / R . \tag{2-7}$$

Here, experimental part is simpler since the measurable quantity dI_r/I_r is identical with required quantity and does not have I_0 value. One can decide the thickness of the electrolyte and the concentration of a colored substance arbitrarily. In this respect, the author showed that the main focus of the semiconductor investigations was the solid-state phase. Hence, he only considered the effect of modulation in semiconductor part of the double layer. He also assumed that the electrolytic part of the double layer was unaffected by the modulation. On metal electrodes the double layer is only established in the electrolyte and only the potential drop across the electrolytic double layer is modulated. In this respect, Plieth found that when metal electrodes are used, specific investigations can be carried out in the double layer, and results are unaffected by light absorption in the electrolyte and are unambiguous in the local coordination (Plieth, 1970).

Many other researchers conducted optical and electrochemical studies on metal electrodes (Adzic et al., 1974). In this part of this chapter, I will review some of these studies briefly.

Kolb et al. (1974) studied the relative reflectivity changes, $\Delta R/R$, of a gold electrode surface caused by the deposition of monolayers of thallium, copper and lead

from electrolytic solutions at underpotentials in situ and calculated optical constants of the surface layer giving rise to this measured reflectivity change and compared to the results of the electroreflectance effect on bare gold surfaces. It is stated that a change in the gold electrode surface layer which changes in the optical properties of the substrate metal surface is the reason for the reflectance change observed during the monolayer deposition.

Bewick and Thomas (1975) conducted a series of researches (Bewick and Thomas, 1975; 1977a; 1977b) to investigate optical and electrochemical studies of the underpotential deposition of metals. In the first paper, underpotential deposition of thallium deposition on single crystal silver electrodes for orientations 100, 110 and 111 is examined (Bewick and Thomas, 1975). It is stated that the deposition process for the first monolayer was shown to be the formation of a layer of adsorbed atoms initially, followed by a phase transformation to form a crystal plane by two-dimensional nucleation and growth. Bewick and Thomas (1975) emphasized that the effect of the substrate structure was seen on the formation of the second thallium monolayer and stated that the formation of this layer also involved adsorption followed by transformation into a crystal plane (Bewick and Thomas, 1975). In the second part, Bewick and Thomas (1977a) studied thallium and lead underpotential deposition on silver single crystals and discussed the nature of phase transitions occurring during the underpotential deposition of metal layers and the question of the involvement of two-dimensional nucleation. It is showed that the order of transitions is determined by the substrate. In the third paper (Bewick and Thomas, 1977b), only a single monolayer of lead was formed on the (111) and (100)

substrates, but on the (110) orientation, the deposition of a second layer started before the onset of bulk deposition.

Adzic et al. (1979) studied UPD of bismuth on gold electrode in 1979 by specular reflectance spectroscopy and linear sweep voltammetry and determined the spectral dependence of $\Delta R/R$ caused by Bi adatoms and compared with the calculated spectrum and achieved a satisfactory agreement between experimental and calculated spectra. Adzic et al. (1979) used ΔR/R values have been used to determine the surface concentration of Bi, and used this value to calculate the electrosorption valence of Bi_{ad} (Adzic et al., 1979).

2.4. Reflectance Studies of Gold/Electrolyte Interface

One of the earlier studies of the system was Cahan et al.'s (1970) research on the gold/electrolyte interface with both single and multiple reflection techniques.

For the multiple reflection methods, Cahan et al. (1970) found significant errors stemming from the use of large number of reflections. In order to take consideration of the sensitivity of the reflectivity of gold electrodes to potential and to adsorbed ionic and neutral species, Cahan and his colleagues proposed an explanation which involved transitions of electrons in surface states (5d to 6s). Cahan et al. (1970) also claimed that the previous explanations involving changes in the Fermi level relative to non-surface electronic states were untenable. Also, they developed a new method to study the refractive index within the double layer if it is lower than that of the bulk solution.

In their study, Cahan and his colleagues base their approach on the Surface State Theory and explain the procedure as follows (Cahan et al., 1970 pp 40-41)[1]: At a temperature of absolute zero, for a perfect crystal, if the primary mechanism of light absorption in gold is the 5d→6s transition, there should be an abrupt step in the (reflectivity, photon energy) curve. At higher temperatures, the step should become rounded as shown by the Fermi distribution function. This rounding should be symmetric around the inflection point, whereas the actual reflectivity curve still shows significant excess absorption, more than 0.5 eV below the actual absorption edge while only 2-3 kT is attributable to thermal fluctuations in the electron distribution (Cahan et al., 1970 pp 40-41).

Cahan et al. (1970) underline the fact that the theoretical considerations of the electronic surface states of finite lattices imply that the impact of truncation of an infinite lattice generates highly localized surface eigenstates with energies in the band gap, i.e., for gold, the top of the 5d band is raised and the bottom of the 6s band is lowered at the surface. Below figure shows a possible diagrammatic representation of the 5d and 6s bands at a metal-vacuum interface. The states induced by introducing a boundary in the crystal are illustrated with the cross-hatched areas. Cahan et al. (1970) argue that the existence of these states in the forbidden band is related for the shape of the reflectivity curve of gold. In this respect, the $(5d)_{surface}$→Fermi level transitions are possible with photon energies lower than the absorption edge due to the existence of these occupied states. In contrary, the shape of the $(5d)_{surface}$ band might be calculated from the excess absorption (Cahan et al., 1970).

[1] The expalanation regarding Cahan et al.'s experimental procedure and results are directly taken from Cahan et al. 1970.

Figure 2-4 (Figure from Cahan et al., 1970) demonstrates the surface immersed in an electrolyte. It is stated that the 5d and 6s bands are distorted due to the potential across the interface. Hence, the (energy, distance) relationship of the surface bands is likewise changed, and in this way the shape of the excess absorption spectrum can be shifted significantly. In this regard, Cahan and his colleagues argued that if the hypothesis that rounding in the reflectivity curve is caused by the excess absorption due to the surface states is correct, and then there are sufficiently large energy changes to account for electro-modulation over a wide range. Consequently, only a small region in the metal is affected by the modulation of the double layer. The results of their analysis also show that very large effects can be produced by the relatively small charge (33 $\mu C/cm^2$ for the 0.7 V in the work of Hansen and Prostak, 1967; 1968) associated with the modulation of this double layer (Cahan et al., 1970).

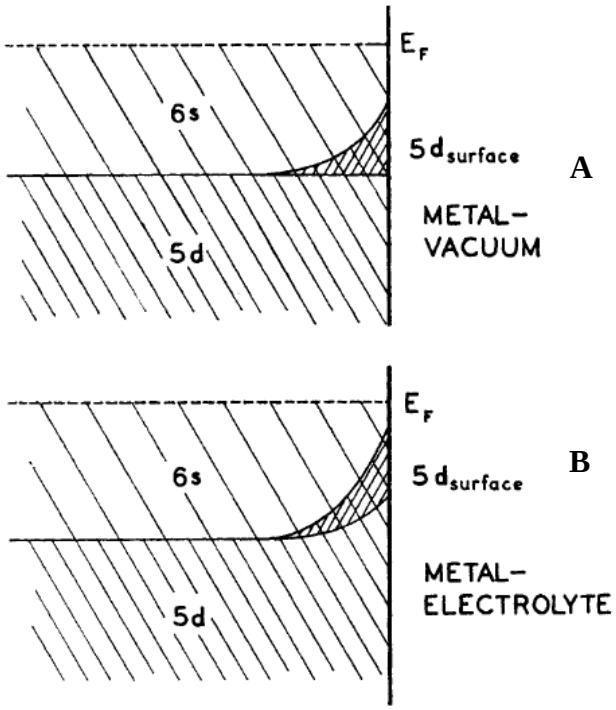

Figure 2-4. Schematic representation of energy bands and surface states (cross hatched-area) in gold. (A) Metal-vacuum interface, (B) Metal-solution interface.

Cahan et al. (1970) also showed that the small shifts in photon energy (0.0076 to 0.076 eV) used by Hansen and Prosak in their calculations of $\Delta R/R$ against λ can be considered as approximating differentials, and their resultant curve is equivalent to the derivative of the (*reflectivity*, λ) curve. The energy shift does not change the half-width of the peak in the ($\Delta R/R$, λ) curve extracted by Hansen and Prostak (1967; 1968) (Cahan et al., 1970).

Based on these findings, Cahan et al. (1970) argued that the shifts of a size that can no longer be considered as linear produce a broadening and a shift of the peak. Further, Cahan et al. (1970) underlined that with surface states of the type represented in Figure 2-4, even a few tenths of a volt should be sufficient to produce such non-linear effects and surface heterogeneity would also contribute to broadening (Cahan et al., 1970).

An important question that Cahan and his colleagues pose is whether there are any significant electro-modulation effects specifically due to changes in the refractive index and/or thickness of the double layer. Cahan et al. (1970) assume that these effects do exist and propose a method to observe them independent of the effects within the metal (Cahan et al., 1970).

Cahan et al. (1970) programmed a three-layer calculation to calculate the reflectivity for high angles of incidence varying the index of refraction of the double

layer. At each incident angle, the predicted dip in the reflectivity is associated with a unique index of refraction. As the index of refraction approaches that of the bulk solution, the required angle of incidence approaches 90°. For perpendicular polarization, the change of reflectivity can be greater than 20% for a 0.05 change in the index of refraction. The following experimental set up is being implemented to study this effect. A flat electrode is to be mounted at the center of rotation of a scanning θ-2θ goniometer. A small modulation of the fixed average electrode potential will be impressed potentiostatically and the goniometer scanned through small angles. The modulation will be detected and divided by the average reflectivity. Any electro-modulation of index of refraction will show up as a blip at the corresponding angle. From this angle, the index of refraction of the double layer can be calculated, and hence its dielectric constant (Cahan et al., 1970).

Briefly, Cahan et al. (1970) explained the sensitivity of the reflectivity of gold to potential which involves surface electronic states. Their results showed that specular reflection on gold electrodes is very sensitive to adsorbed species, including neutral species, and provides a means for studying adsorption phenomena. In addition, it is emphasized that the multiple reflection studies can produce gross errors particularly associated with scattering phenomena which indicates the desirability of performing future work with single or at most a few reflections. (Cahan et al., 1970).

2.5. Cyclic Voltammetry

Cyclic voltammetry (CV) is a type of the electroanalytical method which is being used to study the electrode-electrolyte interface (Schmickler, 1996; Bard and Faulkner, 2002; Plieth, 2008; Brett and Brett, 1993), and it is the most common technique to obtain preliminary information about an electrochemical process. Fundamentals of CV rely on sweeping of the potential from an initial potential (E_1) to a vertex potential (E_2) and back to the initial potential at a constant scan rate. Figure 2-5A shows linear variation of the applied potential versus time.

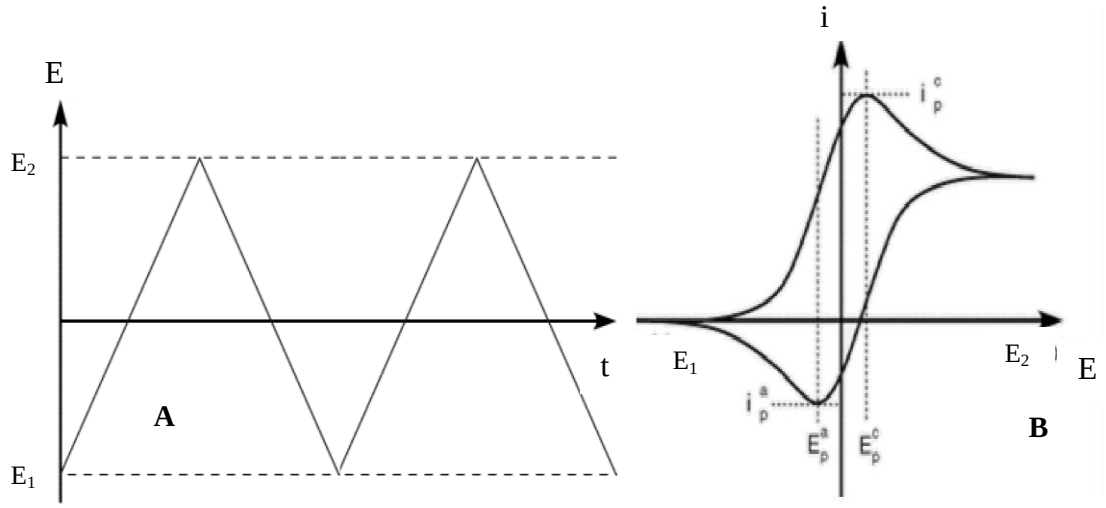

Figure 2-5. (A) Potential waveform of cyclic voltammogram - Potential vs. time graph, (B) A typical cyclic voltammogram (CV) - Current vs. potential graph.

In a cyclic voltammetry, a potentiostat is used to control the potential difference between the reference electrode and working electrode and to measure the current flow across the counter electrode and working electrode. The significant criteria which affect the reproducibility and reliability of the cyclic voltammetry are electrolyte, electrode quality, potential range, and scan rate during potential scan, change in the current

depends on reaction kinetics and diffusion of the electroactive species at the associated potential. Recorded current represents the sum of the Faradic current of the actual electrode and capacitive current due to double-layer charging. When the anodic reaction starts, the current value increases at the associated potential and reaches the maximum value which is called the cathodic peak, where the highest flux is observed. When the peak point is reached depletion leads to decrease in the current. In cathodic reaction, current values turn negative and they vary depending on the diffusion. The peak point at the negative current curve refers to anodic peak current as a reflection of the anodic reaction (Schmickler, 1996; Gokcen, 2010).

Diffusion-controlled current and peak current equations can be derived as a function of time and expressed as follows (Bard and Faulkner, 2002; Hamann and Hamnett, 2007). In an electron transfer reaction, $O + ne^- \leftrightarrow R$, where the O and R species concentration ratio is defined with the Nernst equation as (Gokcen, 2010)

$$\frac{C_O}{C_R} = \exp\left[\frac{nF}{RT}\left(E(t) - E_0\right)\right]. \tag{2-8}$$

In this equation, the potential is a function of time, $E(t)$, and is calculated by the linear change of the initial potential (E_1) with a constant scan rate (vt): $E(t) = E_1 - vt$. C_R can be neglected since there is no product at the beginning of the reaction. Thus, laplace transformation of the diffusion equation is written as (Gokcen, 2010)

$$\overline{C}_O(x,s) = \frac{C_O^*}{s} + A(s)\exp\left[-\left(\frac{s}{D_O}\right)^{\frac{1}{2}} x\right]. \tag{2-9}$$

The current and the flux of O species through the electrode are proportional to each other, and boundary conditions ($x = 0$) are considered at the electrode surface. The relation of flux with the current is given in the form of a Laplace transform by (Gokcen, 2010)

$$\frac{\bar{i}(s)}{nFA} = D_O\left[\frac{\partial \bar{C}_O(x,s)}{\partial x}\right]. \tag{2-10}$$

When this equation is inverted into the time domain, it can be expressed as

$$i(t) = -nFAC_O^*(\pi D_O \sigma)^{\frac{1}{2}}\chi(\sigma t)\ . \tag{2-11}$$

Here, $\sigma = (nF/RT)v$ and $\pi^{\frac{1}{2}}\chi(\sigma t)$ represent current function. The corresponding maximum value of the current function at the peak potential is 0.4958. When this value is substituted into the current equation, the peak current can be defined as

$$i_p = -(2.99\times10^5)n^{\frac{3}{2}}AC_O^* D_O^{\frac{1}{2}} v^{\frac{1}{2}}\ . \tag{2-12}$$

The difference in peak potential and half-peak potential is expressed as

$$\left|E_p - E_{p/2}\right| = 1.857\frac{RT}{nF}. \tag{2-13}$$

2.6. Pb UPD on Au (111)

Researches performed a great number of Pb electrodeposition studies on gold single crystal substrate (Budevski at al., 1996; Jütner and Lorenz, 1980; Engelsman et al., 1980). Electrochemical results indicate that Pb UPD on Au (hkl) depends strongly on the

crystallographic orientation. The peak structure of cyclic voltammograms in these systems was explained by the formation of different superlattice structures on atomically flat terraces. The UPD process was found to be influenced by the presence of monatomic steps on the substrate (Jütner and Lorenz, 1980). Figure 2-6 (Gokcen et al., 2011) shows the cyclic voltammogram for Pb UPD on Au (111). The presence of small D_1 deposition peak indicates initial deposition on surface defects, such as dislocations, and steps. Sharp D_2 peak corresponds to nucleation and growth of Pb UPD layer on terraces (Gokcen et al., 2011).

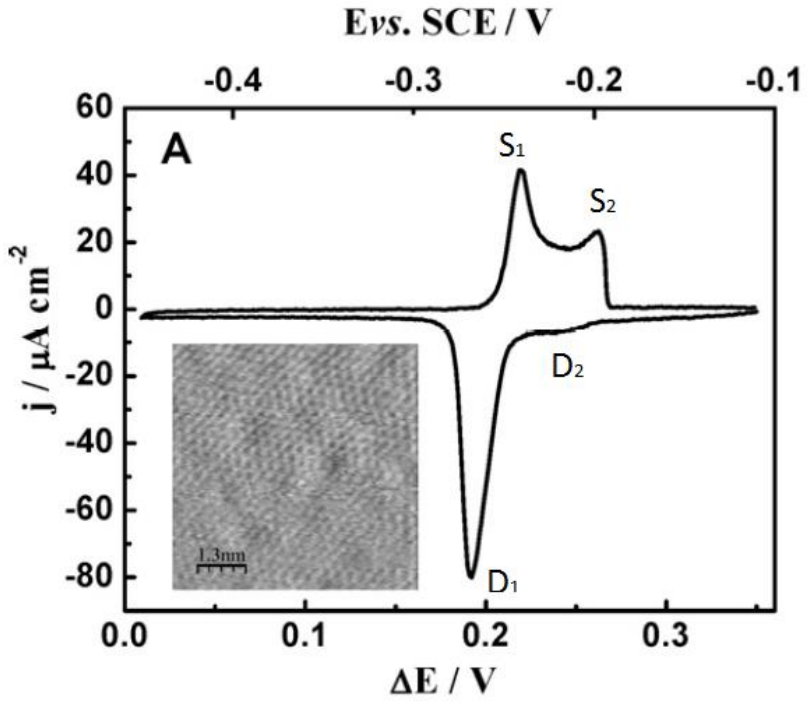

Figure 2-6. Cyclic voltammogram and current density vs. potential graph of lead UPD/Au (111) from 0.1M $HClO_4$ + 1mM Pb^{2+} with a $v=|dE/dt|$= 10 mV/s sweep rate.

Figure 2-7 illustrates cyclic voltammetry of Au (111) single crystal we obtained in $5x10^{-3}$M Pb^{2+} + 0.1M $HClO_4$ electrolyte. As it is seen from the graph, anodic and

cathodic peaks are almost symmetrical. Initial start of deposition due to the surface defects can be seen around 0.45V at the small deposition peak, and most of the deposition occurs around the sharp deposition peak, 0.22V.

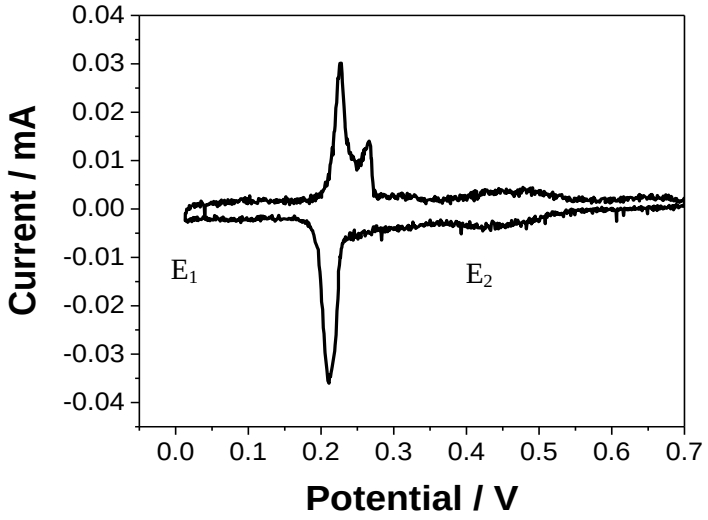

Figure 2-7. Cyclic voltammetry Pb UPD on Au (111) crystal in $5x10^{-3}$M Pb^{2+} + 0.1M $HClO_4$ solution with 10 mV/s scan rate.

By using the UPD cyclicvoltammogram, charge can be integrated from anodic or cathodic reaction and expressed as

$$q(E) = \frac{1}{v}\int_{E_1}^{E_2} i(E)dE\,. \qquad (2\text{-}14)$$

Here, q is the charge, v is the sweep rate and E_1 and E_2 are the potential limits ($E_1 = 0.005\,\mathrm{V}$ to $E_2 = 0.4\,\mathrm{V}$). Integrating the anodic curve from the CV we obtained during the Pb UPD on Au (111) experiments gives charge vs. potential graph in Figure 2-8A, and normalizing charge values by dividing curve by maximum charge, qE/Q_0, the curve will be directly transformed into coverage values, and then coverage vs. potential graph can be obtained as in Figure 2-8B. This normalization can be expressed as

$$\theta = \frac{q(E)}{Q_0} = \frac{\frac{1}{\nu}\int_{E_1}^{E} i(E)dE}{\frac{1}{\nu}\int_{E_1}^{E_2} i(E)dE}. \qquad (2\text{-}15)$$

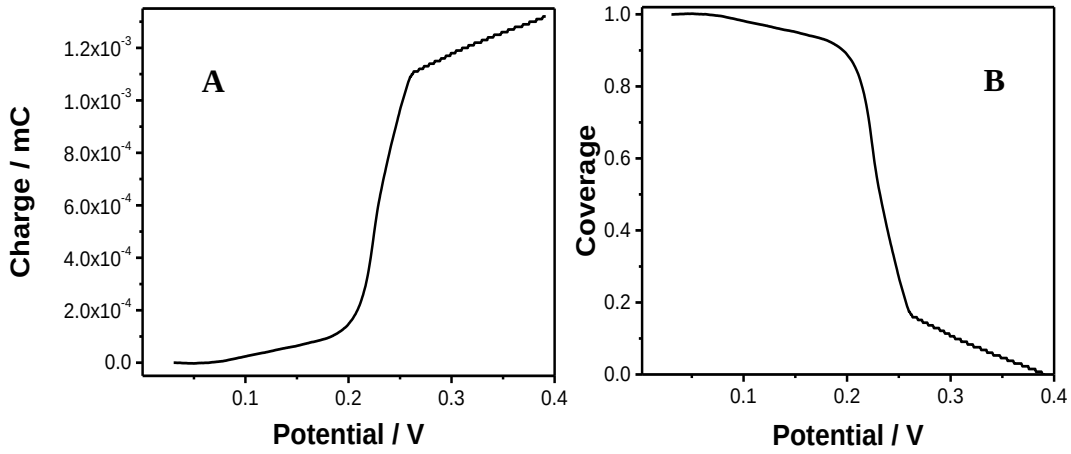

Figure 2-8. (A) Charge vs. potential graph, (B) Coverage vs. potential graph.

2.7. Chronoamperometry

Chronoamperometry (CA) is one of the very significant techniques which are used for the quantitative analysis of a nucleation process. This useful method enables the initial information about nucleation and growth mechanism in a studied system and is used in our research to investigate the main mechanisms beyond the UPD and SLRR process. Moreover, it leads to determine the amount of charge for deposition (dissolution). Additionally, nucleation rate constant and an adsorption isotherm can also be determined by this technique. In chronoamperometry, a (sequence of) potential pulse is applied to the working electrode and the current is measured and recorded versus time as a response. The current can be analyzed and its nature can be identified from the variations with time (Bard and Faulkner, 2002; Brett and Brett, 1993).

Figure 2-9 shows a typical CA potential-time profile and corresponding current vs time graph. As it can be seen in the Figure 2-9A, at the beginning of the transient experiment the potential of the working electrode is held at E_1, and then, at t=0 the potential is instantaneously changed to a new value E_2. Figure 2-9B shows the corresponding current time response.

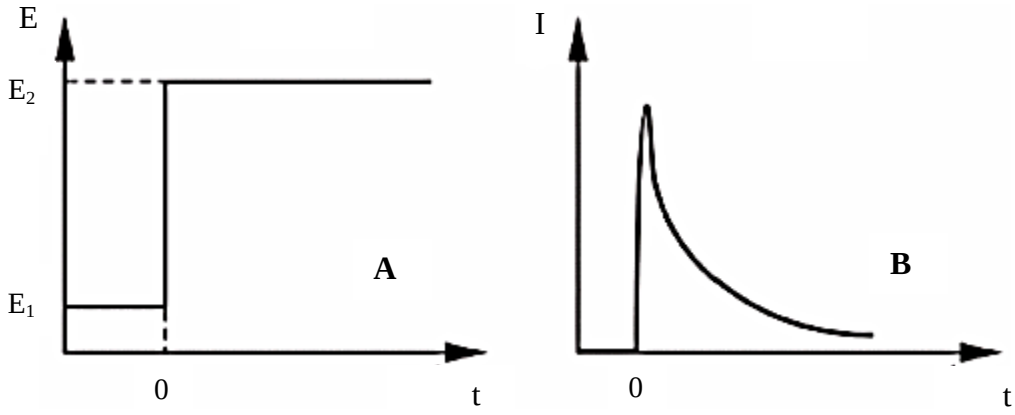

Figure 2-9. (A) The potential-time profile applied during the chronoamperometric experiment, E_1 is initial value and E_2 is the stepped potential value, (B) The corresponding response of the current due to changes of the potential.

Cottrell equation is used to determine the exact form of current-time dependence for a planar electrode the current density and expressed as

$$i(t) = nF\sqrt{\frac{D_0}{\pi}}\frac{C_O^*}{\sqrt{t}}. \tag{2-16}$$

The charge can be generated by integrating the current as a function of time, $Q = \int i(t)dt$ and expressed as

$$Q(t) = 2nF\sqrt{\frac{D_0}{\pi}}C_O^*. \tag{2-17}$$

The cathodic charge is proportional to the level of deposited species, and the anodic charge is proportional to the level of stripped species in electrodeposition. Thus, CA leads to do the quantitative analysis for the electrodeposition process as

$$Q = \int_{t_1}^{t_2} j dt \,. \tag{2-18}$$

Chapter 3: Experimental

This chapter describes our surface reflectivity measurement system explaining our set up, sample preparation, image analysis, and data acquisition.

3.1. Description of Our System

Using the goniometer set ups in the literature as a guide, we implemented our own reflectivity measurement system. The experimental setup system used in our lab to measure reflectivity during UPD and SLRR is composed of a CCD camera, a halogen lamp as the light source, an integrating mirror to collect all the spread light, an electrochemical cell to immerse all three electrodes (working, reference, and counter electrodes), data acquisition device (DAQ), connector block, a potentiostat, several ThorLabs bases and holders to allow durability and flexibility to adjust laser beam easily and to fix the equipment on the optical table.

3.2. CCD Camera

ThorLabs DCU223M, black and white, 8-bit CCD camera is used. The camera has 1024x768 resolution, and the reason to choose monochromatic version instead of color version is that the overall sensitivity of the color image is three times lower than that achievable with a monochromatic sensor. The CCD camera features USB 2.0 connection which allows interfacing with many programs easily. CCD camera comes with an extensive Windows compatible software package on CD which can be used to adjust camera parameters easily. It also has camera viewer feature which is used to adjust

the image as it is desired before starting to run the experiments. Camera is fully compatible with Thorlabs C-mount and also other camera lenses. In our system a Pentax Cosmicar Television lens which has 8.5 mm focal length and 1:1.5 maximum aperture ratio is used for iris adjustments to prevent saturation.

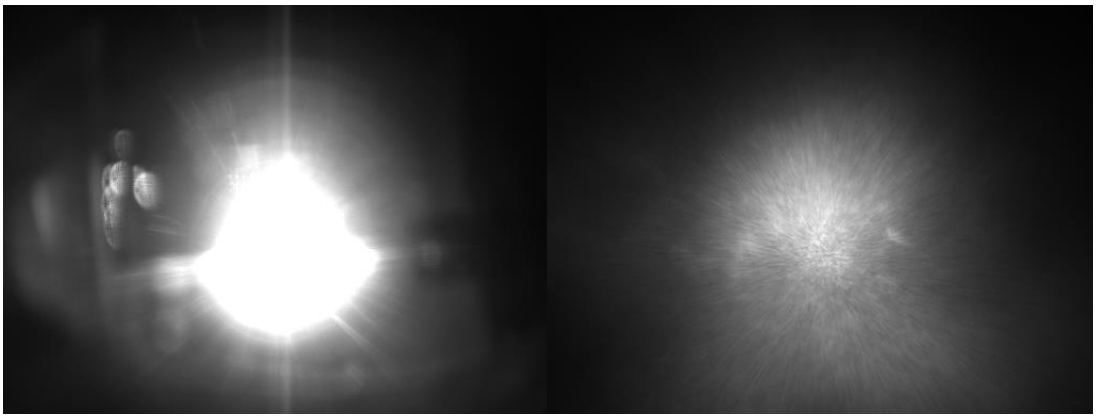

Figure 3-1. Images are taken by CCD camera with different iris adjustments.

Figure 3-1 shows two different images with different brightness of the light source. The image in the right side has a significant amount of saturated pixels while the left side image is adjusted for no saturation by choosing optimum iris setting and using a filter when it is necessary. The iris adjustment on the Cosmicar lens allows setting for desired image without saturation. When optimizing the dynamic range of the image, it is very important to avoid saturation effects. Saturation occurs when grey levels exceed the maximum available. When a spot becomes saturated, any differences in high pixel intensities cannot be resolved. No reliable quantitative data will be generated from a saturated spot, and saturated spots may also have an overall effect on normalization. Thus, it is one of the most significant steps to achieve optimum camera settings and to avoid oversaturation by adjusting camera's shutter and iris, and also by applying a filter when it is necessary before starting experiments.

As it is mentioned earlier, reflectivity of the reflected beam is proportional to the pixel intensity of the outcome image, and this intensity values will have a linear relation with the cell potential. However, this relation can be neglected since it is very small compared to the change due to intensity. This topic will be discussed in greater detail in the Section 3-9.

3.3. Light Source

Since building the initial set up of our system, we have tried a variety of light sources to obtain maximum intensity change for more reliable results. First, we have used an incandescent lamp, and then we moved to a red He-Ne laser with 632 nm wavelength, LED lamp and a halogen light source. Comparing all light sources we have tried, halogen lamp gave us more reproducible, reliable results in terms of intensity. Therefore, as a light source, we have finally used Thorlabs SLS201 halogen light source. This light source allows applying filters with different wavelengths easily with a built-in filter hole in the light source. Thus, this allowed us to compare white light measurements with red light measurements by applying a 633 nm line pass filter.

3.4. Potentiostat

EG&G Princeton Applied Research 273A Potentiostat was used as potentiostat in our reflectivity measurement experiments. Potential range was between 5 mV and 0.7V for lead UPD on Au (111) crystal. Different scan rates were set to obtain optimum results and in general, 10 mV/s scan rate gave better results in terms of deposition and adsorbtion peaks in potential vs. current curves.

3.5. LabVIEW Data Acquisition Algorithm and Program

A LabVIEW program is written to capture time, current, and potential values during the experiments. This LabVIEW program communicates with potentiostat by using a multifunction DAQ PCI 6052 E integrated device and NI BNC 2110 connector block. The DAQ integrated device was programmed and communicated with the potentiostat via the connector block. The program is coded and modified so that whenever the voltage and the current are read out and recorded, this program creates a software trigger for capturing an image. Thus, the CCD camera is initialized with each potential values and displays and saves an image corresponding each data points (time, potential, and current). The software measures intensity of each recorded image by taking mean intensity of all pixels in the image array and displays intensity vs. time or intensity vs. potential graphs in the front panel of LabVIEW file. This feature allowed us to observe the images that are taken by the camera before and during the experiment simultaneously on the front panel and displays the intensity vs. time and intensity vs. potential graphs. Panel also has an oversaturation detector which counts the saturated pixels and displays it with yellow, orange, or red light indicating no saturation, a few pixels saturation, and high number of pixels saturation respectively (Figure 3-2).

The user-friendly graphical user interface also displays current vs. potential graph in the front panel to observe the deposition and adsorption peaks simultaneously with the experiment. The front panel also has other useful graphs such as potential vs. time and intensity vs. time graphs which allows user to make simultaneous observation during the experiments.

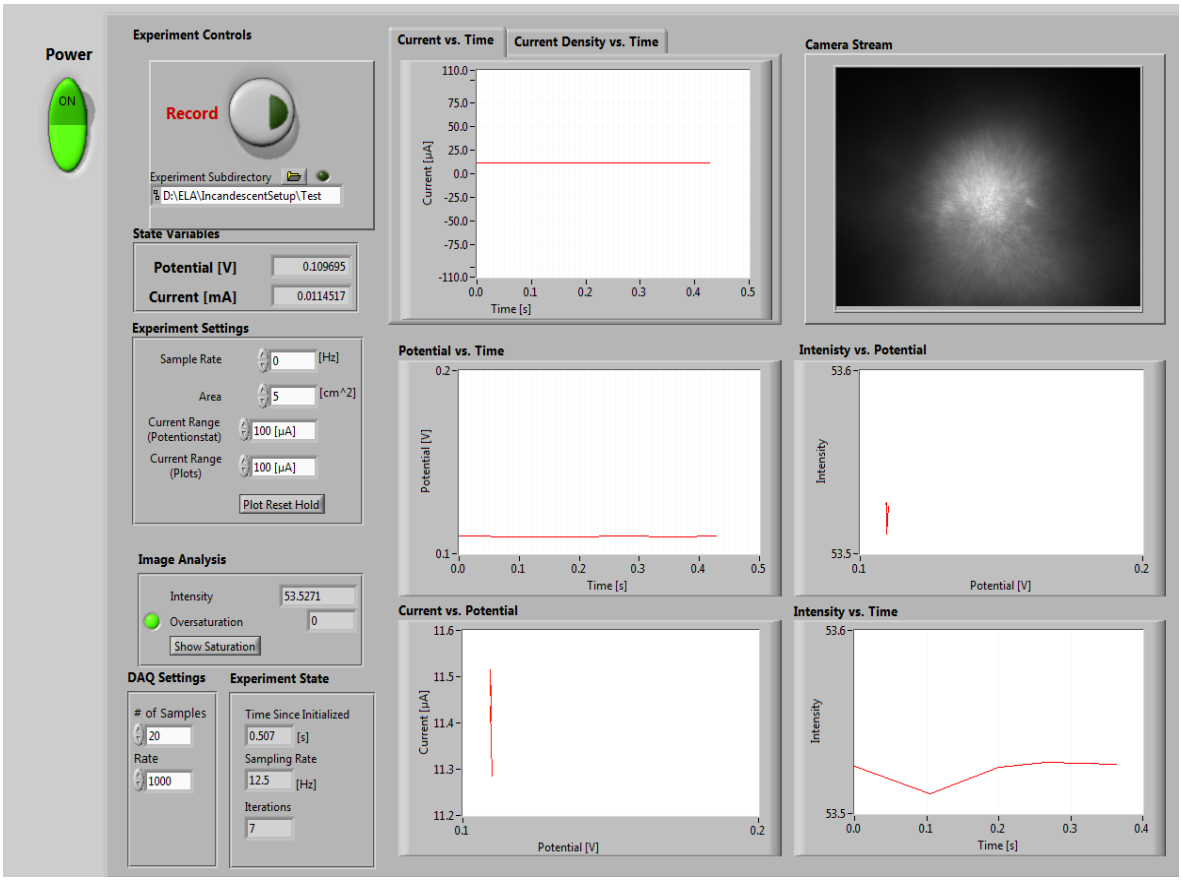

Figure 3-2. Front panel of our LabVIEW Program.

The LabVIEW program we built will start by pushing operate and then clicking on start button to display or capture data. The software allows us to observe the images before recording to make the shutter adjustments to provide optimum shutter and iris conditions in order to achieve images without any saturation. Thus, we do not have to record and save unnecessary images and data to the computer which will take too much space on the hard drive. Potential, current and time values are displayed on the panel allowing us to do all the final adjustments before starting to record the actual experiments. “Plot reset/hold” button on the panel functions to reset or hold the graphs

when it is desired. Default adjustment is to reset the plots in every 10 seconds which makes it easy to adjust the intensity of the reflected beam before the experiments.

Once the desired image for reflected beam is obtained, then clicking again on this button will hold the graphs and display all the data without resetting. This feature helps us to observe if the intensity of the images is constant or not before the deposition. It is very significant to achieve constant intensity to get meaningful intensity data during the deposition. Any draft or change in the intensity due to outside effects (any impact unrelated to deposition, such as wrong incident angle, light changes in the environment) will affect the quality and validity of the intensity data. Therefore, we test our intensity for a while (more than 2-3 cycles) to see if there is any draft. Once the record button is pushed, whenever a potential value and a current value are recorded, the CCD camera will capture an image and save it in the specified file location. The software measures the average intensity of the each image and display intensity vs. time graph simultaneously with other desired graphs, such as Potential vs. time, current vs. potential, and intensity vs. potential graphs. The LabVIEW program saves all the other data (time, current, potential, intensity etc.) in a ".lvm" file, which can be opened with a notepad or excel program for further data analysis.

3.6. NI DAQ Device and NI Connector Block

NI BNC 2110 connector block is used to connect the potentiostat with the Multifunction NI PCI 6052 E DAQ integrated device in order for interfacing. Channel

AI4 (A05) was connected to potential output of the potentiostat while channel AI5 (A04) was connected to the current output.

3.7. Sample Preparation

An Au (111) single crystal, with a diameter of 10 mm and thickness of 3 mm, was used as the working electrode (WE). First, the crystal was mechanically polished by using 9, 3, 1 and 0.25 μm diamond suspensions until visible clean and smooth surface were obtained, and after each polishing gold crystal is rinsed and immersed in distilled 18.2 MΩ ultra-pure water (Milipore Direct Q-UV with Barnstead A1007 pre-distillation unit) and sonificated. After completing all mechanical polishing steps, the surface was electropolished by anodization in a 2.5:1.5:1 solution of ethylene glycol, hydrochloric acid and ethanol. Then, Au (111) crystal was annealed in the hydrogen flame (Figure 3-3). In order to create a clean and smooth surface, as electropolishing, hydrogen flame annealing is also a significant step of the surface preparation process.

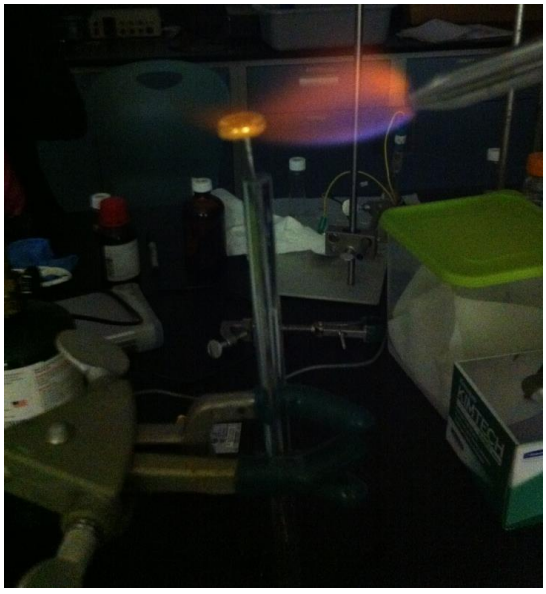

Figure 3-3. Flame annealing of the Au (111) crystal.

A platinum wire was used as the counter electrode (CE) while lead wire was being used as the reference electrode (RE). 0.1M $HClO_4$ +1mM Pb^{2+} solution and all other solutions were prepared by using ultrapure chemicals (99.999%, Alfa Aesar, J.T.Baker) and 18.2 MΩ ultra-pure water. Cell, glass tubes, and all components were cleaned with piranha solution (1:3 H_2O_2, H_2SO_4) prior to the experiments. After the annealed crystal cooled down, sides and back of the crystal, and the attached platinum wire is covered with nail polish to prevent any interaction of platinum with solution during the experiment. Since vibrations or shaking of the crystal will affect the reflected beam while taking the pictures during the experiment, the gold crystal was fixed to the lid of the cell very tightly. All electrodes and components are fixed with rubber stoppers or teflon tape on the outer end in order to prevent any vibrations or shaking during the reflectivity measurements (Figure 3-4). The lid of the cell was sealed with parafilm to prevent any leakage and air outlet. After sealing every component and the cell completely, the electrolyte was de-aerated for two hours with high purity nitrogen gas to reduce the content of dissolved oxygen and minimize the effect of oxygen reduction reaction on our measurements.

Experiments are done on the Newport research series plus high performance sealed hole table top which allowed mounting all the equipment firmly and also prevented vibrations. The camera is fixed to the optical table with ThorLabs holder modules which provide motion flexibility of the light beam vertically. Since our aim was to measure the change in the intensity of the reflected beam, and this could be done without changing the camera angle, unlike Ward's (1992) and Ke's (1993) systems, our setup was fixed in one angle, and experiments were run with this fixed angle. The module

used to hold the cell is also flexible by providing adjustment easily via screws in different directions. In the experimental set up we built, the light beam also passed through a 633 nm line pass filter to compare results for different wavelengths. The beam hits the gold crystal that is placed in the cell, and then reflects from the crystal to the focus of the camera when we do the specular light reflectivity measurements (Figure 3-5B). However, when we do the diffuse light reflectivity measurements, an integrating mirror is used to collect all the spread light beams and focus them to the camera (Figure 3-5A). Camera lens and shutter were adjusted manually prior to each experiment while checking the real time video with the LabVIEW program.

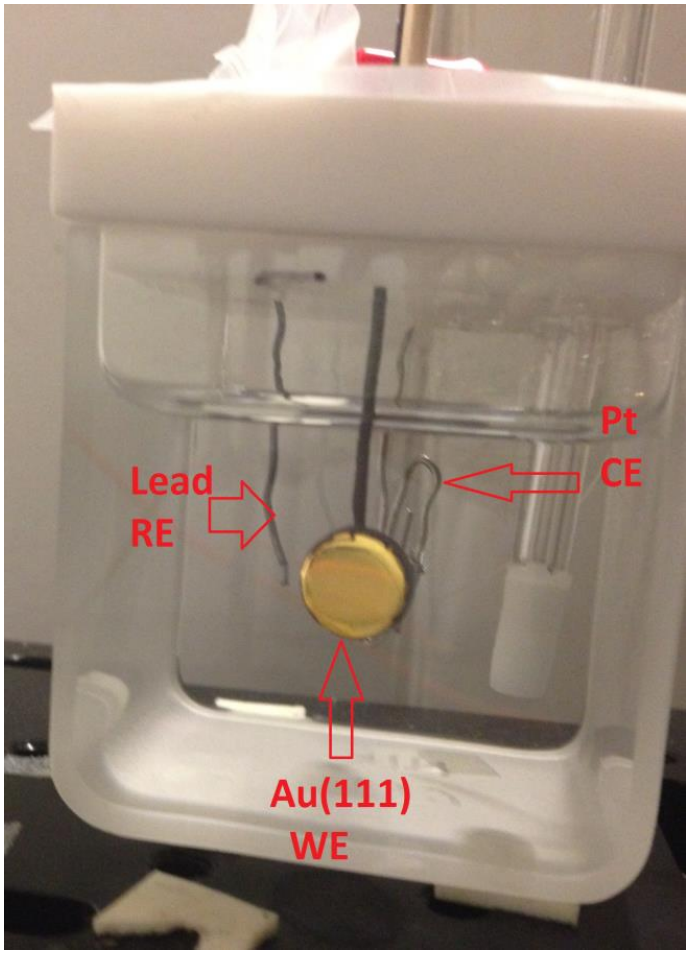

Figure 3-4. Electrochemical cell with the three electrodes and solution.

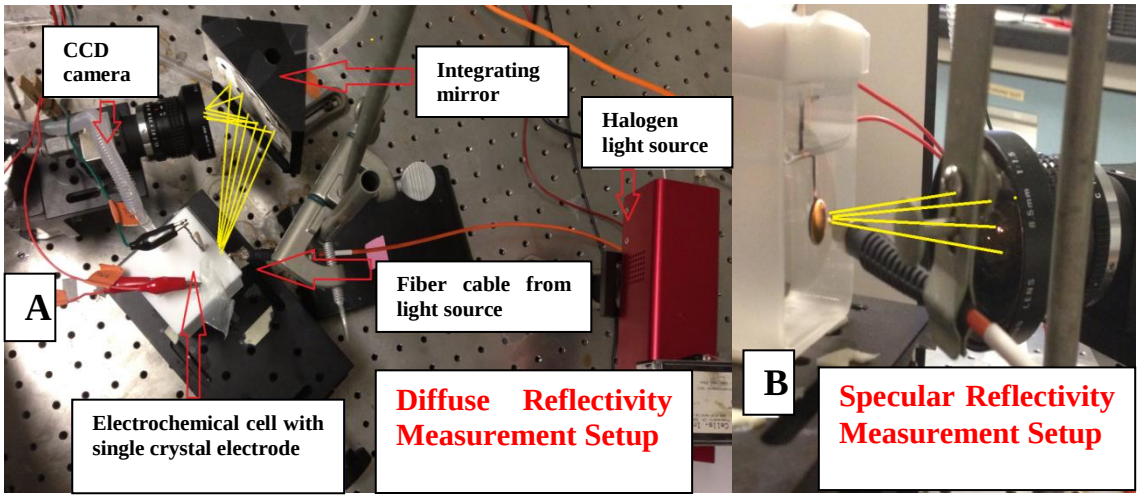

Figure 3-5. (A) Experimental set up of diffuse reflectivity measurements with integrating mirror, (B) Experimental set up of specular reflectivity measurements without integrating mirror.

3.8. Our Surface Reflectivity Measurements

Reflectivity can be measured from pixel intensities of an image (Ke, 1993). In other words, change in the reflectivity of a surface has a linear relationship with changing intensity of the reflected light from a surface. In addition to this, it is also proved that UPD monolayer coverage has a direct correlation with intensity of the reflected light beam in many optical and electrochemical studies (Bewick and Thomas, 1975, 1977a; Kolb et al., 1974; Adzic et al., 1974; Kolb and Kotz, 1977a, 1977b; Mo et al., 1996). Therefore, we can normalize our pixel intensity vs. potential graphs into normalized intensity vs. potential graph to estimate change in the UPD ML coverage with respect to potential difference. Finally, the correlation between the reflectivity and UPD ML coverage for Pb UPD on Au (111) can be expressed as

$$R = R_{Pb/Au} + (1-\theta_{UPD})R_0 . \qquad (3\text{-}9)$$

When the Eq. (3-9) is rearranged to calculate UPD monolayer coverage, it will be written as

$$\theta_{UPD} = \frac{R_0 - R}{R_0 - R_{Pb/Au}} \quad . \tag{3-10}$$

Here, R_0 is the reflectivity from the bare gold surface right, R refers to the recorded reflectivity values of the reflected light beam during the experiment, and $R_{Pb/Au}$ represents the reflectivity of fully covered Au (111) surface. The reflectivity values are obtained by multiplying the pixel intensities with a factor which is calculated by using relevant camera parameters (R=Ix$const$) (Ke, 1993). Due to the fact that in our formula θ_{UPD} represents the UPD ML coverage, which is the ratio of the reflectivity values, we can directly use the measured intensity values to calculate coverage without converting them into reflectivity values. In that case, for Pb UPD on Au (111), while I represents intensity, UPD ML coverage formula can be arranged as

$$\theta_{UPD} = \frac{I_0 - I}{I_0 - I_{Pb/Au}} . \tag{3-11}$$

The optical properties of an electrode surface are a function of the applied potential (Kolb, 1974; Bewick and Thomas, 1975). Therefore, the pixel intensities of an image will have a linear relationship with the cell potential. However, comparing the change in the reflectivity due to deposition is much bigger than the change in the reflectivity caused by potential difference. This will be illustrated and explained more in future text.

3.9. Sensitivity Verification of the Surface Reflectivity System

The experimental surface reflectivity setup designed and built during this PhD work has been tested for sensitivity on the change in Pb UPD layer coverage on Au (111) electrode. The experimental set up described previously has been employed to record the relative reflected light intensity change i.e., reflectivity change of the Au (111) surface during CV in the solution containing 10^{-3} M Pb^{2+} + 0.1 M $HClO_4$ (Figure 3-6). The scan limits were between 0.005 V underpotential (E_1) and 0.4 V underpotential with respect to Pb/Pb^{2+} (E_2). The first scan limit is chosen as underpotential where full Pb UPD layer is formed, θ=1, and the second one is chosen as potential where there is no Pb UPD layer on Au (111) surface, θ=0. The representative CV of such measurement in solution 10^{-3} M Pb^{2+} + 0.1 M $HClO_4$ with sweep limit, 0.01 V/s is shown in Figure (3-6A). The obtained CV-UPD current data obtained in anodic sweep from E_1 to E_2 were integrated and normalized to obtain the Pb UPD coverage as a function of potential (θ vs. E data, UPD isotherm) and this data are compared with θ vs. E data-isotherm obtained from surface reflectivity measurements. Several different geometries of the reflectivity systems and incident light to the Au electrode were examined in order to find the most sensitive option (Figure 3-6B, 3-6C, and 3-6D). The coverage of the Au surface was estimated from relative change of the intensity of reflected light to the CCD camera during the potential sweep in described limits (see previous chapters). In Figure 3-6B, comparison between the θ vs. E data estimated from charge integration and reflectivity measurements using diffuse reflected light system geometry and white light source are shown. In Figure 3-6C, θ vs. E data estimated from charge integration and reflectivity measurements using specular reflected light system geometry and white light as a source are shown as well.

Finally, the results from the last iteration of our set up are shown in Figure 3-6D. It represents the comparison between θ vs. E data estimated from charge integration and reflectivity measurements using specular reflected light system geometry and red light (632 nm wavelength band-pass filtered) as a light source. As one can see, the best agreement among these three comparisons in terms of θ vs. E data represents the diffused reflected light geometry with white light source (Figure 3-6B).

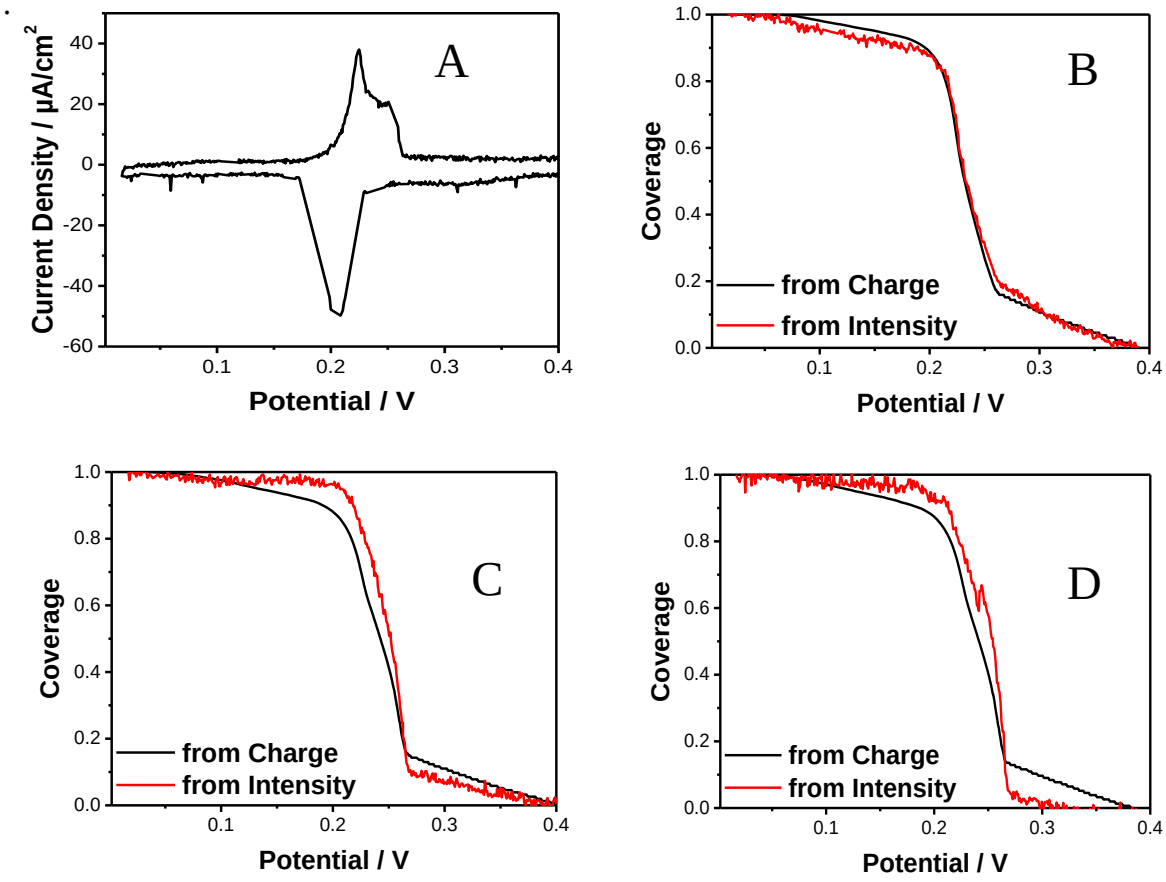

Figure 3-6. (A) CV of Pb UPD on Au (111), (B, C, and D) θ vs. E data estimated by surface reflectivity measurements using diffuse-white light scattering (B), specular-white light scattering (C), and specular-red light scattering (D).

The agreement is actually is very good. The relative difference between these data is less than 2% which shows that our system is capable of recording the slightest change

in the Pb UPD layer coverage in the entire potential range of the Pb UPD layer presence on Au (111) surface, $0 \leq \theta \leq 1$ (from E_1 to E_2). The small difference between the isotherms obtained by these two measurements is observed at $\theta \rightarrow 1$, and $\theta \rightarrow 0$ limit where almost no change in coverage occurs as a function of potential. This is attributed to a slight dependence of the Au surface reflectivity on the potential of the electrode surface. To estimate this effect and its contribution to the discrepancy between charge based isotherm and reflectivity based isotherm measurements we have measured the change of the Au (111) reflectivity as a function of potential in a broad potential range (Figure 3-7A).

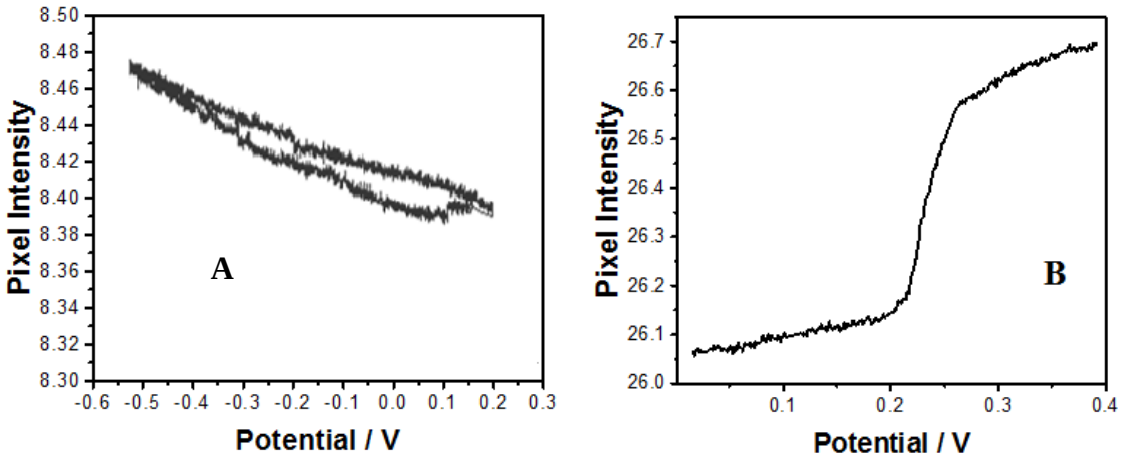

Figure 3-7. Reflected light intensity change during (A) potential sweep in limits of 0.7 V, (B) Pb UPD layer stripping from Au surface with potential sweep in limit of 0.4 V.

We could see that the change of the signal due to a potential change of the Au surface obtained with in the same potential window as during CV of Pb UPD is only a 3% (ΔI=0.03) , Figure 3-7A, of the total signal change obtained during the UPD process (ΔI=0.7), Figure 3-7B. This indicated that the most of the reflectivity change of the Au surface that we have observed is due to a change of the electronic state of Au surface

related to Pb UPD process. More importantly, surface reflectivity measurements are very accurate in recording large change in Pb UPD coverage, $0.1 \leq \theta \leq 0.9$, which is the most relevant for our future SLRR reaction kinetics studies. Therefore, the surface reflectivity system we have built and tested is capable of truthful measurement of the Pb UPD coverage change with minimal discrepancy with the conventional charge integration approach. Thus, the experimental system geometry and light source described under Figure 3-6B and in previous text is confirmed as appropriate to be used in our further studies of the SLRR reaction kinetics.

Obviously, one of the crucial part of our experimental potential-time scheme used in SLRR kinetics study is potential pulse from the value of E_1 (bare Au (111) surface, ΔE=0.7 V - underpotential) to the potential E_2 (ΔE=0.005 V - underpotential) where the full Pb UPD on Au (111) is formed. The time duration of the potential pulse (t_p) is decided after analyzing a set of chrono-amperometric data recorded for the different duration of the pulse time at E_2, and after integration of the current-time transient's data in order to obtain charge-potential pulse time dependence in solutions having different concertation of Pb^{2+} ion. These data are shown in Figure 3-8. One can see that accumulated charge as a function of the length of the potential pulse to E_2 (t_p) saturates in each solution after approximately two to three seconds. This means that shortest necessary time for formation of the full Pb UPD monolayer is ≈ 3 seconds even for the solution with lowest Pb^{2+} ion concentration (10^{-3} M). For this reason, the t_p=3 seconds in all our experiments was adopted knowing that this is the shortest time which ensures complete Pb UPD layer formation even in the solutions that are most diluted in terms of Pb ions.

As previously discussed our SLRR solution contains both Au^{3+} and Pb^{2+} ions. This means that during the potential pulse to E_2, to ensure a formation of Pb UPD layer on Au (111), inevitably some Au^{3+} discharge will occur as a result of overpotential Au deposition together with Pb UPD formation. To assess the magnitude of this effect, and to estimate if there is any potential Au surface roughening, we performed chrono-ameperometric studies in solution containing 0.1 M $HClO_4$ + X M of Au^{3+}, (X=0÷3x10^{-4} M of Au^{3+}) and performing the potential pulse from OCP (no deposition) to E_2 (same potential where Pb UPD would form in SLRR solution with Au co-deposition) with 3 seconds duration. The aim was to estimate how much of the Au is deposited to Au surface in this step, and what percentage of Au monolayer this represents. The data are shown in Figure 3-9.

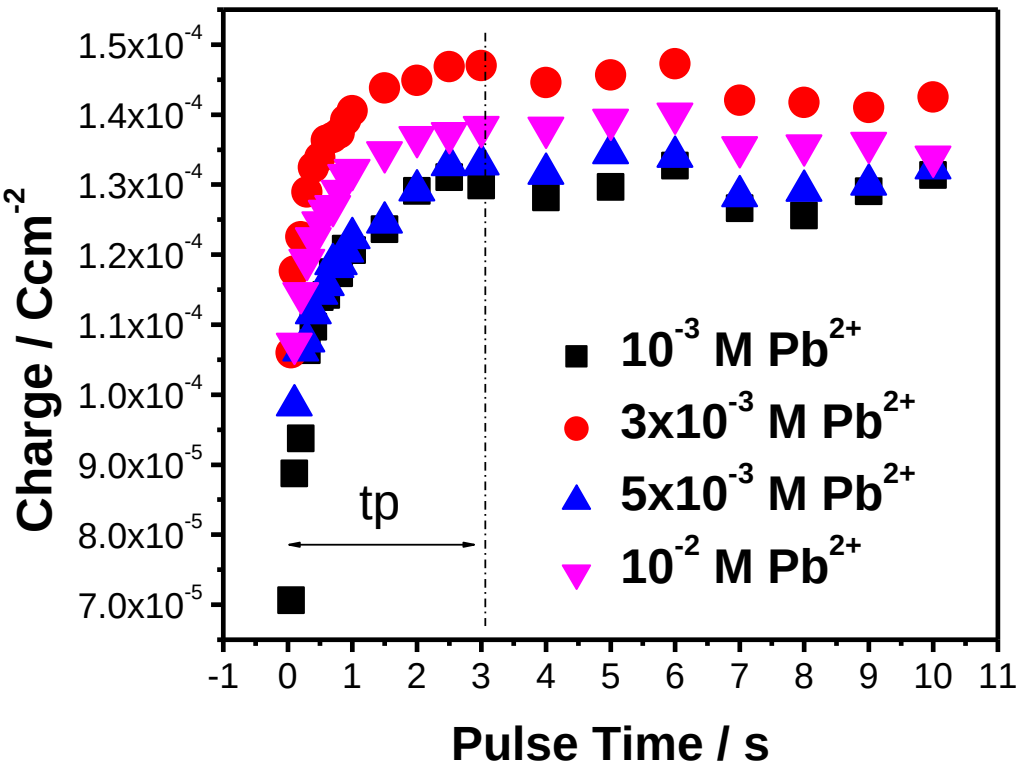

Figure 3-8. Charge-pulse duration at E_2=0.005 V where the full Pb UPD on Au (111) is formed. The base solution is 0.1 M $HClO_4$ + X M Pb^{2+}. The actual molarity of Pb^{2+} in each solution is indicated in the graph.

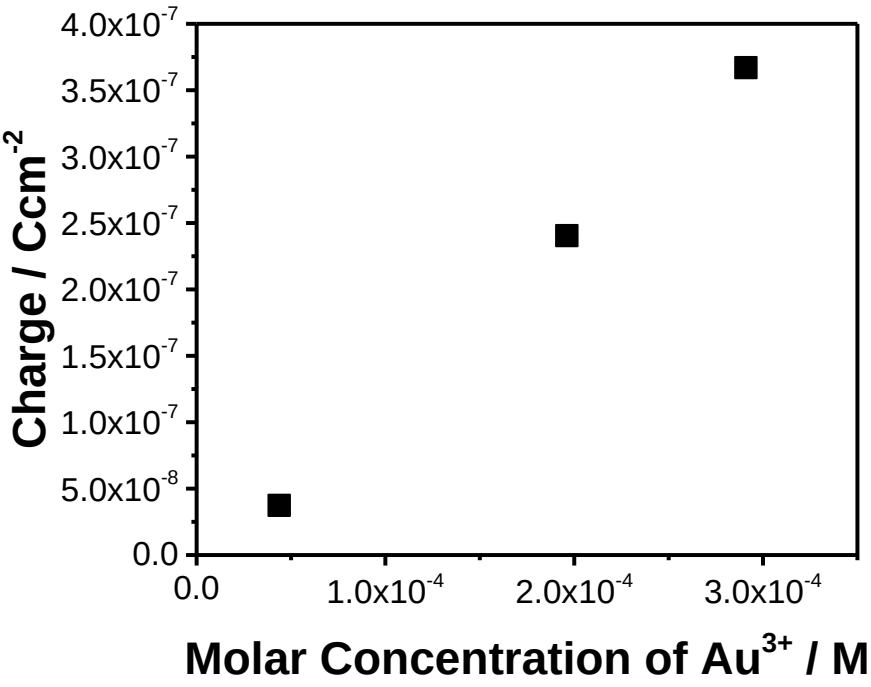

Figure 3-9. Charge accumulated during pulse duration of 3 seconds at E_2=0.005 V underpotential (E_2=-0.4 V vs. SCE) where the full Pb UPD on Au (111) would be formed as a function of Au^{3+} concentration in the solution.

As one can see, the charge accumulated corresponds to Au deposition and increases linearly as the concentration of Au^{3+} in solution is increased. The actual molarity of Au^{3+} can be red from the value on the axis. For the worst case scenario it is necessary to focus to the charge accumulated during Au deposition from $3x10^{-4}$ M solution as the upper limit of our experimental routine for SLRR kinetics studies (most concentrated Au^{3+} solution). The total charge is $\approx 4x10^{-7}$ Ccm^{-2}. The charge of full Au monolayer assuming it is formed from Au^{3+} ions on Au (111) with atomic areal density

of $1.5x10^{15}$ cm^{-2} is $7.2x10^{-4}$ Ccm^{-2}. Obliviously, the amount of Au co-deposited with Pb UPD is less than 1/1000 of a gold monolayer. This is very small amount of Au co-deposited with Pb UPD layer on the surface and we assume it is immediately covered with Pb UPD adatoms since the concentration of Pb^{2+} in each experiment is much larger than Au^{3+}. The Pb UPD process occurs much faster than Au deposition as indicated by the relative charge difference accumulated during the potential pulse in Pb^{2+} only and Au^{3+} only containing solutions (Figure 3-8 vs. Figure 3-9, about 1000 times faster). Therefore we can assume that the Au co-deposition with Pb UPD does not affect the morphology of our surface, and that the conditions at the potential E_2 truly correspond to Au surface covered with full Pb UPD layer.

3.10. SLRR Experimental Procedure in One Cell Configuration

In general, redox replacement of UPD monolayer is initialized with the UPD monolayer of the metal *M* on the *S(h,k,l)* substrate. The formed monolayer of metal *M* serves as a sacrificial material to allow deposition of a more noble metal *P*. After obtaining the required UPD monolayer coverage of the metal *M*, process is completed by immersion of the crystal in a more noble metal solution where the sacrificial less noble UPD metal layer is displaced by the more noble metal P^{p+} ions at the open circuit potential (OCP). Instead of this traditional method, we used **one cell configuration** technique for the experimental routine for Au deposition by SLRR of Pb(UPD)/Au(lll) (Figure 3-10). "*One cell, one solution*" configuration which was used by Fayette et al. in 2011 simplified the process significantly. In this technique, we used a solution which contains both ions (Pb^{2+} and Au^{3+}) involved in the SLRR reaction in this step (Figure 3-

10). Before each experiment, we run a few cycles of CVs to make sure the surface is good enough to proceed in the experimental routine. The cathodic current at the more negative limit in the anodic direction sweep during CV is also used to estimate zero order reaction rate constant (TLRR), k_0, for Pb UPD oxidation by O_2 from the solution using the literature data for D_{O_2}, $C_{O_2}^{\infty}$, δ, and Γ_{Pb}^{UPD}.

The basic procedure for our experiments is given as below.

- The crystal is immersed in 10^{-3}M Pb^{2+} + 0.1M $HClO_4$ base solution and deaerated for two hours.
- Camera iris and shutter are adjusted and tested for optimum intensity change.
- Cyclic voltammogram is performed.
- SLRR reaction routine is performed in 10^{-3}M Pb^{2+} + 0.1M $HClO_4$ base solution to observe effect of oxygen reduction during SLRR.

  Step 1: Potentiostat is set to step function starting from 0.7 V (E_1) (Figure 3-11).

  Step 2: Potential stepped to 0.005 V (E_2) where full UPD monolayer coverage occurs and stayed at that potential for 3 seconds (Figure 3-11).

  Step 3: After 3 seconds, applied potential is off, and cell is at OCP. This is the step where SLRR reaction takes place (Figure 3-11).
- After completing SLRR to measure oxygen reduction kinetics, a 3 ml 10^{-4} M $AuCl_3$ solution is added to the cell, and the new solution which contains both Pb^{2+} and Au^{3+} ions are deaerated for 4-5 minutes. Then, three steps above are repeated for this new solution and data recorded.

- After that, another 3 ml 10^{-4} M $AuCl_3$ solution is added to the cell, electrolyte is again deaerated for another 4-5 minutes, and SLRR reaction routine is repeated for this new concentration.
- Later, SLRR routine is repeated again for different concentrations of Au^{3+} by adding another 3 ml 10^{-4} M $AuCl_3$ solution each time to examine the effect of gold concentration in the electrolyte. These experimental data are collected and analyzed up to 8 different Au^{3+} concentrations.

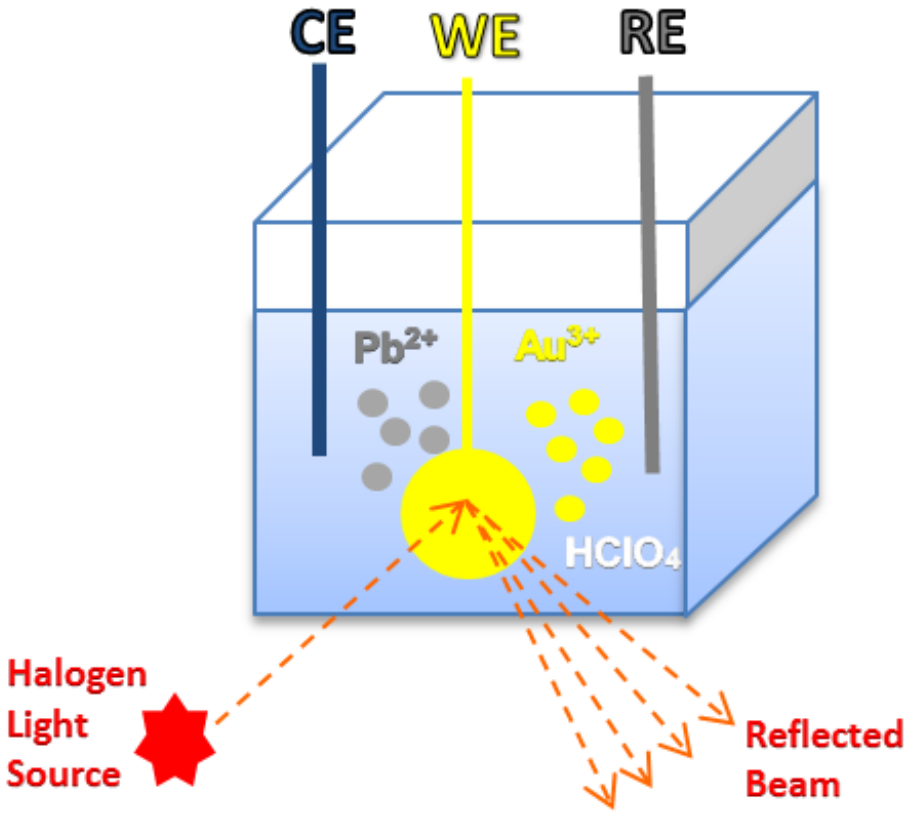

Figure 3-10. Sketch of one cell configuration of electrochemical cell used for SLRR reaction system.

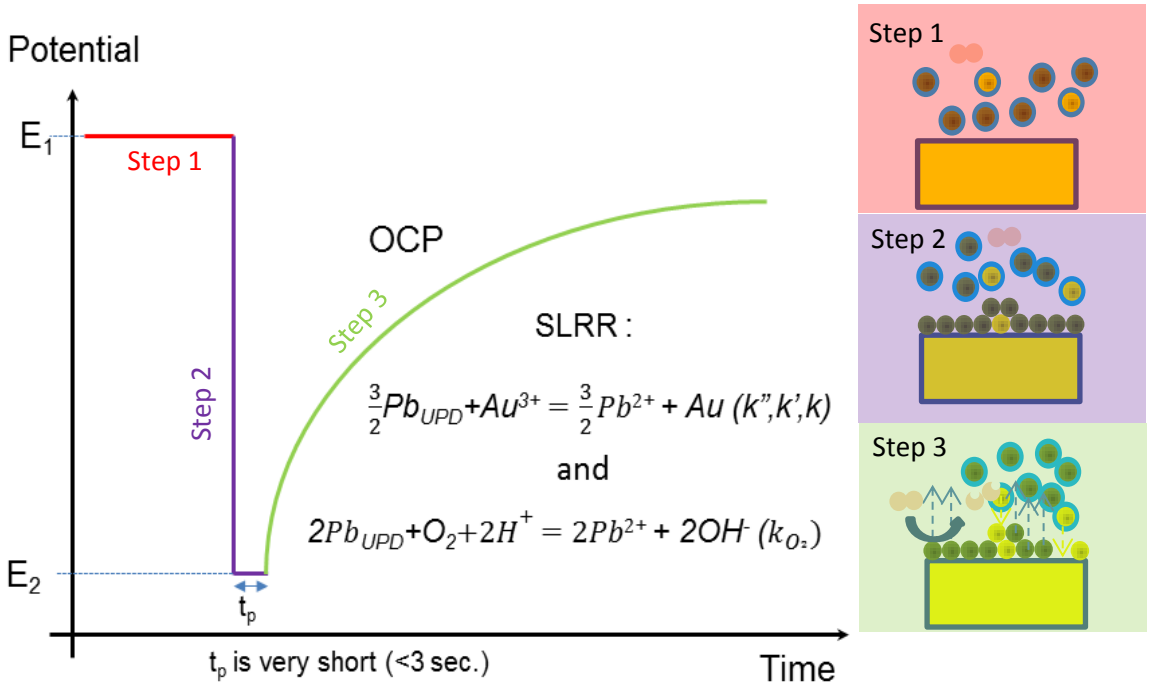

Figure 3-11. Sketch of SLRR reaction system.

Figure 3-10 illustrates our one cell configuration for the SLRR reaction system. Here, our electrochemical cell holds our three electrodes as it was mentioned earlier. Working electrode is our Au (111) crystal on which we shine the light. The incident beam hits on the crystal surface and reflects to the camera by an integrating mirror. We examine our OCP data and intensity data which were saved during our experiment to investigate and compare reaction rates. In the Figure 3-11, red line represents Step 1 on which, potential E_1 is applied to the working electrode (WE). In our case it was selected as 0.7 V due to the fact that there is no lead UPD at this potential. Then, Step 2 is represented with purple in the graph (Figure 3-11). Here, the cell potential is stepped to E_2 and stayed at this potential for t_p (3 seconds in our case). During this step, underpotential depositon of lead takes place with a very small Au co-deposition. The amount of Au co-deposition can be neglected since it is 1/1000 of a gold monolayer as it

was mentioned earlier. 3 seconds is the optimum time for UPD reaction for our experimental conditions and it is chosen according to the experiment which has the smallest lead concentration in the solution (10^{-3}M Pb^{2+} + 0.1 M $HClO_4$). Then after 3 seconds, the cell voltage is cut off and step 3 begins. This step is represented with the green line in the graph. During this step, cell potential goes to OCP and two parallel SLRR reactions take place as it was mentioned earlier.

Even though the solution is deaerated for two hours, there will still be some oxygen content left in solution. Due to this oxygen content, two parallel reactions, which will be explained in detail in the next chapter, will take place during our SLRR experiment. One of them is oxygen reduction SLRR reaction, and the other one is Au deposition SLRR of Pb_{UPD}.

Chapter 4: Results and Discussions

4.1. Model Equations of Reaction Kinetics for Au deposition via SLRR of Pb UPD Monolayer on Au (111)

The main SLRR reaction occurring during Au deposition in our experiments is presented below with corresponding stoichiometry

$$Pb^{0}_{UPD}/Au(111)+\frac{2}{3}Au^{3+}_{solv}\rightarrow Pb^{2+}_{solv}+\frac{2}{3}Au^{0}_{s}/Au(111). \quad (4\text{-}1a)$$

The initial studies using reflectivity and OCP measurements show that this reaction follows first order reaction kinetics. The general description of this process is discussed previously in the introduction, and here we just mention brief remarks. The first reaction kinetics in terms of lead UPD monolayer coverage change in time is represented by Eq. (4-2) as

$$\theta=\theta_0 e^{-k't}. \quad (4\text{-}2)$$

For all experiments, the conditions are such that θ_0 is 1 so that the Eq. (4-2) is simplified to

$$\theta=e^{-k't}. \quad (4\text{-}3)$$

The details of the *k'* definition is described in the introduction part of the thesis.

On the other hand, the Pb UPD monolayer oxidation also occurs via oxygen reduction which also represents a SLRR reaction. The traces of dissolved oxygen in solution cannot be removed completely and this means that Pb UPD monolayer oxidation by oxygen reduction always occurs in parallel to main process which is Au deposition.

The Pb UPD oxidation via oxygen reduction is SLRR reaction with corresponding stoichiometry written as

$$Pb^{0}_{UPD}/Au(111)+O_2+2H^{+}\rightarrow Pb^{2+}+2OH^{-}. \quad (4\text{-}1b)$$

The initial study and measurements show that the level of dissolved oxygen is of order of 10^{-6} M which also leads to conditions that reaction kinetics of this SLRR is controlled by transport, i.e., follows zero order reaction kinetics. Assuming that starting Pb UPD layer coverage is 1, the Pb UPD coverage as a function of time during this reaction can be written in terms of reaction rate constant, $k_{0,}$ as

$$\theta = 1-k_0 t\,. \quad (4\text{-}4)$$

As described in introduction part, the k_0 is function of the surface concentration of Pb UPD monolayer at coverage 1, stoichiometry coefficients, bulk concentration of oxygen molecules, oxygen diffusivity in solution, and diffusion layer thickness. For the Pb UPD monolayer oxidation via oxygen reduction described by Eq. (4-5), the k_0 is described as

$$k_0 = \left(\frac{1}{2}\right)\cdot\frac{D_{O_2}\cdot C^{\infty}_{O_2}}{\Gamma^{UPD}_{Pb}\cdot\delta}\,. \quad (4\text{-}5)$$

The Eq. (4-4) is used fit the θ vs. t transients obtained from reflectivity measurements in solutions where no Au^{3+} ions are present and only Pb UPD monolayer oxidation occurs via oxygen reduction, Eq. (4-1b). For the same case, the model used to analyze the OCP data is obtained by combining the Eq. (4-4) with *Bruckenstein-Swathirajan* (BS) isotherm (Gokcen, 2011) as

$$E = E_{\theta\rightarrow 0} - 0.013\,\mathrm{V}\cdot\left[\ln\left(\frac{1-k_0 t}{k_0 t}\right)+ f\cdot(1-k_0 t)+ g\cdot(1-k_0 t)^{3/2}\right]. \quad (4\text{-}6)$$

The details in the model are already described in the introduction part. However, when both Au^{3+} and dissolved O_2 molecules are present in the solution, both SLRR reactions occur in parallel, Eq. (4-1a) and Eq. (4-1b). To take this into account, and to some extent eliminate the effect of oxygen on the measurements of reaction kinetics of Au deposition via SLRR of Pb UPD monolayer, we derived new rate/model equations which are used for θ vs. t transient's analysis and OCP transients' analysis during our deposition experiments.

The change of the Pb UPD layer coverage in time when both Au^{3+} and O_2 are present in solution can be presented as the first order linear differential equation with constant coefficients, k' and k_0. One should note that k' is the rate constant of for Au deposition via SLRR of Pb UPD monolayer, Eq. (4-1a), and k_0 is the rate constant for Pb UPD oxidation/dissolution via oxygen reduction occurring at transport limited control, Eq. (4-1b). The change in the coverage which takes both reactions (Eq. (4-1a) and Eq. (4-1b)) can be expressed as

$$-\frac{d\theta}{dt} = k'\theta + k_0 . \tag{4-3a}$$

After re-arrangement, it can be written as

$$\frac{d\theta}{dt} + k'\theta = -k_0 . \tag{4-3b}$$

By multiplying both sides by $e^{k't}$, it will be

$$e^{k't}\frac{d\theta}{dt} + ke^{k't}\theta = -k_0 e^{k't} . \tag{4-3c}$$

If we substitute $ke^{k't} = \frac{de^{k't}}{dt}$ in Eq. (4-3c) , we get

$$e^{k't}\frac{d\theta}{dt}+\frac{de^{k't}}{dt}\theta=-k_0e^{k't}. \qquad \text{Eq. (4-3d)}$$

After applying the product rule of derivation [$(fg)'=f'g+g'f$, here, $f=\theta$ and $g=e^{k't}$], we get

$$\frac{d}{dt}e^{k't}\theta=-k_0e^{k't}. \qquad \text{Eq. (4-3e)}$$

The both sides of equation now can be integrated as

$$\int\frac{d}{dt}e^{k't}\theta dt=\int-k_0e^{k't}dt \qquad \text{Eq. (4-3f)}$$

which leads to the solution with free constant as

$$e^{kt}\theta=-\frac{k_0}{k'}e^{k't}+const. \qquad \text{Eq. (4-3g)}$$

Solving for θ, we get

$$\theta=(e^{-k't}const)-\frac{k_0}{k'}. \qquad \text{Eq. (4-3h)}$$

From boundary and initial conditions we can evaluate the constant. For t=0, θ=1, and it follows that $constant=(1+\frac{k_0}{k'})$. Therefore, the model rate equation so called, O_2 corrected first order rate equation, is defined as

$$\theta(t)=(1+\frac{k_0}{k'})e^{-k't}-\frac{k_0}{k'}. \qquad (4\text{-}7)$$

This equation is used to analyze θ vs. t transients form our reflectivity measurements.

Similarly, combining the Eq. (4-7) with BS isotherm (Eq. (1-7)), we can get the O_2 corrected first order rate equation that can be used to model the OCP transients from our deposition experiments. The final equation used to model OCP transients from deposition experiments is presented as

$$E = E_{\theta\to 0} - 0.013\,\mathrm{V}\left\{\ln\frac{\left((1+\frac{k_0}{k'})e^{(-k't)} - \frac{k_0}{k'}\right)}{\left(1+\frac{k_0}{k'} - (1+\frac{k_0}{k'})e^{(-k't)}\right)} + f\left((1+\frac{k_0}{k'})e^{(-k't)} - \frac{k_0}{k'}\right) + g\left((1+\frac{k_0}{k'})e^{(-k't)} - \frac{k_0}{k'}\right)^{3/2}\right\}. \quad (4\text{-}8)$$

4.2. Effect of Au^{3+} Concentration on Reaction Kinetics of Au deposition via SLRR of Pb UPD Monolayer

4.2.1 Rate Constants Obtained from Surface Reflectivity Measurements

The first set of results represents eight measurements of reaction kinetics for Au deposition via SLRR of Pb UPD obtained from reaction solution containing 0.1 M $HClO_4$ + 10^{-3} M Pb^{2+} + X M Au^{3+} (X=0; 4.3×10^{-5} M; 8.5×10^{-5} M; 1.2×10^{-4} M; 1.6×10^{-4} M; 2.0×10^{-4} M; 2.3×10^{-4} M; and 2.6×10^{-4} M). The individual Pb UPD coverage transients measurements data together with model equation fits to extract the rate constant are shown in Figure 4-1. Here, fits of the rate equation to the data are shown with red line and the experimental data are represented with black circles. The Figure 4-1A is the experiment where solution did not contain Au^{3+} ions and this Pb UPD coverage transient is fitted with Eq. (4-4) to extract the value of k_0 which is the rate constant for Pb UPD oxidation/dissolution via oxygen reduction reaction. The obtained value of k_0 is then used as a parameter in the model represented by Eq. (4-7) - oxygen corrected first order reaction kinetics, to fit the data in Figure 4-1(B-H) and extract the value of rate constant *k'* as a function of the Au^{3+} concentration. The obtained values of *k'* for this reaction solution are plotted as function of the Au^{3+} concentration in Figure 4-5 - black squares

and they are summarized in Table 4-1. As one can see, the model equation used succeeds very well in interpretation of the experimental data (Figure 4-1). In each case, the quality of the fits obtained was characterized by r^2 values better than 0.98. The obtained dependence of *k'* vs. [Au^{3+}] is linear and shows increase in *k'* value with increasing concentration of gold ions. Considering previous work of Gokcen et al. (2011) the *k'* is defined as

$$k' = k\left(C_P^{is}\right)^L . \tag{4-9}$$

Here, *k* is the fundamental rate constant, while $C_{Au^{3+}}^{is}$ is the surface concentration in [mol/cm^2] of Au^{3+} ions at the gold electrode surface which are participating in the SLRR reaction. The exponent *L* is the order of the SLRR reaction in terms of surface concentration of Au^{3+} ions, $C_{Au^{3+}}^{is}$. The surface concentration of Au^{3+} at the electrode surface could be approximately expressed as a product of the interface width, ξ=0.5x10^{-9} m (Smickler 2010), and the bulk value of Au^{3+} concentration in the solution ($C_{Au^{3+}}^{\infty}$ or [Au^{3+}] notation),

$$C_{Au^{3+}}^{is} = C_{Au^{3+}}^{\infty} \cdot \xi . \tag{4-10}$$

Therefore, we can rewrite the expression for k' in terms of bulk Au^{3+} concentration as

$$k' = k\left(C_P^{is}\right)^L = k\left(C_{Au^{3+}}^{\infty} \cdot \xi\right)^L = k \cdot \xi^L \cdot \left(C_{Au^{3+}}^{\infty}\right)^L . \tag{4-11}$$

Obviously, following from his discussion, the linear trend in our *k'* vs. [Au^{3+}] data, Figure 4-5, indicates that the value of *L* is 1, i.e., that the Au deposition via SLRR of Pb UPD monolayer is the first order in terms of bulk Au^{3+} ion concentration. To some extent this was expected if we assume that Au deposition via SLRR of Pb UPD monolayer is elementary reaction, and that stoichiometry coefficients can be taken as the order of the

chemical reaction in terms of its reactants. From stoichiometry of the SLRR reaction, Eq. (4-3), one Au atom reacts with 1.5 Pb UPD atoms, and therefore, one can assume L=1 which is experimentally confirmed in our study.

Table 4-1. Summary of reaction rate constants from intensity model equation for reaction solution containing 0.1 M $HClO_4$ + 10^{-3} M Pb^{2+} + X M Au^{3+}.

Base Electrolyte: 0.1 M $HClO_4$ + 10^{-3} M Pb^{2+}								
[Au^{3+}] / M	**0**	**4.3×10^{-5}**	**8.5×10^{-5}**	**1.2×10^{-4}**	**1.6×10^{-4}**	**2.0×10^{-4}**	**2.3×10^{-4}**	**2.6×10^{-4}**
k' or k_0 /s^{-1}	0.00873	0.02039	0.08058	0.09296	0.15288	0.19537	0.24296	0.27780
±σ / s^{-1}	4.76E-5	0.00002	0.00073	0.00099	0.00179	0.00338	0.00230	0.00384

The second set of results represents eight measurements of reaction kinetics for Au deposition via SLRR of Pb UPD obtained from reaction solution containing 0.1 M $HClO_4$ + $3x10^{-3}$ M Pb^{2+} + X M Au^{3+} (X=0; $4.3x10^{-5}$ M; $8.5x10^{-5}$ M; $1.2x10^{-4}$ M; $1.6x10^{-4}$ M; $2.0x10^{-4}$ M; $2.3x10^{-4}$ M; and $2.6x10^{-4}$ M). The individual Pb UPD coverage transients measurements data together with model equation fits to extract the rate constant are shown in Figure 4-2. Here, fits of the rate equation to the data are shown with red line and the experimental data are represented with black circles. The Figure 4-2A is the experiment where solution did not contain Au^{3+} ions and this Pb UPD coverage transient is fitted with Eq. (4-4) to extract the value of k_0 which is the rate constant for Pb UPD oxidation/dissolution via oxygen reduction reaction. The obtained value of k_0 is then used as a parameter in the model represented by Eq. (4-7) - oxygen corrected first order reaction kinetics to fit the data in Figure 4-2(B-H) and extract the value of rate constant k' as a function of the Au^{3+} concentration in reaction solution. The obtained values of k' for this reaction solution is plotted as function of the Au^{3+} concentration in Figure 4-5 - green diamonds and they are summarized in Table 4-2.

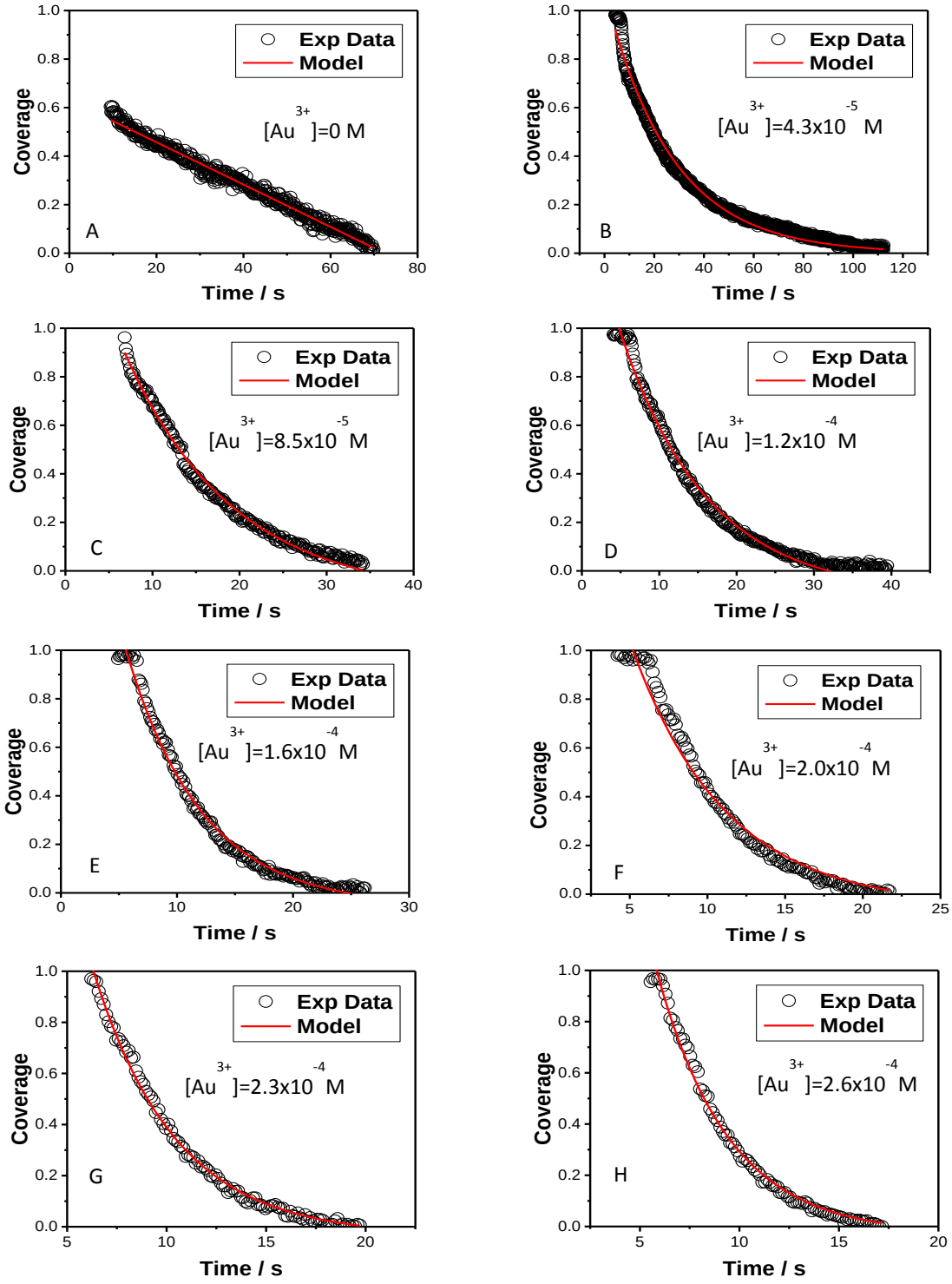

Figure 4-1. The Pb UPD monolayer coverage transients obtained from surface reflectivity measurements in solution: 0.1 M $HClO_4$ + 10^{-3} M Pb^{2+} + X M Au^{3+}.

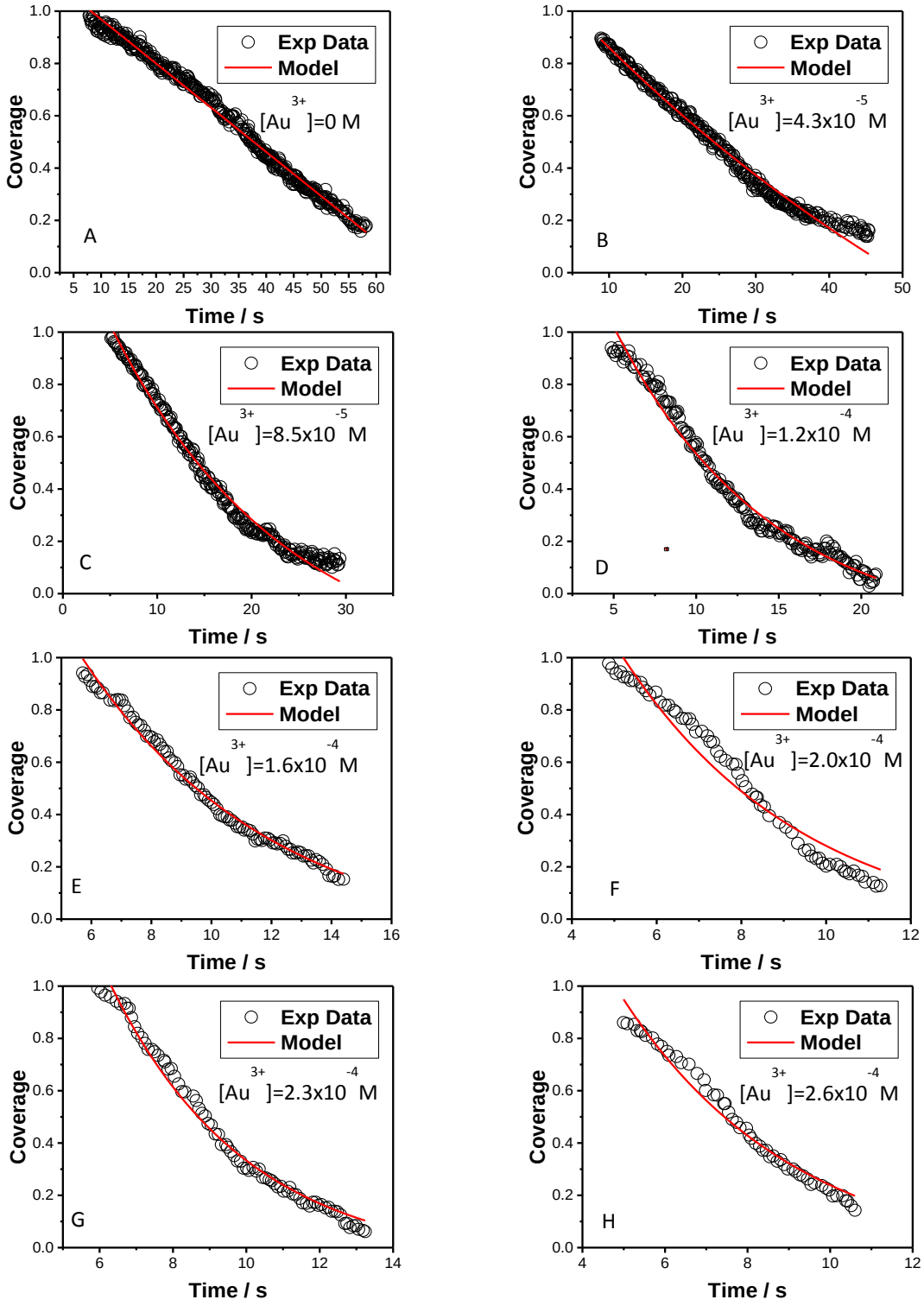

Figure 4-2. The Pb UPD monolayer coverage transients obtained from surface reflectivity measurements in solution: 0.1 M $HClO_4$ + $3x10^{-3}$ M Pb^{2+} + X M Au^{3+}.

As one can see, the model equation used in our study succeeds very well in interpretation of the experimental data, Figure 4-2. In each case, the quality of the fits obtained was characterized by r^2 values better than 0.96. The same as in previous case, obtained dependence of *k'* vs. [Au^{3+}] is linear showing an increase in *k'* value as the concentration of Au ions in the solution is increased. This reconfirms the *L*=1, in terms of Au^{3+} reactants as discussed previously. One important thing that is observed is that an increased concentration of Pb^{2+} in reaction solution leads to a slightly higher value of *k'*. This trend will be re-examined latter in more details.

Table 4-2. Summary of reaction rate constants from intensity model equation for reaction solution containing 0.1 M $HClO_4$ + 3x10^{-3} M Pb^{2+} + X M Au^{3+}.

Base Electrolyte: 0.1 M $HClO_4$ + 3x10^{-3} M Pb^{2+}								
[Au^{3+}] / M	**0**	**4.3×10^{-5}**	**8.5×10^{-5}**	**1.2×10^{-4}**	**1.6×10^{-4}**	**2.0×10^{-4}**	**2.3×10^{-4}**	**2.6×10^{-4}**
***k'* or k_0 /s^{-1}**	0.01690	0.01232	0.05409	0.10597	0.15789	0.23217	0.26798	0.23780
$\pm\sigma$/ s^{-1}	7.12E-5	3.13E-4	0.00070	0.00152	0.00218	0.00860	0.004773	0.00631

The third set of results represents eight measurements of reaction kinetics for Au deposition via SLRR of Pb UPD obtained from reaction solution containing 0.1 M $HClO_4$ + 5x10^{-3} M Pb^{2+} + X M Au^{3+} (X=0; 4.3x10^{-5} M; 8.5x10^{-5} M; 1.2x10^{-4} M; 1.6x10^{-4} M; 2.0x10^{-4} M; 2.3x10^{-4} M; and 2.6x10^{-4} M). The individual Pb UPD coverage transients measurements data together with model equation fits to extract the rate constant are shown in Figure 4-3. Here, fits of the rate equation to the data are shown with red line and the experimental data are represented with black circles. The Figure 4-3A is the experiment where solution did not contain Au^{3+} ions and this Pb UPD coverage transient is fitted with Eq. (4-4) to extract the value of k_0 which is the rate constant for Pb UPD

oxidation/dissolution via oxygen reduction reaction. The obtained value of k_0 is then used as a parameter in the model represented by Eq. (4-7) - oxygen corrected first order reaction kinetics, to fit the data in Figure 4-3(B-H) and extract the value of rate constant *k'* as a function of the Au^{3+} concentration in reaction solution. The obtained values of *k'* for this reaction solution is plotted as function of the Au^{3+} concentration in Figure 4-5 - blue-gray triangles and they are summarized in Table 4-3. As in previous case, the model equations used in our study succeed very well in interpretation of the experimental data, Figure 4-3. The quality of the fits obtained was characterized by r^2 values which were in each individual case better than 0.96. As previously discussed, the obtained dependence of *k'* vs. [Au^{3+}] is linear and shows an increase in *k'* value as the concentration of Au ions in the solution is increased. This again reconfirms the *L*=1, in terms of Au^{3+} reactant as we have discussed previously. The increased concentration of Pb^{2+} in reaction solution leads to a higher value of *k'*.

Table 4-3. Summary of reaction rate constants from intensity model equation for reaction solution containing 0.1 M $HClO_4$ + 5x10^{-3} M Pb^{2+} + X M Au^{3+}.

Base Electrolyte: 0.1 M $HClO_4$ + 5x10^{-3} M Pb^{2+}								
[Au^{3+}] / M	**0**	**4.3×10^{-5}**	**8.5×10^{-5}**	**1.2×10^{-4}**	**1.6×10^{-4}**	**2.0×10^{-4}**	**2.3×10^{-4}**	**2.6×10^{-4}**
***k'* or k_0 /s^{-1}**	0.00467	0.03897	0.09899	0.17997	0.24319	0.29162	0.34231	0.37922
$\pm\sigma$ / s^{-1}	1.45E-4	0.00020	0.00067	0.00152	0.00206	0.00375	0.00363	0.00718

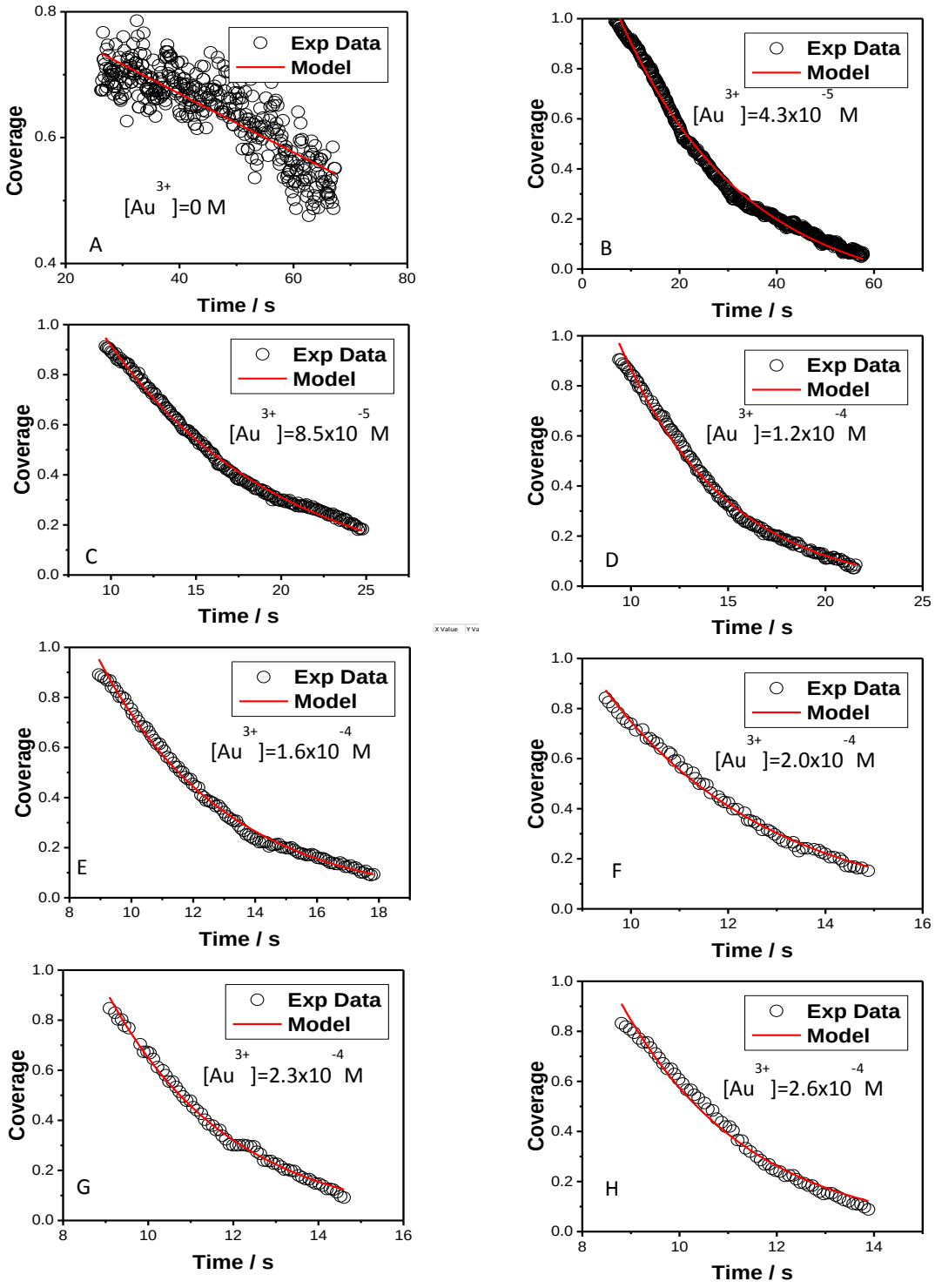

Figure 4-3. The Pb UPD monolayer coverage transients obtained from surface reflectivity measurements in solution: 0.1 M $HClO_4$ + $5x10^{-3}$ M Pb^{2+} + X M Au^{3+}.

The fourth set of results represents eight measurements of reaction kinetics for Au deposition via SLRR of Pb UPD obtained from reaction solution containing 0.1 M $HClO_4$ + 10^{-2} M Pb^{2+} + X M Au^{3+} (X=0; $4.3x10^{-5}$ M; $8.5x10^{-5}$ M; $1.2x10^{-4}$ M; $1.6x10^{-4}$ M; $2.0x10^{-4}$ M; $2.3x10^{-4}$ M; and $2.6x10^{-4}$ M). The individual Pb UPD coverage transients measurements data together with model equation fits to extract the rate constant are shown in Figure 4-4. Here, fits of the rate equation to the data are shown with red line and the experimental data are represented with black circles. The Figure 4-4A is the experiment where solution did not contain Au^{3+} ions and this Pb UPD coverage transient is fitted with Eq. (4-4) to extract the value of k_0 which is the rate constant for Pb UPD oxidation/dissolution via oxygen reduction reaction. The obtained value of k_0 is then used as a parameter in the model represented by Eq. (4-7) - oxygen corrected first order reaction kinetics, to fit the data in Figure 4-3(B-H) and extract the value of rate constant k' as a function of the Au^{3+} concentration in reaction solution. The obtained values of k' for this reaction solution is plotted as function of the Au^{3+} concentration in Figure 4-5 - red circles and they are summarized in Table 4-4. As in previous cases, the model equations provided very good fits of our experimental data, Figure 4-4. The r^2 values in each individual fit were better than 0.98. As it was previously discussed, the obtained dependence of k' vs. [Au^{3+}] is linear showing an increase in k' value as the concentration of Au ions in the solution is increased. This again reconfirms the L=1, in terms of Au^{3+} reactant as previous data suggested as well. The further increase in concentration of Pb^{2+} in reaction solution leads to a much higher values of k' measured.

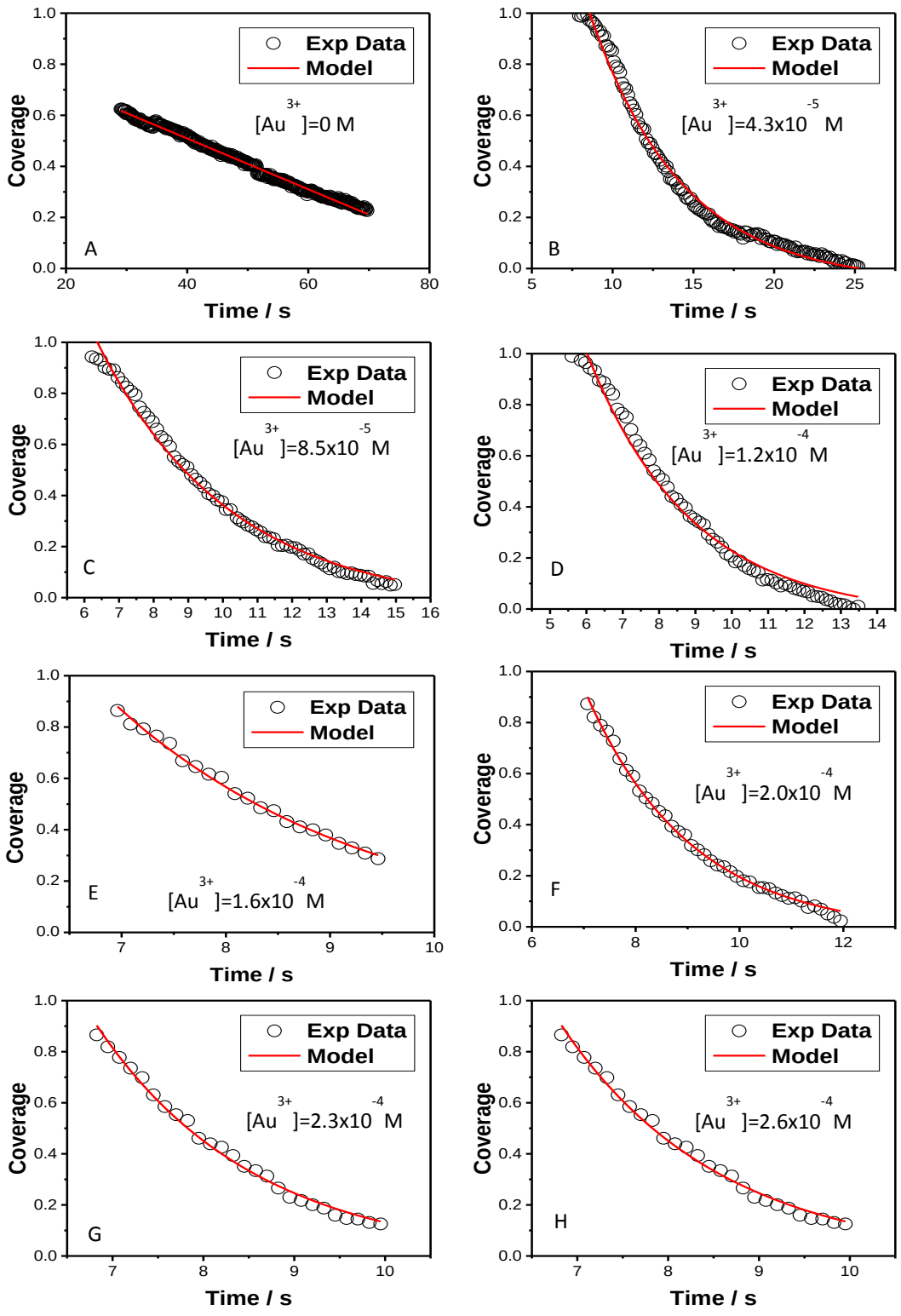

Figure 4-4. The Pb UPD monolayer coverage transients obtained from surface reflectivity measurements in solution: 0.1 M $HClO_4$ + 10^{-2} M Pb^{2+} + X M Au^{3+}.

Table 4-4. Summary of rate constants from intensity model equation for reaction solution containing 0.1 M $HClO_4$ + 10^{-2} M Pb^{2+} + X M Au^{3+}.

Base Electrolyte: 0.1 M $HClO_4$ + 10^{-2} M Pb^{2+}								
$[Au^{3+}]$ / M	**0**	**4.3×10^{-5}**	**8.5×10^{-5}**	**1.2×10^{-4}**	**1.6×10^{-4}**	**2.0×10^{-4}**	**2.3×10^{-4}**	**2.6×10^{-4}**
***k'* or k_0 /s^{-1}**	0.00994	0.17487	0.26258	0.34861	0.40956	0.49651	0.57528	0.65082
$\pm\sigma$/ s^{-1}	4.53E-5	0.00235	0.00396	0.00879	0.00727	0.00589	0.01149	0.02062

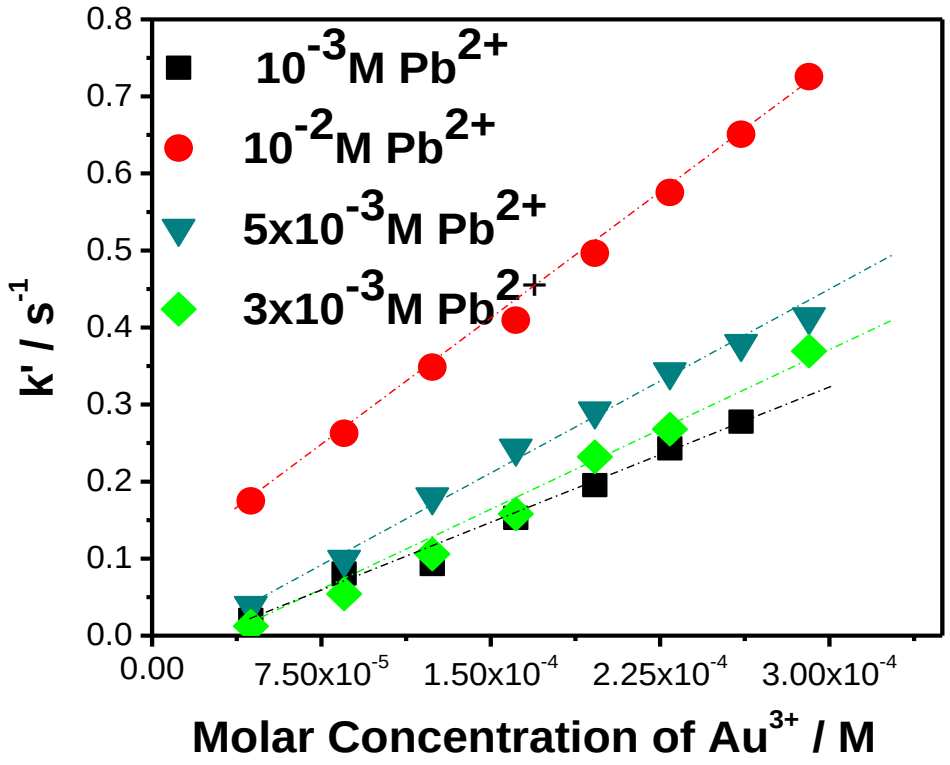

Figure 4-5. The *k'* vs. Au^{3+} concentration dependence obtained from Pb UPD monolayer coverage transients during Au deposition via SLRR of Pb UPD monolayer with reaction solution for different concentration of Pb^{2+} ions.

4.2.2. Rate Constants Obtained from OCP Transients Measurements

The first set of results represents eight measurements of reaction kinetics for Au deposition via SLRR of Pb UPD obtained from reaction solution containing 0.1 M $HClO_4$

+ 10^{-3} M Pb^{2+} + X M Au^{3+} (X=0; $4.3x10^{-5}$ M; $8.5x10^{-5}$ M; $1.2x10^{-4}$ M; $1.6x10^{-4}$ M; $2.0x10^{-4}$ M; $2.3x10^{-4}$ M; and $2.6x10^{-4}$ M). The individual OCP transients measurements data together with model equation fits to extract the rate constant are shown in Figure 4-6. Here, fits of the rate equation to the data are shown with red line and the experimental data are represented with black circles. The Figure 4-6A is the experiment where solution did not contain Au^{3+} ions and this OCP transient is fitted with Eq. (4-6) to extract the value of k_0 which is the rate constant for Pb UPD oxidation/dissolution via oxygen reduction reaction. The obtained value of k_0 is then used as a parameter in the model represented by Eq. (4-8)-oxygen corrected first order reaction kinetics to fit the data in Figure 4-6(B-H) and extract the value of rate constant *k'* as a function of the Au^{3+} concentration. The obtained values of *k'* for this reaction solution is plotted as function of the Au^{3+} concentration in Figure 4-10 -black squares and they are summarized in Table 4-5. From Figure 4-6 it is obvious that the model equations used succeeds very well in interpretation of the experimental OCP transients-data. In each case, the quality of the fits obtained was characterized by r^2 values better than 0.98. The obtained dependence of *k'* vs. [Au^{3+}] is linear showing an increase in k' value with increasing concentration of gold ions. This is the same trend that has been observed in this solution studying Pb UPD coverage transients using surface reflectivity. Thus, the OCP transients analysis and Pb UPD coverage transients analysis are in qualitative agreement reconfirming previous conclusion that the reaction order in terms of the Au^{3+} reactant is 1.

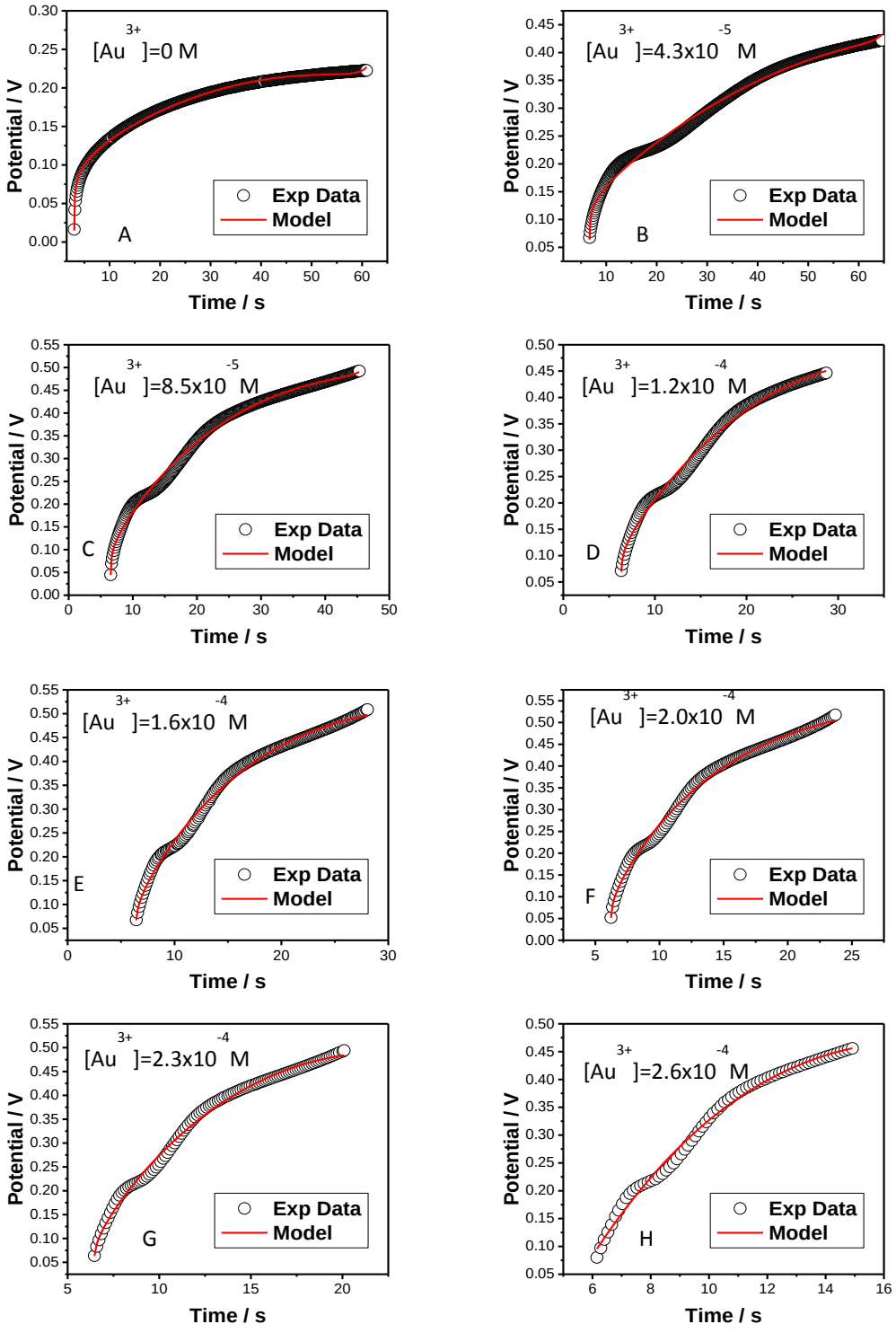

Figure 4-6. The OCP transients obtained during Au deposition via SLRR of Pb UPD monolayer on Au (111) in solution: 0.1 M $HClO_4$ + 10^{-3} M Pb^{2+} + X M Au^{3+}.

Table 4-5. Summary of reaction rate constants extracted from OCP fittings for reaction solution containing 0.1 M $HClO_4$ + 10^{-3} M Pb^{2+} + X M Au^{3+}.

Base Electrolyte: 0.1 M $HClO_4$ + 10^{-3} M Pb^{2+}								
[Au^{3+}] / M	**0**	**4.3×10^{-5}**	**8.5×10^{-5}**	**1.2×10^{-4}**	**1.6×10^{-4}**	**2.0×10^{-4}**	**2.3×10^{-4}**	**2.6×10^{-4}**
***k'* or k_0 /s^{-1}**	0.01693	2.35E-6	0.01788	0.00453	0.03440	0.06150	0.02667	2.35E-6
$\pm\sigma$/ s^{-1}	5.07E-5	0.00028	0.00097	0.01037	0.00952	0.01631	0.01687	0.00028

The second set of results represents eight measurements of reaction kinetics for Au deposition via SLRR of Pb UPD obtained from reaction solution containing 0.1 M $HClO_4$ + $3x10^{-3}$ M Pb^{2+} + X M Au^{3+} (X=0; $4.3x10^{-5}$ M; $8.5x10^{-5}$ M; $1.2x10^{-4}$ M; $1.6x10^{-4}$ M; $2.0x10^{-4}$ M; $2.3x10^{-4}$ M; and $2.6x10^{-4}$ M). The individual OCP transients measurements data together with model equation fits to extract the rate constant are shown in Figure 4-7. Here, fits of the rate equation to the data are shown with red line and the experimental data are represented with black circles. The Figure 4-7A is the experiment where solution did not contain Au^{3+} ions and this OCP transient is fitted with Eq. (4-6) to extract the value of k_0 which is the rate constant for Pb UPD oxidation/dissolution via oxygen reduction reaction. The obtained value of k_0 is then used as a parameter in the model represented by Eq. (4-8) - oxygen corrected first order reaction kinetics to fit the data in Figure 4-7B-H and extract the value of rate constant *k'* as a function of the Au^{3+} concentration in reaction solution. The obtained values of *k'* for this reaction solution is plotted as function of the Au^{3+} concentration in Figure 4-10 - red circles and they are summarized in Table 4-6. From Figure 4-7 it is evident that the model equations used in our study succeed very well in interpretation of the experimental OCP data. This is illustrated by r^2 values being better than 0.92 in each individual fit.

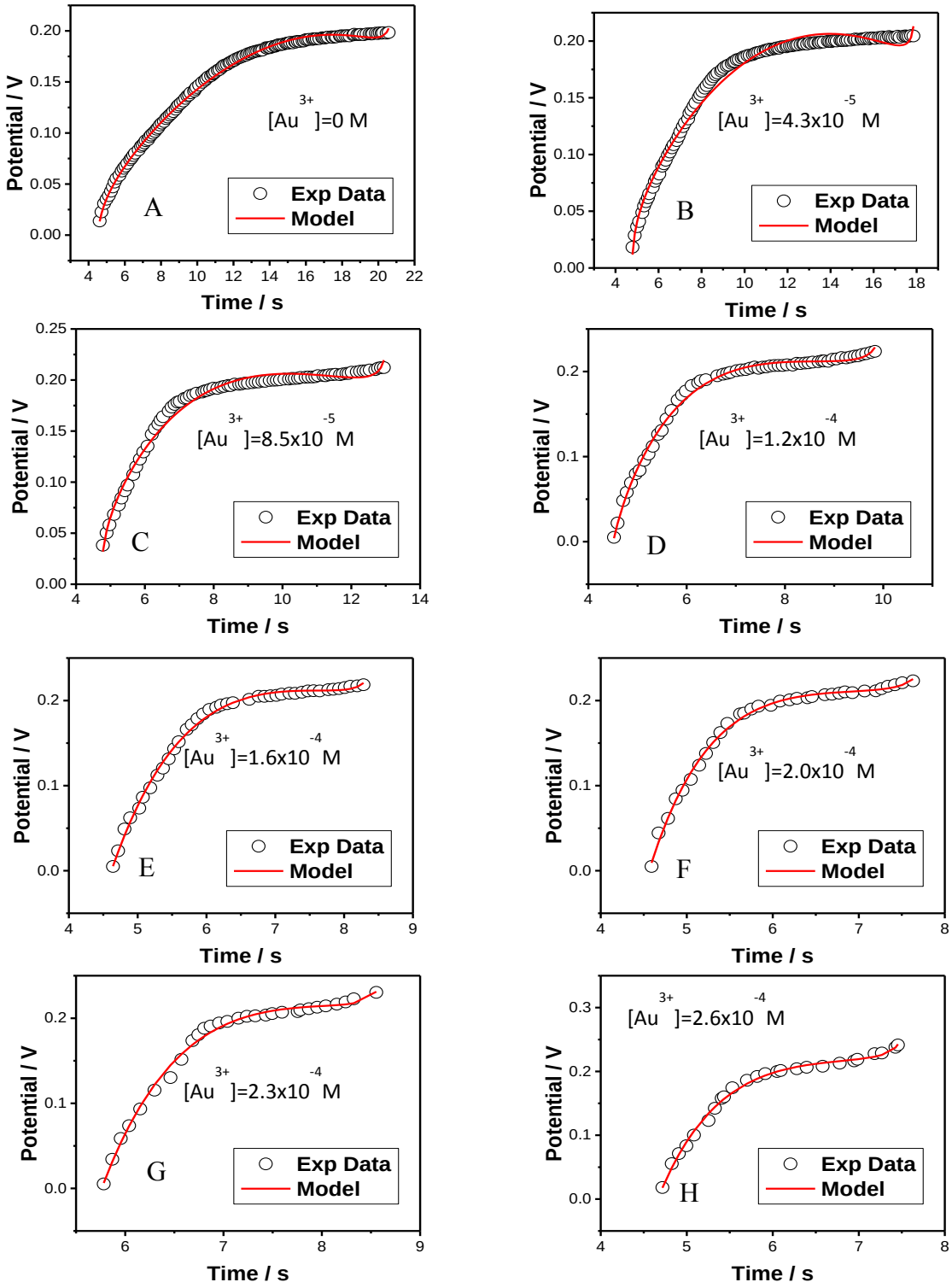

Figure 4-7. The OCP transients obtained during Au deposition via SLRR of Pb UPD monolayer in solution: 0.1 M $HClO_4$ + $3x10^{-3}$ M Pb^{2+} + X M Au^{3+}.

The same as in previous case, the obtained dependence of *k'* vs. [Au^{3+}] is linear showing an increase in *k'* value as the concentration of Au ions in the solution is increased. This reconfirms the *L*=1, in terms of Au^{3+} reactants as discussed previously. One important thing that is observed is that an increased concentration of Pb^{2+} in reaction solution leads to a slightly higher value of *k'*. The OCP data analysis and observed trend is in qualitative agreement with the previous results and trend obtained from reaction kinetics study using surface reflective. It is apparent, that OCP transient analysis yields the overall *k'* values which are slightly larger than the ones obtained from surface reflectivity studies in the same solution.

Table 4-6. Summary of reaction rate constants extracted from OCP fittings for reaction solution containing 0.1 M $HClO_4$ + $3x10^{-3}$ M Pb^{2+} + X M Au^{3+}.

Base Electrolyte: 0.1 M $HClO_4$ + $3x10^{-3}$ M Pb^{2+}								
[Au^{3+}] / M	**0**	**4.3×10^{-5}**	**8.5×10^{-5}**	**1.2×10^{-4}**	**1.6×10^{-4}**	**2.0×10^{-4}**	**2.3×10^{-4}**	**2.6×10^{-4}**
***k'* or k_0 /s^{-1}**	0.06124	0.03147	0.14762	0.34060	0.41915	0.67855	0.58264	0.70710
$\pm\sigma$/ s^{-1}	0.00019	0.00054	0.00189	0.00551	0.03976	0.05377	0.09404	0.10038

The third set of results represents eight measurements of reaction kinetics for Au deposition via SLRR of Pb UPD obtained from reaction solution containing 0.1 M $HClO_4$ + $5x10^{-3}$ M Pb^{2+} + X M Au^{3+} (X=0; $4.3x10^{-5}$ M; $8.5x10^{-5}$ M; $1.2x10^{-4}$ M; $1.6x10^{-4}$ M; $2.0x10^{-4}$ M; $2.3x10^{-4}$ M; and $2.6x10^{-4}$ M). The individual OCP transients measurements data together with model equation fits to extract the rate constant are shown in Figure 4-8. Here, fits of the rate equation to the data are shown with red line and the experimental data are represented with black circles. The Figure 4-8A is the experiment where solution did not contain Au^{3+} ions and this OCP transient is fitted with Eq. (4-6) to extract the

value of k_0 which is the rate constant for Pb UPD oxidation/dissolution via oxygen reduction reaction. The obtained value of k_0 is then used as a parameter in the model represented by Eq. (4-8)-oxygen corrected first order reaction kinetics, to fit the data in Figure 4-8(B-H) and extract the value of rate constant *k'* as a function of the Au^{3+} concentration in reaction solution. The obtained values of *k'* for this reaction solution are plotted as function of the Au^{3+} concentration in Figure 4-10 - blue triangles and they are summarized in Table 4-7. The quality of the fits obtained was characterized by r^2 values which were in each individual case better than 0.96. As previously discussed, the obtained dependence of *k'* vs. [Au^{3+}] is linear showing an increase in *k'* value as the concentration of Au ions in the solution is increased. This again reconfirms the *L*=1, in terms of Au^{3+} reactant as we have discussed previously. These data and analysis are in qualitative agreement with surface reflectivity measurements and analysis discussed previously.

Table 4-7. Summary of reaction rate constants extracted from OCP fittings for reaction solution containing 0.1 M $HClO_4$ + 5x10^{-3} M Pb^{2+} + X M Au^{3+}.

Base Electrolyte: 0.1 M $HClO_4$ + 5x10^{-3} M Pb^{2+}								
[Au^{3+}] / M	**0**	**4.3×10^{-5}**	**8.5×10^{-5}**	**1.2×10^{-4}**	**1.6×10^{-4}**	**2.0×10^{-4}**	**2.3×10^{-4}**	**2.6×10^{-4}**
***k'* or k_0 /s^{-1}**	0.00136	0.17908	0.32837	0.38908	0.53721	0.47640	0.63730	0.56155
$\pm\sigma$/ s^{-1}	0.04657	0.00596	0.02419	0.08484	0.08883	0.23377	0.26553	0.31982

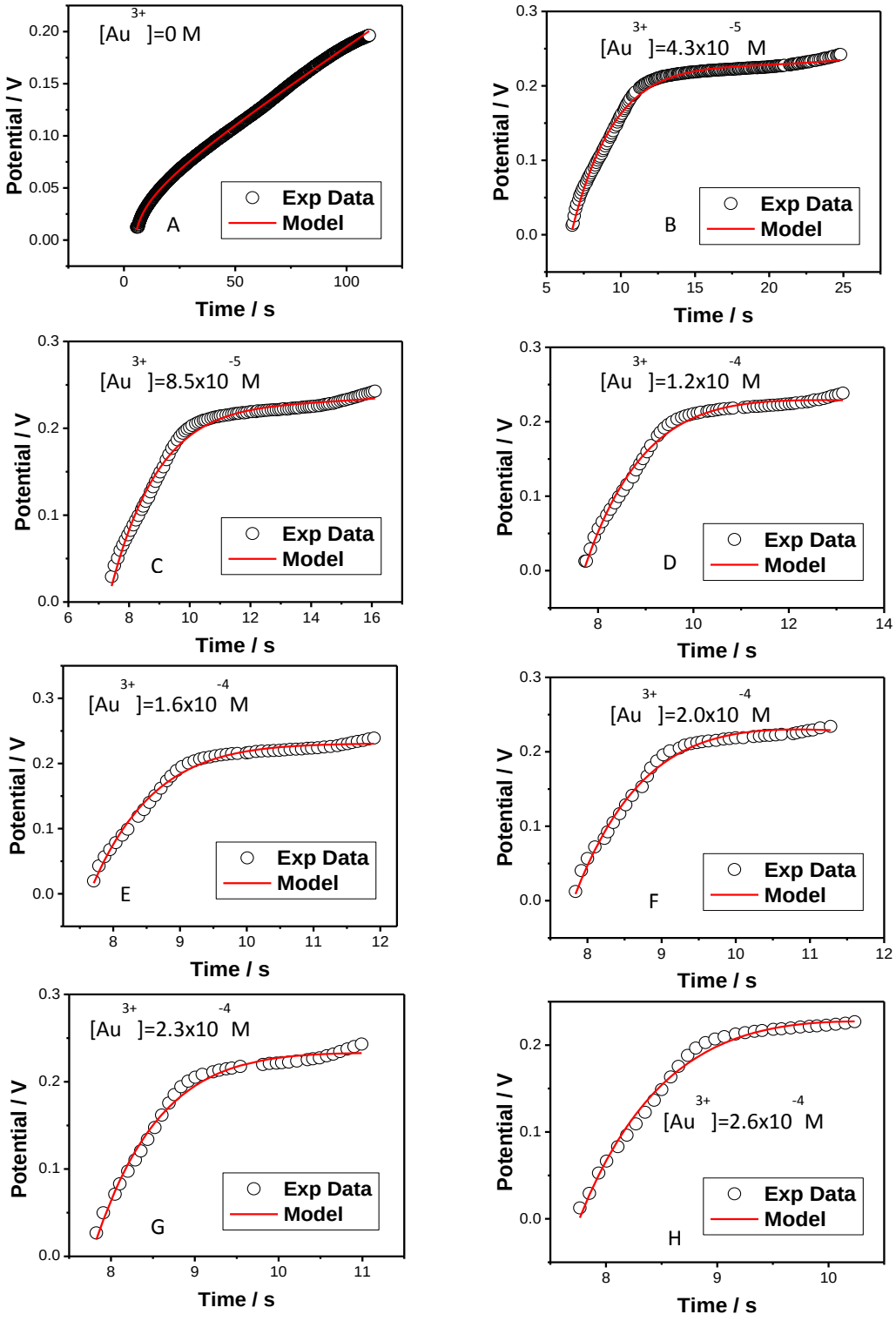

Figure 4-8. The OCP transients obtained during Au deposition via SLRR of Pb UPD monolayer in solution: 0.1 M $HClO_4$ + $5x10^{-3}$ M Pb^{2+} + X M Au^{3+}.

The fourth set of results represents eight measurements of reaction kinetics for Au deposition via SLRR of Pb UPD obtained from reaction solution containing 0.1 M $HClO_4$ + 10^{-2} M Pb^{2+} + X M Au^{3+} (X=0; $4.3x10^{-5}$ M; $8.5x10^{-5}$ M; $1.2x10^{-4}$ M; $1.6x10^{-4}$ M; $2.0x10^{-4}$ M; $2.3x10^{-4}$ M; and $2.6x10^{-4}$ M). The individual OCP transients measurements data together with model equation fits to extract the rate constant are shown in Figure 4-9. Here, fits of the rate equation to the data are shown with red line and the experimental data are represented with black circles. The Figure 4-9A is the experiment where solution did not contain Au^{3+} ions and this OCP transient is fitted with Eq. (4-6) to extract the value of k_0 which is the rate constant for Pb UPD oxidation/dissolution via oxygen reduction reaction. The obtained value of k_0 is then used as a parameter in the model represented by Eq. (4-8)-oxygen corrected first order reaction kinetics, to fit the data in Figure 4-8(B-H) and extract the value of rate constant k' as a function of the Au^{3+} concentration in reaction solution. The obtained values of k' for this reaction solution is plotted as function of the Au^{3+} concentration in Figure 4-10 - pink triangles and they are summarized in Table 4-8. As in previous cases, the model equations provided very good fits of our experimental data, Figure 4-9. The r^2 values in each individual fit were better than 0.98. As it was previously discussed, the obtained dependence of k' vs. [Au^{3+}] is linear showing an increase in k' value as the concentration of Au ions in the solution is increased. This again reconfirms the L=1, in terms of Au^{3+} reactant as previous data suggested as well. The increase in concentration of Pb^{2+} in reaction solution leads to a much higher values of k' measured.

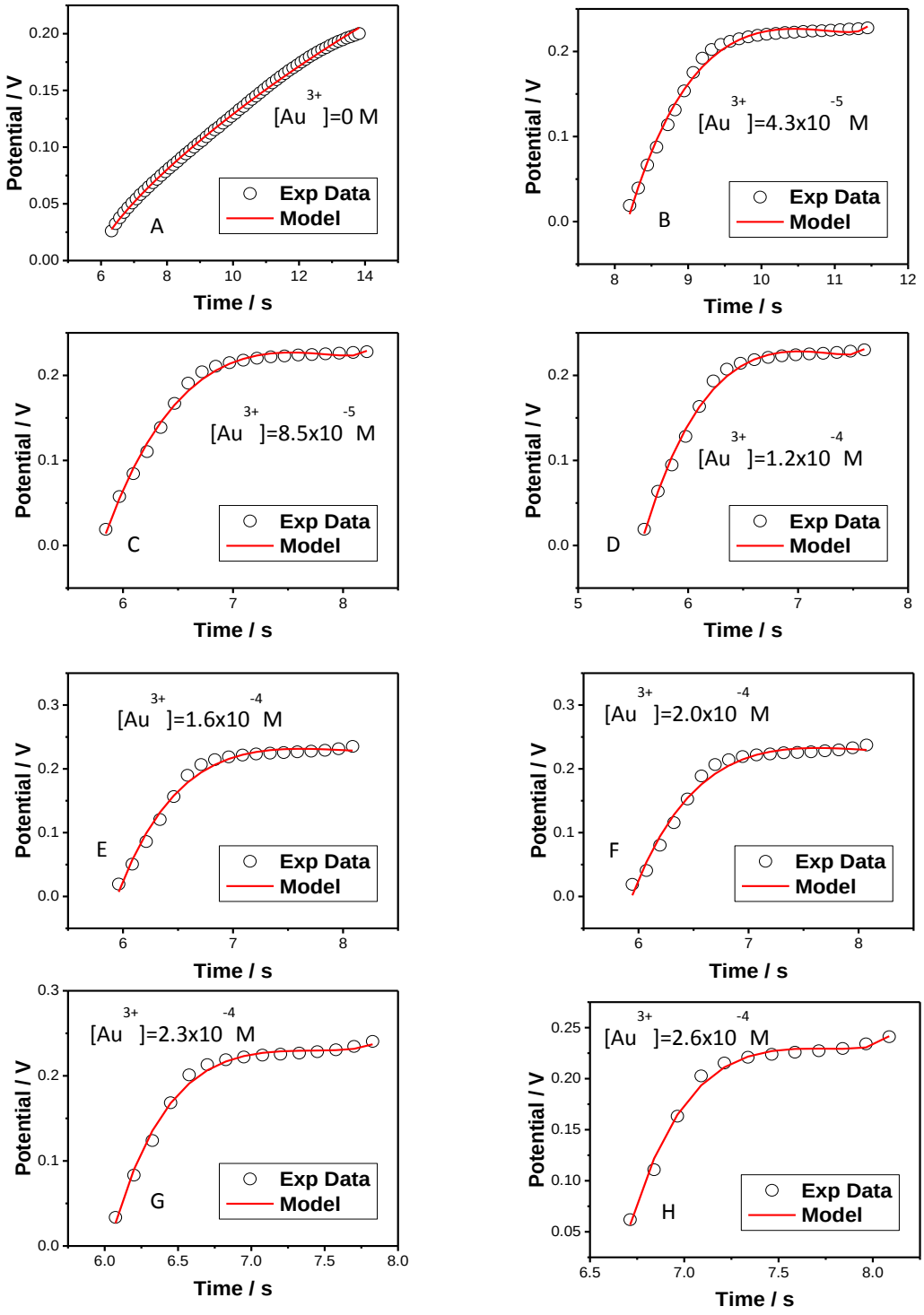

Figure 4-9. The OCP transients obtained during Au deposition via SLRR of Pb UPD monolayer in solution: 0.1 M $HClO_4$ + 10^{-2} M Pb^{2+} + X M Au^{3+}.

Table 4-8. Summary of reaction rate constants extracted from OCP fittings for reaction solution containing 0.1 M $HClO_4$ + 10^{-2} M Pb^{2+} + X M Au^{3+}.

Base Electrolyte: 0.1 M $HClO_4$ + 10^{-2} M Pb^{2+}								
[Au^{3+}] / M	**0**	**4.3×10^{-5}**	**8.5×10^{-5}**	**1.2×10^{-4}**	**1.6×10^{-4}**	**2.0×10^{-4}**	**2.3×10^{-4}**	**2.6×10^{-4}**
***k'* or k_0 /s^{-1}**	0.06589	0.45688	0.55804	0.68049	0.79077	0.74972	1.21496	1.39606
$\pm\sigma$/ s^{-1}	0.69889	0.06277	0.09858	0.13434	0.16876	0.26981	0.32389	0.32728

The physical relevance of our reflectivity measurements for kinetics of TLRR can be evaluated if the value of the reaction constant k_0 calculated from literature data and CV information of the system, and then this result compared with estimated k_0 values from the fittings of model equations for coverage transients and OCP transients. As an example, if we consider the case for Au deposition via SLRR of Pb UPD monolayer in solution 0.1 M $HClO_4$ + 10^{-2} M Pb^{2+}, we need to examine the zero order reaction kinetics values when there are no gold ions in the solution. These results are represented in Figure 4-1a for coverage transients and in Figure 4-6a for OCP transients. Here, rate constant values are extracted as follows:

k_0(4-1a)=0.00873

k_0(4-6a)=0.01693 .

From the stoichiometry of the deposition reaction (Eq. 4-1b), the ratio of m/p = 0.5. The diffusion constant for O_2, D_{O_2} is calculated from the equation below (Han and Bartels 1996) for room temperature, T=298° K:

$$\log_{10}[D_{O_2}/\mathrm{cm^2 s^{-1}}] = -4.410 + 773.8/T - (506.4/T)^2 . \qquad (4\text{-}12)$$

D_{O_2} = 1.6×10^{-5} cm^2s^{-1} (Han and Bartels 1996), while the value of the diffusion layer thickness, δ, in stagnant electrolyte is taken as 0.05 cm (Prentice 1991), and faraday

constant, F is 96500 C/mol, and oxygen reduction current density at 5mV is j= 13.18 μA/cm^2 from our CV, so oxygen concentration can be calculated as

$$C_{O_2}^{\infty} = \frac{\delta \cdot j}{4 \cdot F \cdot D_{O_2}} = 1.07\text{x}10^{-7}\ \text{mol cm}^{-3}. \quad (4\text{-}13)$$

The full Pb(UPD)/Au (111) deposited from 10^{-3} M Pb^{2+} + 0.1 M $HClO_4$ solution has a packing density of 0.66 with respect to Au (111). After taking the atomic areal density of Au (111) as 1.5×10^{15} cm^{-2} (Bard 2002), the surface concentration of the full Pb(UPD)/Au (111) is calculated as; $\Gamma_{i,Pb}^{UPD}$ =(1.5x10^{15}x0.66)/(6.023x10^{23})= 0.164×10^{-8} mol·cm^{-2}. Having $C_{O_2}^{\infty}$ =1.07x10^{-4} mol·lit^{-1} (10^{-8} mol·cm^{-3}), k_0 is calculated as

$$k_0 = \left(\frac{m}{p}\right) \cdot \frac{D_{O_2} \cdot C_{O_2}^{\infty}}{\Gamma_{i,Pb}^{UPD} \cdot \delta} = 0.01041 s^{-1}. \quad (4\text{-}14)$$

As it can be seen here, the estimate of k_0 from the literature data is in better agreement with the value of the k_0 obtained from model fit of intensity–coverage transients than the one in OCP transients. k_0 is the parameter to be used in the oxygen corrected first order reaction kinetic equation to obtain k values for two different gold concentrations in the solution.

The overall comparison between the data in Figure 4-5 and Figure 4-10 shows that both experimental approaches yield the same qualitative trends in k' vs. [Au^{3+}] data. The trends are expected from the basic definition of the k' and stoichiometry of SLRR reaction, thus reconfirming that the definition of k' developed by Gokcen et al. (2011) are correct and capture the full phenomenological description of the reaction kinetics of metal deposition via SLRR. One important thing that transpires is that OCP transient analysis yield overall larger values of k' as compared to the surface reflectivity studies.

The difference is not large, yet it points to a slight drawback of the OCP model in terms of its robustness due to its complexity and number of fitting parameters (4 parameters) as compared to the model equation used to fit Pb UPD coverage transients (1 parameter).

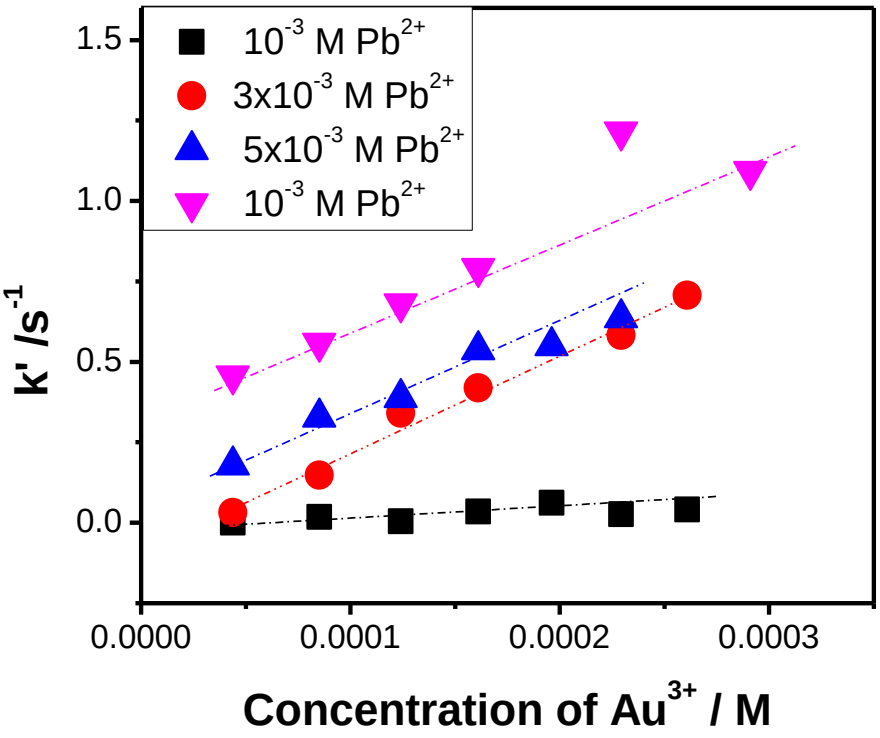

Figure 4-10. The *k'* vs. Au^{3+} concentration dependence obtained from OCP transients during Au deposition via SLRR of Pb UPD monolayer. The different sets of data indicated by different color for different concentration of Pb^{2+} ions.

4.3 Effect of Pb^{2+} Concentration on Reaction Kinetics of Au deposition via SLRR of Pb UPD Monolayer

A more detailed analysis of the *k'* vs. [Au^{3+}] data presented in Figure 4-5 (reflectivity measurements) and in Figure 4-10 (OCP measurements) indicate that the observed slope in the *k'* vs. [Au^{3+}] linear trends has a very strong dependence on the Pb^{2+}

concentration in the reaction solution. This is shown in Figure 4-11. Both type of measurements yield also linear dependence in slope of *k'* vs. [Au^{3+}] data vs. [Pb^{2+}] concentration with almost identical slopes. The only difference is that the extracted *k'* vs. [Au^{3+}] slopes from OCP data are shifted upward reflecting the slightly higher values of rate constants extracted in this measurements as compared to the reflectivity measurements. Having in mind definition of *k'* presented and discussed in introduction and in previous sections, Eq. (4-11) one can conclude that the slope in *k'* vs. [Au^{3+}] data is equal to

$$slope = k \cdot \xi^{L} = k\xi . \tag{4-15}$$

Here, *k* represents the fundamental rate constant of SLRR reaction which is the function of collision frequency between Au^{3+} ions and Pb UPD adatoms, *Z*, and the activation energy for the redox process E_a, viz (Gokcen et al., 2011),

$$k = Ze^{-Ea/RT} . \tag{4.16}$$

Considering that ξ is a constant representing the interface width, which is of order of the inner Helmholtz plane separation from the metal electrode surface, $0.5x10^{-9}$ m, one cannot see a direct effect of Pb^{2+} ion concertation from the definition of the fundamental constant. However, we can conclude that experimental measurements do show that the Pb^{2+} ion concentration has a direct effect on the value of the fundamental rate constant for SLRR reaction-redox process. This effect as obvious from the Figure 4-11 and it is very strong. The increase in the value of *k* for 100% is observed for an order of magnitude increase in Pb^{2+} ion concentration. At this point we cannot deduct exact phenomenological description of this relation, yet its direct relevance to activation energy of the red-ox process on the frequency factor is evident if one looks the definition of the

exchange current density for an electrode/metal surface in contact with tis ions in solution. One thing that transpires from basic electrode kinetics is that exchange current density of the Pb UPD layer with its ions in the solution is a strong function of their concentration in the solution. Therefore, this effect is expected to influence the frequency factor in the fundamental rate constant as it means that larger exchange between Pb UPD adatoms and Pb^{2+} ions in the solution would mean also a larger attempt frequency for formation of the activated complex between Pb UPD-adatoms and Au^{3+} ions in solution.

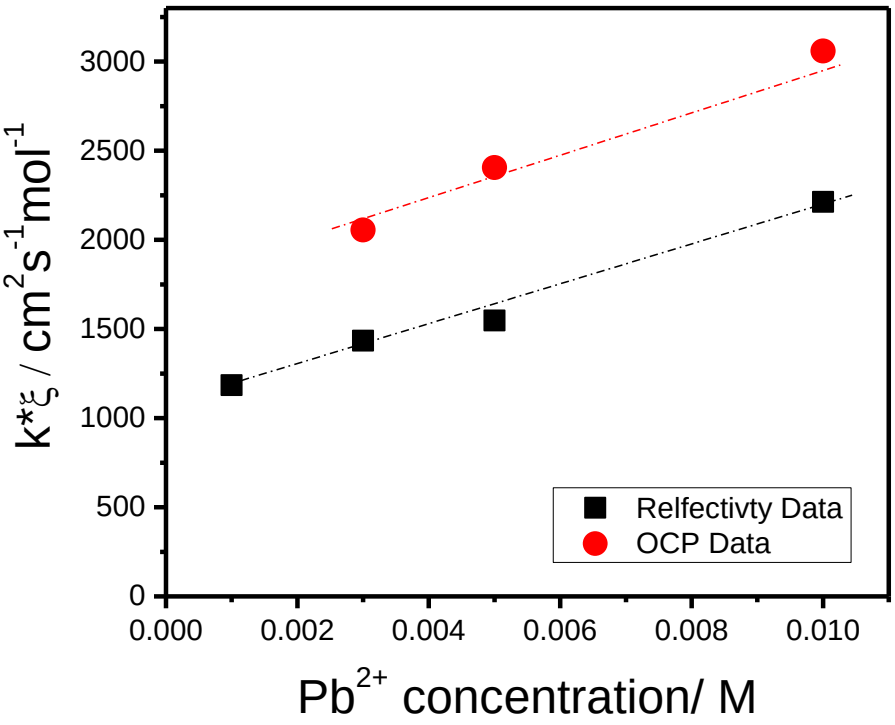

Figure 4-11. The slope in *k'* vs. Au^{3+} concentration linear trends obtained from OCP transients and Pb UPD coverage transients during Au deposition via SLRR of Pb UPD monolayer. See text for more details.

4.4. Effect of Supporting Electrolyte on Reaction Kinetics of Au deposition via SLRR of Pb UPD Monolayer

4.4.1. Rate Constants Obtained from Surface Reflectivity Measurements

In this study we have performed the set of eight measurements of reaction kinetics for Au deposition via SLRR of Pb UPD obtained from reaction solution containing X M $HClO_4$ + 10^{-3} M Pb^{2+} + $1.35x10^{-4}$ M Au^{3+} (X=0.01 M; 0.04 M; 0.07 M; 0.095 M; 0.12 M; 0.14 M; 0.17 M; and 0.19 M). The individual Pb UPD coverage transients together with model equation fits to extract the rate constant are shown in Figure 4-12. The experiments where solution did not contain Au^{3+} ions were used to determine the value of k_0 which is the rate constant for Pb UPD oxidation/dissolution via oxygen reduction reaction (transients not shown for brevity reason). The obtained value of k_0 is then used as a parameter in the model represented by Eq. (4-7)-oxygen corrected first order reaction kinetics, to fit the data in Figure 4-12(A-H) and extract the value of rate constant *k'* as a function of the $\{ClO_4\}^-$ ion concentration. The obtained values of *k'* for this reaction solution is plotted as function of the $\{ClO_4\}^-$ ion concentration in Figure 4-13 - black squares and they are summarized in Table 4-9. In each case, the quality of the model fits to experimental data was very good. The obtained r^2 values were better than 0.98. The obtained dependence of *k'* vs. $[ClO_4^-]$ is linear showing a decrease in *k'* values with increasing concentration of perchlorate ions. The perchlorate ion does not have any complexing ability towards either Pb^{2+} or Au^{3+} ions. Furthermore, it is likely that Au^{3+} is in its chloride complex in the solution as $\{AuCl_4\}^-$ ($AuCl_3$ is the source of Au ions) which is more stable than Au^{3+} complexed with water molecules. Therefore, at first look,

our data look surprising since there is no obvious relation between the concentration of the perchlorate ions and reacting species in SLRR reaction or in activated complex. However, it seems that our trend can be explained by considering a basic postulates of Debye-Hückel theory of electrolyte. A stronger presence of supporting anions in the solution reflects on the Debye length, λ_D, which is a distance at which the ion charge and Coulomb potential is completely screened by surrounding ions in the electrolyte. The relation between Debye length and concentration of the perchlorate ions as supporting electrolyte has $\lambda_D \sim [ClO_4^-]^{-0.5}$ dependence.

Therefore, one expects that more perchlorate ions in the solution will reduce the value of Debye length. This means that the effective coulomb field surrounding a potentially reacting $\{AuCl_4\}^-$ ion at the interface will be felt at the shorter distance if reaction solution contains more perchlorate ions. Indirectly this means that the potential interaction and distance of the approach between gold ions and Pb adatoms is weaker in solution containing more perchlorate ions. Therefore, one could expect a slower kinetics of a red-ox process and lower values of the rate constant.

Table 4-9. Summary of reaction rate constants extracted from intensity model fittings for reaction solution containing X M $HClO_4$ + 10^{-3} M Pb^{2+} + $1.35x10^{-4}$ M Au^{3+}.

Base Electrolyte: 10^{-3} M Pb^{2+} + $1.35x10^{-4}$ M Au^{3+}								
$[ClO_4^-]$ / M	**0.01**	**0.04**	**0.07**	**0.095**	**0.12**	**0.14**	**0.17**	**0.2**
k' / s^{-1}	0.04913	0.06085	0.05734	0.04769	0.04405	0.03952	0.03074	0.02474
$\pm\sigma$ / s^{-1}	0.00140	1.51E-3	0.00162	0.00049	0.00184	0.00166	0.00150	0.00106

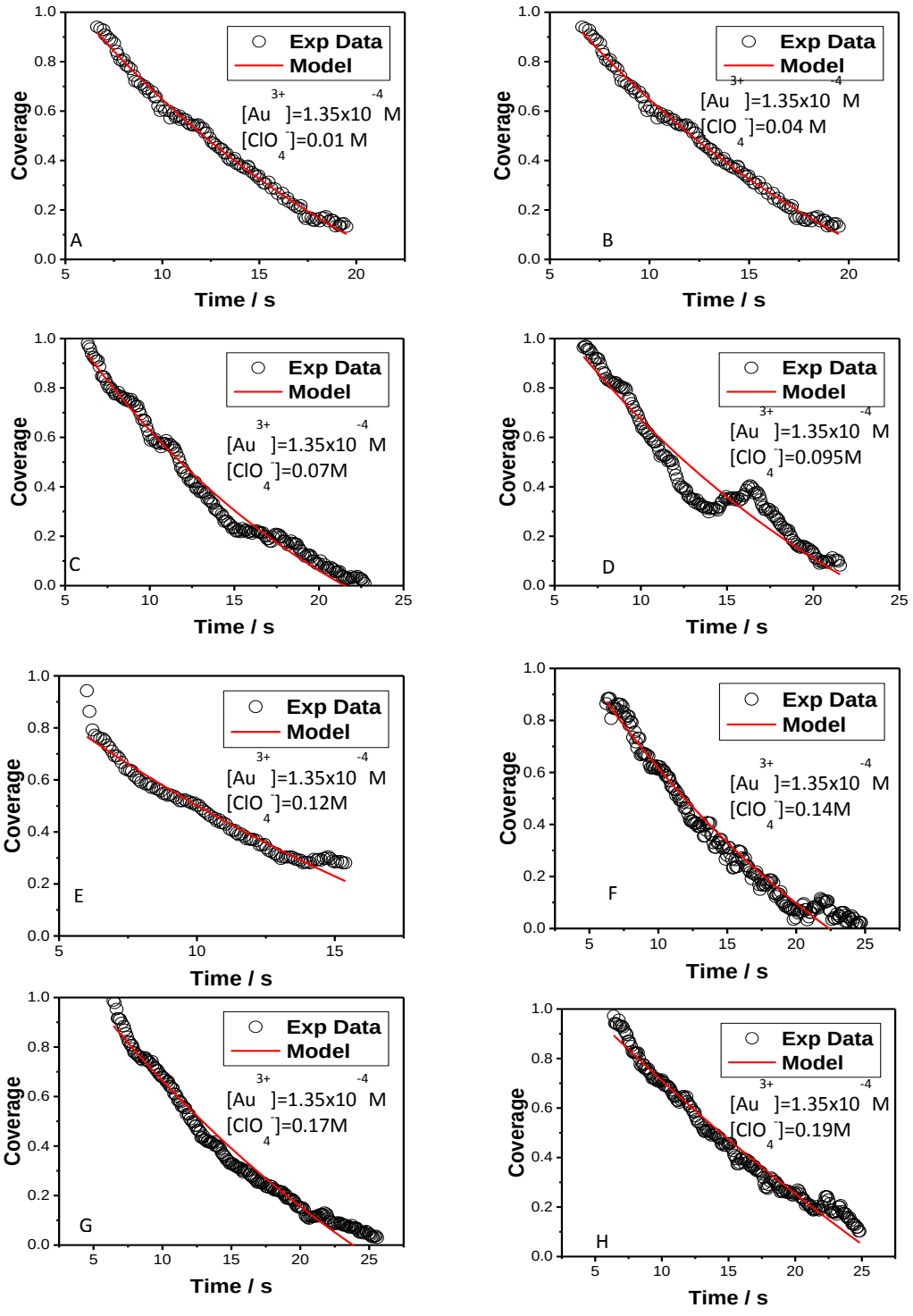

Figure 4-12. The Pb UPD layer coverage transients during Au deposition via SLRR of Pb UPD monolayer in solution containing X M $HClO_4$ + 10^{-3} M Pb^{2+} + $1.35x10^{-4}$ M Au^{3+}.

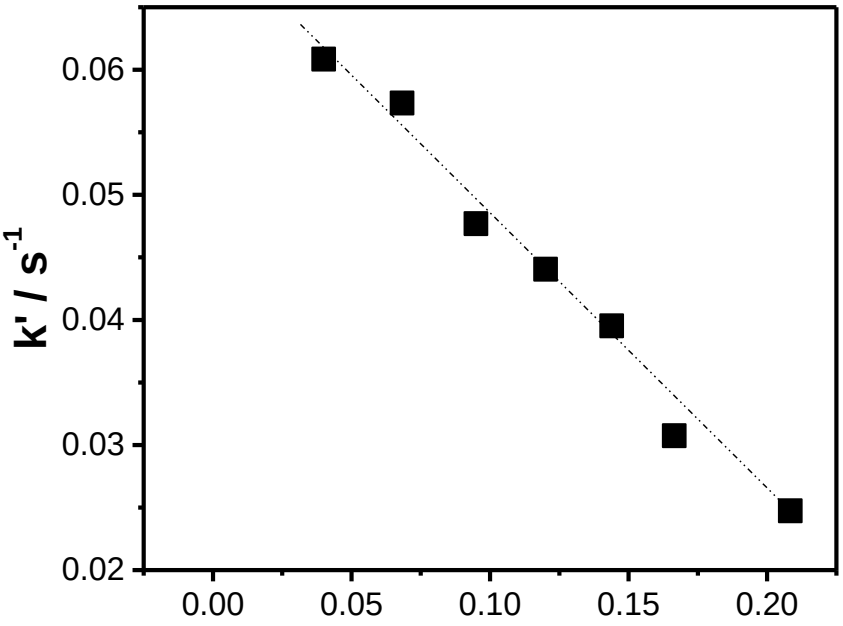

Figure 4-13. *k'* vs. [ClO_4^-] dependence for Au deposition via SLRR of Pb UPD monolayer in reaction solution containing 10^{-3} M Pb^{2+} + $1.35x10^{-4}$ M Au^{3+}. The rate constants extracted from surface reflectivity measurements.

4.4.2. Rate Constants Obtained from OCP Transients Measurements

Same as in previous case, we have performed the set of eight measurements of reaction kinetics for Au deposition via SLRR of Pb UPD obtained from reaction solution containing X M $HClO_4$ + 10^{-3} M Pb^{2+} + $1.35x10^{-4}$ M Au^{3+} (X=0.01 M; 0.04 M; 0.07 M; 0.095 M; 0.12 M; 0.14 M; 0.17 M; and 0.19 M). The individual OCP transients together with model equation fits to extract the rate constant are shown in Figure 4-14. Here, fits of the rate equation to the data are shown with red line and the experimental data are represented with black circles. The experiments where solution did not contain Au^{3+} ions were used to determine the value of k_0 which is the rate constant for Pb UPD

oxidation/dissolution via oxygen reduction reaction (transients not shown for brevity reason). The obtained value of k_0 is then used as a parameter in the model represented by Eq. (4-8)-oxygen corrected first order reaction kinetics, to fit the data in Figure 4-14(A-H) and extract the value of rate constant *k'* as a function of the $\{ClO_4\}^-$ ion concentration. The obtained values of *k'* for this reaction solution is plotted as function of the $\{ClO_4\}^-$ ion concentration in Figure 4-15 - black squares and they are summarized in Table 4-10. In each case, the quality of the model fits to experimental data was very good. The obtained r^2 values were better than 0.92. The obtained dependence of *k'* vs. $[ClO_4^-]$ is linear for the most part of the data and showing a decrease in *k'* values with increasing concentration of perchlorate ions. These trend and results are consistent with the trends observed in experiments using surface reflectivity. Interestingly, even approximately the same values of *k'* were extracted for a given concentration of perchlorate ions in the solution, compare Figure 4-13 and Figure 4-15. This shows a great complementarity between these two types of measurements which are shown to be enabling methodology for study of the kinetics of metal deposition via SLRR of Pb UPD monolayer.

Table 4-10. Summary of reaction rate constants extracted from OCP fittings for reaction solution containing X M $HClO_4$ + 10^{-3} M Pb^{2+} + $1.35x10^{-4}$ M Au^{3+}.

Base Electrolyte: 10^{-3} M Pb^{2+} + $1.35x10^{-4}$ M Au^{3+}								
$[ClO_4^-]$ / M	**0.01**	**0.04**	**0.07**	**0.095**	**0.12**	**0.14**	**0.17**	**0.2**
***k'* / s^{-1}**	0.01346	0.04506	0.05624	0.05521	0.04679	0.03613	0.44878	0.17392
$\pm\sigma$ / s^{-1}	0.03185	0.32872	0.58408	0.40622	0.46579	0.27997	0.13444	0.44345

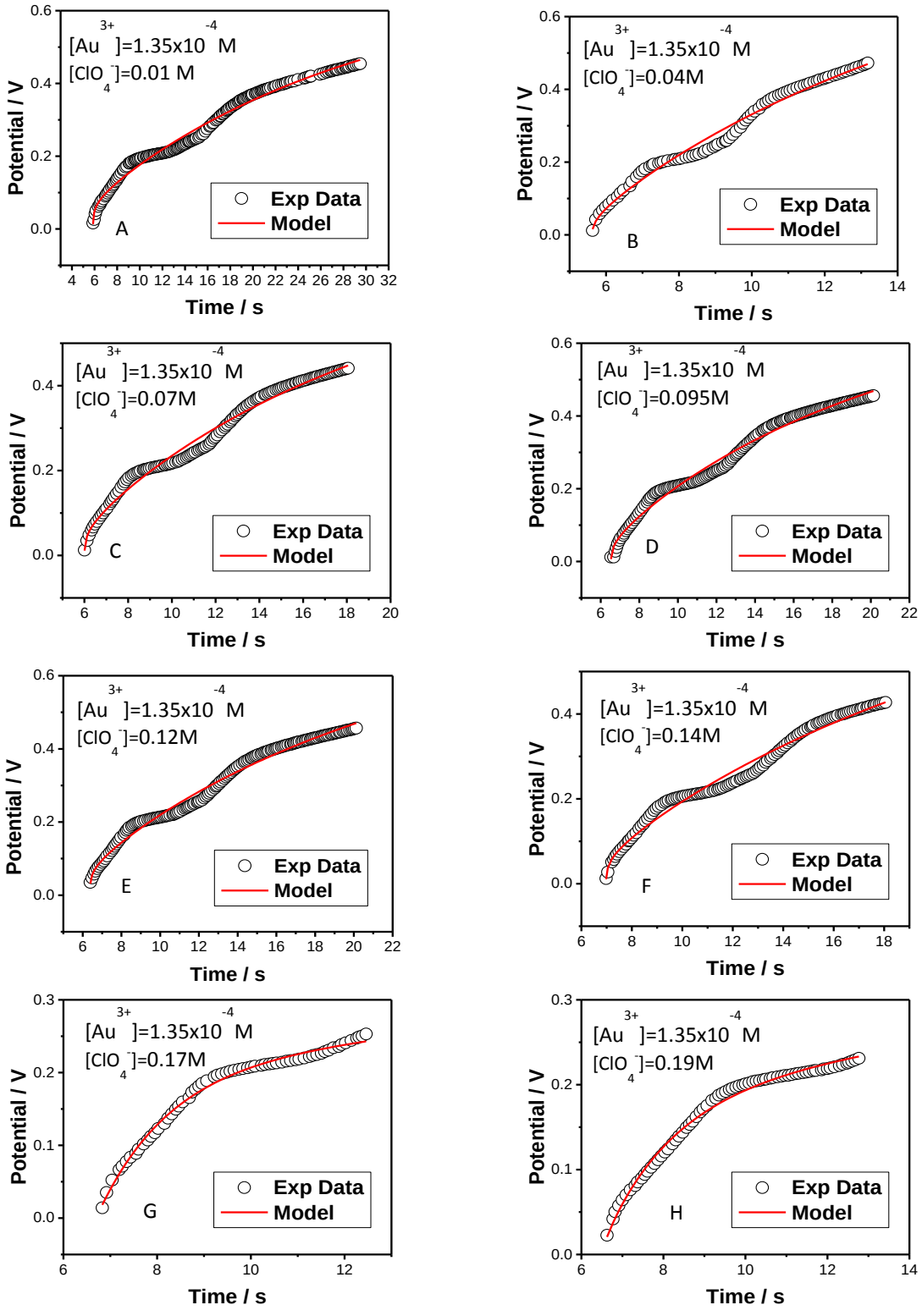

Figure 4-14. The OCP transients during Au deposition via SLRR of Pb UPD monolayer in solution containing X M HClO4 + 10^{-3} M Pb^{2+} + $1.35x10^{-4}$ M Au^{3+}.

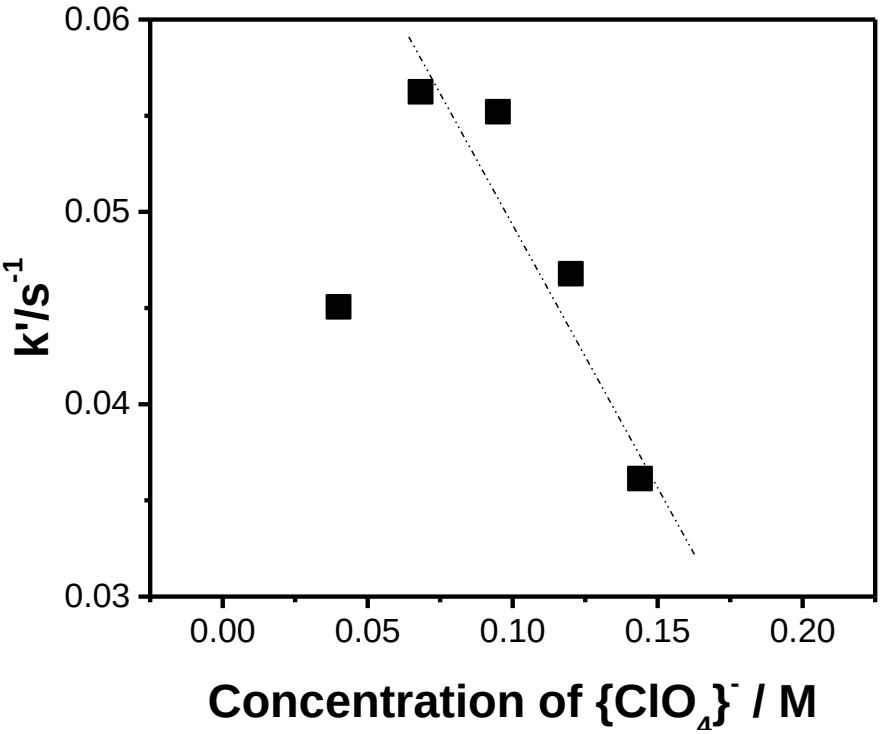

Figure 4-15. *k'* vs. $[ClO_4^-]$ dependence for Au deposition via SLRR of Pb UPD monolayer in reaction solution containing 10^{-3} M Pb^{2+} + $1.35x10^{-4}$ M Au^{3+}. The rate constants extracted from OCP transients measurements**.**

Chapter 5: Conclusions

Underpotential deposition (UPD) and Surface Limited Redox Replacement (SLRR) reactions are two significant monolayer deposition methods, which have gained more attention lately in catalyst design community. Determining the parameters of the reaction kinetics, such as reaction rate constant and half time of the reaction gives the opportunity to have a better control on monolayer catalysts deposition and morphology. The current state of the art technique used to determine SLRR kinetics uses OCP transients and fits these data to OCP model equations to extract reaction rate constant. Due to the complexity of the model equations and having many parameters results in overestimate of rate constants of SLRR reaction kinetics. To overcome this issue, we developed a new system to measure SLRR reaction kinetics using surface reflectivity measurements. This dissertation presents the reaction kinetics study of Au deposition via SLRR of Pb UPD ML using surface reflectivity measurements for which complete experimental system and the LabVIEW data acquisition program was developed.

Initially, we tested the experimental surface reflectivity setup designed and built during this PhD for sensitivity on the change in Pb UPD layer coverage on Au (111) electrode by comparing coverage estimation from our intensity measurements with the coverage extraction from conventional charge measurements from adsorption isotherm of the charge stripping measurements for lead UPD monolayer on Au (111) single crystal. This test is done for several light measurements set ups, such as diffuse and specular measurements for white and red light. All systems agreed very well with the results of charge measurements. However, diffuse white light reflectivity measurements gave us the

best agreement. For this reason, we conducted all of our future experiments with this system. To estimate the effect of potential change on intensity and its contribution to the discrepancy between charge based isotherm and reflectivity based isotherm measurements, we have measured the change of the Au (111) reflectivity as a function of potential in a broad potential range. It is shown that the change of the signal due to a potential change of the Au surface obtained with in the same potential window during CV of Pb UPD is only a 3 % of the total change. This showed that the most of the reflectivity change of the Au surface observed is due to a change of the electronic state of Au surface related to Pb UPD process and our surface reflectivity measurement system is proven as very accurate in recording large change in Pb UPD coverage range between, 10 and 90%, which is the most relevant for our SLRR reaction kinetics studies.

As the next step, we studied reaction kinetics of Au deposition by surface-limited redox replacement (SLRR) of lead underpotential deposited (UPD) mono layer (ML) on Au (111) single crystal by surface reflectivity measurements in one cell configuration. For these measurements, we calculated the amount of Au co-deposition with lead UPD formation to see if it will cause a significant change in the surface morphology. It is shown that the amount of gold co-deposition is 1/1000 of a gold monolayer, so its effect can be neglected.

Since it is impossible to remove all of the oxygen content from the solution no matter how long it is deaerated, oxygen reduction always occurs in parallel to Au deposition. For this reason, we derived new model equations for both our intensity transient models and OCP model to take consideration of the influence of the Pb UPD oxidation via oxygen reduction.

Then, first, we studied the effect of Au^{3+} concentration on reaction kinetics of Au deposition via SLRR of Pb UPD monolayer by increasing Au^{3+} concentration in each experiment. These measurements are conducted for 8 different concentrations. Pb UPD coverage transients obtained from both intensity measurements and OCP transients are fitted to oxygen corrected model equations to extract the reaction rate constant for different gold concentration. The comparison between the rate constants of both experimental approaches showed the same qualitative trend in *k'* vs. [Au^{3+}] data. As it is expected from the basic definition of the k' and stoichiometry of SLRR reaction, increasing gold concentration resulted faster reaction kinetics from both OCP and intensity transients. However, OCP transient analysis yield overall larger values of k' as compared to the surface reflectivity studies due to its complexity and number of fitting parameters (4) as compared to the model equation used to fit Pb UPD coverage transients which has only one parameter.

Then, we studied the effect of Pb^{2+} concentration on reaction kinetics of Au deposition via SLRR of Pb UPD monolayer. As a result, it is shown that slope in the *k'* vs. [Au^{3+}] linear trends has a very strong dependence on the Pb^{2+} concentration in the reaction solution for both OCP and intensity measurements with almost identical slopes. This effect can be explained with influence of the frequency factor in the fundamental rate constant. Larger exchange between Pb UPD adatoms and Pb^{2+} ions in the solution would result a larger attempt frequency for formation of the activated complex between Pb UPD-adatoms and Au^{3+} ions in solution since exchange current density of the Pb UPD layer with its ions in the solution is a strong function of their concentration in the solution. The extracted *k'* vs. [Au^{3+}] slopes from OCP data are shifted upward reflecting

the slightly higher values of rate constants extracted in this measurements as compared to the reflectivity measurements.

Later, we studied the effect of supporting electrolyte on reaction kinetics of Au deposition via SLRR of Pb UPD monolayer. We have performed the set of eight measurements of reaction kinetics for Au deposition via SLRR of Pb UPD for different $HClO_4$ concentrations. The obtained dependence of k' vs. $[ClO_4^-]$ shows a linear trend with a decrease in k' values with increasing concentration of perchlorate ions for both OCP and intensity fittings giving approximately same values of k' for a given concentration of perchlorate ions in the solution. These results were interesting since there is no obvious relation between the concentration of the perchlorate ions and reacting species in SLRR reaction or in activated complex. On the other hand, it can be explained by Debye-Huckel theory of electrolyte. A stronger presence of supporting anions in the solution will reduce the value of Debye length resulting weaker interaction and distance of the approach between gold ions and Pb adatoms which will cause slower kinetics of a red-ox process.

Chapter 6: Future Work

Reflectivity measurement system we built can be improved with further adjustments. A bigger integrating mirror can be used to focus a wider range of reflected/scattered beam on the camera. This will give the opportunity to get more information from intensity data which will result more accurate estimation of reaction kinetics.

In addition to this, also the measurement system can also be improved by fixing the crystal in the electrochemical cell in a certain spot which will allow fixing the end of the fiber cable of the light source, so the angle of the incident beam, the angle of the electrochemical cell, angle of the integration mirror and the camera. To fix all of the elements in the optical table will not only provide reproducible intensity range and much more reliable results for reaction kinetics, but will also make the experimental preparation is much simpler. When all the elements are fixed, the time consuming part of the experimental design part, such as adjusting the incident angle, integrating mirror and camera position, etc. will be eliminated.

Furthermore, our reflectivity measurement system can be used to study the effect choosing different *M* UPD metal ions in the experiments. The reaction kinetics of thallium UPD on Au (111) crystal can be examined and compared to the results of our lead UPD on Au (111). Since thallium and lead have different reversible potentials, and different UPD shift, all these differences might affect the reaction kinetics, and the impact of m/p ratio by choosing different UPD metal in the SLRR measurements can be examined.

Also, the effect of using different supporting electrolyte on SLRR reaction kinetics study can be extended with examining H_2SO_4 and HNO_3 as supporting electrolyte. One can evaluate how the value of the rate constant *k'* change with changing supporting electrolyte. Dependence of the P metal ion deposition via SLRR of M metal UPD on Au (111) on the choice of anion in the supporting electrolyte can be evaluated in addition to our $HClO_4$ study. This will allow altering the rate of *P* metal deposition SLRR of metal UPD on Au (111) by the appropriate choice of the supporting electrolyte.

References

Adžić, R. R., Spasojević, M. D., & Despić, A. R. (1979). Hydrogen evolution on platinum in the presence of lead, cadmium and thallium adatoms. *Electrochimica Acta*, *24*(5), 569-576.

Adžić, R., Yeager, E., & Cahan, B. D. (1974). Optical and electrochemical studies of underpotential deposition of lead on gold evaporated and single-crystal electrodes. *J Electrochem. Soc.: Electrochemical Science and Technology*, Vol. 121, 4.

Adžić, R. R., Zhang, J., Sasaki, K., Vukmirovic, M. B., Shao, M., Wang, J. X., & Uribe, F. (2007). Platinum monolayer fuel cell electrocatalysts. *Topics in Catalysis*, *46* (3-4), 249-262.

Arrhenius, S. (1889). On the reaction velocity of the inversion of cane sugar by acids. *J. Phys. Chem*, 4, 226.

Bae, S. E., Gokcen, D., Liu, P., Mohammadi, P., & Brankovic, S. R. (2012). Size effects in monolayer catalysis—Model Study: Pt Submonolayers on Au (111). *Electrocatalysis*, 3(3-4), 203-210.

Bard, A. J., & Faulkner, L. R. (2002). *Electrochemical methods: fundamentals and applications* (Vol. 2). New York: Wiley.

Bartlett, P. N. (2004). Electrodeposition of nanostructured films using self-organizing templates. *Interface-Electrochemical Society*, 13(4), 28-33.

Bewick, A., & Thomas, B. (1975). Optical and electrochemical studies of the underpotential deposition of metals Part I. Thallium deposition on single crystal silver electrodes. *Journal of Electroanalytical Chemistry and Interfacial Electrochemistry*, 65(2), 911-931.

Bewick, A., & Thomas, B. (1977a). Optical and electrochemical studies of the under-potential deposition of metals: Part III. Lead deposition on silver single crystals. *Journal of Electroanalytical Chemistry and Interfacial Electrochemistry*, 84(1), 127-140.

Bewick, A., & Thomas, B. (1977b). Optical and electrochemical studies of the underpotential deposition of metals: Part II. Phase transitions and two-dimensional nucleation. *Journal of Electroanalytical Chemistry and Interfacial Electrochemistry*, 85(2), 329-337.

Bockris, J. M., & Reddy, A. K. (1970). *Modern electrochemistry: an introduction to an interdisciplinary area. Vol. 1*. Plenum Press.

Brankovic S. R., Wang, J.X & Adzic R. R. (2002). CO Tolerant electrocatalyst with low platinum loading and a process for its application, US Patent 132154.

Brankovic, S. R., & Zangari, G. (2015). Electrochemical surface processes and opportunities for material synthesis. *Electrochemical Engineering Across Scales*, Vol. 15: From Molecules to Processes.

Brankovic, S. R., Dimitrov, N., & Sieradzki, K. (1999). Surfactant mediated electrochemical deposition of Ag on Au (111). *Electrochemical and solid-state letters*, 2(9), 443-445.

Brankovic, S. R., Dimitrov, N., & Sieradzki, K. (1999). Surfactant mediated electrochemical deposition of Ag on Au (111). *Electrochemical and solid-state letters*, *2*(9), 443-445.

Brankovic, S. R., Wang, J. X., & Adžić, R. R. (2001). Metal monolayer deposition by replacement of metal adlayers on electrode surfaces. *Surface Science*, *474*(1), L173-L179.

Brankovic, S. R. (2009). Electrodeposition: Fundamental aspects and methods, in *Functional properties of bioinspired surfaces-properties and technological application,* ed. E. Favret, and N Fuentes, World Scientific, Singapore.

Brankovic, S. R. (in preparation).

Brett, C. M., & Brett, A. M. O. (1993). *Electrochemistry: principles, methods, and applications* (Vol. 4). Oxford: Oxford university press.

Budevski, E. G. Staikov, W. J. Lorenz. (1996). Electrochemical phase formation and growth – An Introduction to the initial stages of metal deposition, VCH, Weinheim,

Cahan, B. D., Horkans, J., & Yeager, E. (1970). Reflectance studies of the gold/electrolyte interface. In *Symposia of the Faraday Society* (Vol. 4, pp. 36-44). Royal Society of Chemistry.

Cao G. (2004). *Nanostructures and nanomaterials: Synthesis, properties and applications.* Imperial College Press, London, UK.

Cardona, M. (1968). Proc. 9th Int. Conf: Phys. Semicond., 1,365.

Cardona, M. (1969). *SoZid State Physics*, suppl. 1 1, Academic Press, New York.

Corcoran, S. G., Chakarova, G. S., & Sieradzki, K. (1994). An in-situ STM investigation of the underpotential deposition of Ag on Au (111) electrodes. Journal of *Electroanalytical Chemistry*, 377(1), 85-90.

Dana, K. J., Van Ginneken, B., Nayar, S. K., & Koenderink, J. J. (1999). Reflectance and texture of real-world surfaces. *ACM Transactions on Graphics (TOG), 18*(1), 1-34.

Edelstein, A. S., & Cammarata, R. C. (1996). Nanoparticles: Synthesis, properties and applications. *Institute of Physical Publishing*, Philadelphia, 170.

Engelsmann, K., Lorenz, W. J., & Schmidt, E. (1980). Underpotential deposition of lead on polycrystalline and single-crystal gold surfaces: Part I. Thermodynamics. *Journal of Electroanalytical Chemistry and Interfacial Electrochemistry*, *114*(1), 1-10.

Evans, M. G., & Polanyi, M. (1935). Some applications of the transition state method to the calculation of reaction velocities, especially in solution. *Transactions of the Faraday Society*, *31*, 875-894.

Evans, M. G., & Polanyi, M. (1937). On the introduction of thermodynamic variables into reaction kinetics. *Transactions of the Faraday Society*, *33*, 448-452.

Eyring, H. (1935). The activated complex in chemical reactions. *The Journal of Chemical Physics*, *3*(2), 107-115.

Eyring, H., & Polanyi, M. (1931). Uber einfache gasreaktionen. *Z Phys Chem Abt B*, *12*, 279-311.

Fayette, M., Liu, Y., Bertrand, D., Nutariya, J., Vasiljevic, N., & Dimitrov, N. (2011). From Au to Pt via surface limited redox replacement of Pb UPD in one-cell configuration. *Langmuir*, *27*(9), 5650-5658.

Garcia, S. G., Salinas, D. R., & Staikov, G. (2005). Underpotential deposition of Cd on Ag (111): an in situ STM study. *Surface science*,*576*(1), 9-18.

Gokcen, D. (2010). Morphology and property control of Pt submonolayers deposited via surface-limited redox replacement reaction, PhD dissertation, University of Houston.

Gokcen, D., Bae, S. E., & Brankovic, S. R. (2010). Stoichiometry of Pt submonolayer deposition via surface-limited redox replacement reaction. *Journal of The Electrochemical Society*, *157*(11), D582-D587.

Gokcen, D., Bae, S. E., & Brankovic, S. R. (2011). Reaction kinetics of metal deposition via surface limited red-ox replacement of underpotentially deposited metal monolayers. *Electrochimica Acta*,56(16), 5545-5553.

Gokcen, D., Miljanic, O., & Brankovic, S. R. (2009, July). Nano-organization and morphology control of metal monolayers deposited by galvanic displacement of UPD monolayers. In *Meeting Abstracts* (No. 33, pp. 2443-2443). The Electrochemical Society.

Gokcen, D., Miljanic, O., & Brankovic, S.R. (2010). 218th The Electrochemical Society Meeting, Abstract #2015, Las Vegas, NV. Oct. 10-15.

Hamann, C. H., Hamnett, A., & Vielstich, W. (2007). *Electrochemistry*, 2nd completely revised and updated ed.

Hamelin, A., & Lipkowski, J. (1984). Underpotential deposition of lead on gold single crystal faces: Part II. General discussion. *Journal of electroanalytical chemistry and interfacial electrochemistry*, 171(1), 317-330.

Herrero, E., Buller, L. J., & Abruna, H. D. (2001). Underpotential deposition at single crystal surfaces of Au, Pt, Ag and other materials. *Chemical Reviews*, 101(7), 1897-1930.

Huang, B. M., Colletti, L. P., Gregory, B. W., Anderson, J. L., & Stickney, J. L. (1995). Preliminary studies of the use of an automated flow-cell electrodeposition system for the formation of CdTe thin films by electrochemical atomic layer epitaxy. *Journal of the Electrochemical Society*, *142*(9), 3007-3016.

Juttner, K. & Lorenz, W. J. (1980). *Z. Phys. Chem*, NF, 122, 163

Ke, L. (1993). A Method of Light Reflectance Measurement, Master Thesis, Tsinghua University.

Kim, Y. G., Kim, J. Y., Vairavapandian, D., & Stickney, J. L. (2006). Platinum nanofilm formation by EC-ALE via redox replacement of UPD copper: studies using in-situ

scanning tunneling microscopy.*The Journal of Physical Chemistry B*, *110*(36), 17998-18006.

Kolb, D. M., Gerischer, H., & Tobias, C. W. (1978). *Advances in electrochemistry and electrochemical engineering*. Vol. 11, Wiley, New York, 125.

Kolb, D. M. & Kotz, R. (1977a). Electroreflectance spectra of Ag(111) electrodes. *Surface Science*, 64 (1977) 96-108.

Kolb, D. M. & Kotz, R. (1977b). Optical properties and electronic structure of copper atoms adsorbed on a platinum electrode. *Surface Science*, 64 (1977) 678-712.

Kolb, D. M., Przasnyski, M., & Gerischer, H. (1974). Underpotential deposition of metals and work function differences. *Journal of Electroanalytical Chemistry and Interfacial Electrochemistry*, *54*(1), 25-38.

Kolb, D. M., Ullmann, R., & Will, T. (1997). Nanofabrication of small copper clusters on gold (111) electrodes by a scanning tunneling microscope. *Science*, *275*(5303), 1097-1099.

Kowal, A., Li, M., Shao, M., Sasaki, K., Vukmirovic, M. B., Zhang, J., ... & Adzic, R. R. (2009). Ternary Pt/Rh/SnO_2 electrocatalysts for oxidizing ethanol to CO_2. *Nature materials*, *8*(4), 325-330.

Laidler, K. J. (1969). *Theories of chemical reaction rates*, McGraw-Hill, New York.

Lax, B. (1968). *Proc. 9th Int. Conf. Phys. Semicond*., 1, 253.

Li, C. Z., Bogozi, A., Huang, W., & Tao, N. J. (1999). Fabrication of stable metallic nanowires with quantized conductance.*Nanotechnology*, *10*(2), 221.

Lipkowski, J., & Ross, P. N. (1998). *Electrocatalysis* (Vol. 3). John Wiley & Sons.

Liu, Y., Bliznakov, S., & Dimitrov, N. (2009). Comprehensive study of the application of a pb underpotential deposition-assisted method for surface area measurement of metallic nanoporous materials. *The Journal of Physical Chemistry C*, *113*(28), 12362-12372.

Marcelin, R. (1915). Physicochemical kinetics. *Ann. Phys*, *3*, 120-184.

Markov, I. V. (1995). *Crystal growth for beginners*. World Scientific.

McC, W. C. (1918). Lewis. *Studies in Catalysis. Part IX. The Calculation in Absolute Measure of Velocity Constants and Equilibrium Constants in Gaseous Systems," J. Chem. Soc*, *113*, 471-492.

Mo, Y., Gofer, Y., Hwang, E., Wang, Z., & Scherson, D. A. (1996). Simultaneous microgravimetric and optical reflectivity studies of lithium underpotential deposition on Au (111) from propylene carbonate electrolytes. *Journal of Electroanalytical Chemistry*, 409(1), 87-93.

Murray-Coleman, J.F. & Smith, A.M. (1990). The Automated Measurement of BRDFs and their Application to Luminaire Modeling. *Journal of the Illuminating Engineering Society*, pp. 87-99.

Nauma, D., Kumar, P.G., & Pregosin, P.S. (2005). *Magn. Reson. Chem*., 43,246.

Nicewarner-Pena, S. R., Freeman, R. G., Reiss, B. D., He, L., Peña, D. J., Walton, I. D., & Natan, M. J. (2001). Submicrometer metallic barcodes. *Science*, 294(5540), 137-141.

Nutariya, J., Fayette, M., Dimitrov, N., & Vasiljevic, N. (2013). Growth of Pt by surface limited redox replacement of underpotentially deposited hydrogen. *Electrochimica Acta*, *112*, 813-823.

Pauling, H. J., & Jüttner, K. (1992). Top-on-top monolayer formation of foreign metals on gold single crystal surfaces. *Electrochimica acta*, *37*(12), 2237-2244.

Pauling, L. (2014). *General chemistry*. Dover Publications, NY.

Pelzer, H., & Wigner, E. (1932). The speed constansts of the exchange reactions. *Z Phys Chem B*, *15*, 445.

Plieth, W. (2008). *Electrochemistry for materials science*. Elsevier.

Plieth, W. J. (1970). Studies of adsorbed states at the electrode/electrolyte interface by specular reflection of light. In *Symposia of the Faraday Society* (Vol. 4, pp. 137-144). Royal Society of Chemistry.

Prentice, G. (1991). *Electrochemical engineering principles*.

Prostak, A., & Hansen, W. N. (1967). Electroreflectance in metals. *Physical Review*, *160*(3), 600.

Rath, D. L. (1983). Studies of electrode resistance in the electrochemical cell. *Journal of Electroanalytical Chemistry and Interfacial Electrochemistry*, 150(1), 521-534.

Rice, O. K., & Gershinowitz, H. (1934). Entropy and the absolute rate of chemical reactions I. The steric factor of bimolecular associations. *The Journal of Chemical Physics*, *2*(12), 853-861.

Rodebush, W. H. (1923). A statistical theory of monomolecular reactions. *Journal of the American Chemical Society*, *45*(3), 606-614.

Rodebush, W. H. (1933). Thermodynamics and the kinetics of gaseous reactions. *The Journal of Chemical Physics*, *1*(7), 440-443.

Rodebush, W. H. (1935). The absolute rate of a chemical reaction. *The Journal of Chemical Physics*, *3*(4), 242-242.

Rodebush, W. H. (1936). The hydrogen bond and coordination. *Chemical Reviews*, *19*(1), 59-65.

Rogers, L. B., Krause, D. P., Griess, J. C., & Ehrlinger, D. B. (1949). The electrodeposition behavior of traces of silver. *Journal of The Electrochemical Society*, *95*(2), 33-46.

Sasaki, K., Wang, J. X., Naohara, H., Marinkovic, N., More, K., Inada, H., & Adzic, R. R. (2010). Recent advances in platinum monolayer electrocatalysts for oxygen reduction reaction: Scale-up synthesis, structure and activity of Pt shells on Pd cores. *Electrochimica Acta*, *55*(8), 2645-2652.

Schmickler W.(1996) *Interfacial Electrochemistry***,** Oxford University Press, Oxford.

Schmidt, E., Gygax, H. R., & Böhlen, P. (1966). Polarographie an Festelektroden IV. Einfluss des Leitelektrolyten auf die submonoatomare Bleibedeckung von Silberelektroden. *Helvetica Chimica Acta*, *49*(1), 733-740.

Schwarzacher, W. (1999). Metal nanostructures: a new class of electronic devices. *The Electrochemical Society Interface*, *8*(1), 20-24.

Sieradzki, K., & Dimitrov, N. (1999). Electrochemical defect-mediated thin-film growth. *Science*, *284*(5411), 138-141.

Sieradzki, K., Brankovic S.R & Dimitrov, N. (1999). Electrochemical defect-mediated thin-film growth. *Science*, *284*(5411), 138-141.

Smith, J. M. (1970). *Chemical engineering kinetics*. McGraw-Hill.

Stamenkovic, V. R., Mun, B. S., Arenz, M., Mayrhofer, K. J., Lucas, C. A., Wang, G., & Markovic, N. M. (2007). Trends in electrocatalysis on extended and nanoscale Pt-bimetallic alloy surfaces. *Nature materials*, *6*(3), 241-247.

Stickney, J. L.(2002). Electrochemical atomic layer epitaxy (EC-ALE): Nanoscale control in the electrodeposition of compound semiconductors. Advances in Electrochemical Science and Engineering 7: 1-106.

Strasser, P. (2009). Dealloyed core-shell fuel cell electrocatalysts.*Reviews in Chemical Engineering*, *25*(4), 255-295.

Sudha, V., & Sangaranarayanan, M. V. (2005). Underpotential deposition of metals–Progress and prospects in modelling. *Journal of Chemical Sciences*,*117*(3), 207-218.

Sun, M., Zangari, G., Shamsuzzoha, M., & Metzger, R. M. (2001). Electrodeposition of highly uniform magnetic nanoparticle arrays in ordered alumite. *Applied Physics Letters*, *78*(19), 2964-2966.

Swathirajan, S., & Bruckenstein, S. (1983). Thermodynamics and kinetics of underpotential deposition of metal monolayers on polycrystalline substrates. *Electrochimica Acta*, *28*(7), 865-877.

Trasatti, S. (1971). Work function, electronegativity, and electrochemical behaviour of metals: II. Potentials of zero charge and "electrochemical" work functions. *Journal of Electroanalytical Chemistry and Interfacial Electrochemistry*, *33*(2), 351-378.

Van Brussel, M., Kokkinidis, G., Hubin, A., & Buess-Herman, C. (2003). Oxygen reduction at platinum modified gold electrodes. *Electrochimica acta*, 48(25), 3909-3919.

Vasilic, R., & Dimitrov, N. (2005). Epitaxial growth by monolayer-restricted galvanic displacement. *Electrochemical and Solid-State Letters*, *8*(11), C173-C176.

Vasilic, R., Viyannalage, L. T., & Dimitrov, N. (2006). Epitaxial growth of Ag on Au (111) by galvanic displacement of Pb and Tl monolayers. *Journal of the Electrochemical Society*, *153*(9), C648-C655.

Viyannalage, L. T., Vasilic, R., & Dimitrov, N. (2007). Epitaxial growth of Cu on Au (111) and Ag (111) by surface limited redox replacement an electrochemical and STM study. *The Journal of Physical Chemistry C*, *111*(10), 4036-4041.

Vukmirovic, M. B., Bliznakov, S. T., Sasaki, K., Wang, J. X., & Adzic, R. R. (2011). Electrodeposition of metals in catalyst synthesis: the case of platinum monolayer electrocatalysts.*Interface-Electrochemical Society*, *20*(2), 33.

Wang, J. X., Inada, H., Wu, L., Zhu, Y., Choi, Y., Liu, P., & Adzic, R. R. (2009). Oxygen reduction on well-defined core-shell nanocatalysts: particle size, facet, and Pt shell thickness effects. *Journal of the American Chemical Society*, *131*(47), 17298-17302.

Ward. G. J. (1992). Measuring and Modeling Anisotropic Reflection. *SIGGRAPH'92 proceedings*, pp. 265-272.

Whitaker, J. D., Nelson, J. B., & Schwartz, D. T. (2005). Electrochemical printing: software reconfigurable electrochemical microfabrication. *Journal of Micromechanics and Microengineering*, *15*(8), 1498.

Whitney, T. M., Searson, P. C., Jiang, J. S., & Chien, C. L. (1993). Fabrication and magnetic properties of arrays of metallic nanowires.*Science*, *261*(5126), 1316-1319.

Will, M., Dietterle, M., & Kolb, D. (1995). Nanoscale Probes of the Solid/ Liquid Interface, in *Nanoscale Probes of the Solid/Liquid Interface*, Ed. A Gewirth & H Siegenthaler, Vvol 288, pp 137-162. Springer, Berlin.

Yang, F. Y., Liu, K., Hong, K., Reich, D. H., Searson, P. C., & Chien, C. L. (1999). Large magnetoresistance of electrodeposited single-crystal bismuth thin films. *Science*, *284*(5418), 1335-1337.

Yerkes, C. (2011). Lecture Notes

http://butane.chem.uiuc.edu/cyerkes/Chem104A_BFA05/Lecture_Notes_104/Lect12c.html

Zach, M. P., Ng, K. H., & Penner, R. M. (2000). Molybdenum nanowires by electrodeposition. *Science*, *290*(5499), 2120-2123.

Zhang, J., Lima, F. H. B., Shao, M. H., Sasaki, K., Wang, J. X., Hanson, J., & Adzic, R. R. (2005). Platinum monolayer on nonnoble metal-noble metal core-shell nanoparticle electrocatalysts for O2 reduction. *The Journal of physical chemistry B*, *109*(48), 22701-22704.